Institute of Crop Science and Rescource Conservation – Plant Diseases and Plant Protection

---

Hyperspectral Imaging for Non-Invasive Characterization of Barley Resistances to Powdery Mildew

Dissertation

zur
Erlangung des Doktorgrades (Dr. rer. nat.)
der
Mathematischen-Naturwissenschaftlichen Fakultät
der
Rheinischen Friedrich-Wilhelms-Universität Bonn

vorgelegt von
Matheus Thomas Kuśka
aus
Rybnik, Polen

Bonn, August 2017

Angefertigt mit Genehmigung der Mathematisch-Naturwissenschaftlichen Fakultät der
Rheinischen Friedrich-Wilhelms-Universität Bonn

1. Gutachter: PD. Dr. Anne-Katrin Mahlein
Institut für Nutzpflanzenwissenschaften und Ressourcenschutz, Universität Bonn

2. Gutachter: Prof. Dr. Dorothea Bartels
Institut für Molekulare Physiologie und Biotechnologie der Pflanzen, Universität Bonn

Tag der mündlichen Prüfung: 03.11.2017
Erscheinungsjahr: 2017

Knowledge is important. But you need to believe in your hypothesis before you can prove it. Only then you will have the energy to get what you desire.

Matheus Thomas Kuśka

Abstract

Determination and characterization of resistance reactions of crop plants against fungal pathogens are essential to select resistant genotypes. In breeding practice phenotyping of genotypes is realized by time consuming and expensive visual plant ratings. During resistance reactions of plants and disease pathogenesis, structural and biochemical changes occur which are assumed to affect the reflectance spectra of plants specifically.

The aim of this study was to establish a non-invasive resistance detection and characterization using hyperspectral imaging. Therefore, a novel hyperspectral imaging microscope was developed to determine subtle changes during plant-pathogen interactions. Reflectance spectra of barley leaves with different susceptibility and resistance against *Blumeria graminis* f.sp. *hordei* (*Bgh*) were recorded at different timepoints after inoculation. Hyperspectral data were manually analyzed and by data driven approaches. Characteristic spectral signatures were described and biologically interpreted using histological and molecular analysis during the compatible and incompatible barley-*Bgh* interactions.

The powdery mildew pathogenesis and mildew locus o (*mlo*) as well as Mildew locus a (*Mla*) based resistance reactions of barley were identified using hyperspectral imaging. Spectral reflectance of barley was affected by each interaction type in a characteristic way. Changes in the spectral pattern and differences in the reflectance intensities differed depending on the development stage of pathogenesis and resistance. Parallel histological and gene expression analysis provided an in-depth attribution of spectral information and temporal interaction processes on a small scale. Beside detection and characterization, *Bgh* pathogenesis and *Mla* based hypersensitive responses have been visualized by binary maps based on hyperspectral imaging data before symptoms become visible for the human eye. Spectral traces were computed by a machine learning process over an experimental period of 14 days after inoculation to uncover hyperspectral dynamics during barley-*Bgh* interactions. These spectral traces showed changes in hyperspectral reflectance and revealed an individual biological development. Relevant wavelengths for pathogenesis, *mlo* and *Mla* responses against *Bgh* were assessed using the Relief algorithm on hyperspectral images which were recorded all 3 hours after inoculation. By this relevant time points and wavelengths to distinguish between the interaction types were revealed. In addition, the Relief algorithm was applied to analyse a functional link between hyperspectral reflectance and observed gene expressions during these early barley-*Bgh* interactions. A interpretation of the relevant wavelengths to the biologic function of the gene transcripts was facilitated.

The results of this study provide a deeper understanding of optical properties of diseased plants and will promote phenotyping in resistance breeding. This information can be integrated in high-throughput phenotyping pipelines in order to evaluate the performance of multiple genotypes. Further analysis of the coherency between hyperspectral reflectance and enzyme activities, changes in secondary metabolites and hormones during barley-*Bgh* interactions will realize a straight forward phenotyping of genotype-pathogen interactions by hyperspectral imaging.

Kurzfassung

Die Erfassung und Charakterisierung von Resistenzreaktionen von Nutzpflanzen gegenüber pilzlichen Schaderregern ist essentiell für die Selektion resistenter Genotypen. Üblicherweise erfolgt die phänotypische Bewertung verschiedener Genotypen in der Züchtungspraxis durch eine zeit- und kostenintensive Bonitur. Während einer pilzlich verursachten Pathogenese oder Resistenzreaktion kommt es zu strukturellen und biochemischen Änderung in der Pflanze. Es wird angenommen das diese Änderungen einen speziellen Einfluss auf die spektrale Reflexion von Pflanzen haben.

Ziel dieser Arbeit war es, Resistenzreaktionen von Pflanzen gegenüber pilzlichen Erregern nicht-invasiv mit hyperspektralen bildgebenden Verfahren zu erkennen, zu untersuchen und zu charakterisieren. Um subtile Änderungen während einer Pflanzen-Pathogen Interaktion zu erfassen wurde ein neues hyperspektrales Mikroskop entwickelt. Blätter von Gerstengenotypen mit unterschiedlichen Anfälligkeiten und Resistenzen gegenüber *Blumeria graminis* f.sp. *hordei* (*Bgh*) wurden zu unterschiedlichen Zeitpunkten nach der Inokulation mit *Bgh* hyperspektral gemessen. Die resultierenden hyperspektralen Daten wurden manuell und datengetrieben analysiert. Histologische und molekularbiologische Untersuchungen wurden durchgeführt um charakteristische, spektrale Reflexions Signaturen während kompatibler und nicht-kompatibler Gerste-*Bgh* Interaktionen biologisch zu interpretieren.

Die *Bgh* Pathogenese, sowie Resistenzreaktionen basierend auf dem mildew locus o (*mlo*) und Mildew locus a (*Mla*) Genen konnten identifiziert werden. Änderungen der spektralen Signaturen während der Pathogenese und der spezifischen Resistenzreaktion unterschieden sich abhängig vom Entwicklungszeitpunkt. Eine genaue Zuordnungen der spektralen Informationen und zeitlichen Interaktionsprozessen wurde mithilfe histologischer und Genexpressionsanalysen mit hoher Präzision erbracht. Binäre Abbildungen auf Basis der hyperspektralen Bilder erbrachten eine frühzeitige Visualisierung der *Bgh* Pathogenese und auf *Mla* basierenden hypersensitiven Reaktionen bevor diese für das menschliche Auge sichtbar waren. Durch den Einsatz von Maschinellen Lernen und der Berechnung von spektralen "Verläufen" konnte die hyperspektrale Dynamik während der Gersten-*Bgh* Interaktionen in einem experimentellen Zeitraum von 14 Tagen nach der Inokulation entschlüsselt werden. Diese spektralen "Verläufe" zeigten Änderungen in den hyperspektralen Signaturen und die individuelle biologische Entwicklung der Genotypen über die Zeit. Die relevanten Wellenlängen während der Pathogenese und während *mlo* und *Mla* Reaktionen gegen *Bgh* wurden mithilfe des Relief-Algorithmus auf hyperspektralen Bildern -welche alle drei Stunden aufgenommen wurden- bewertet. Dadurch konnten wesentliche Wellenlängen und entscheidende frühe Zeitpunkte zur Unterscheidung der Interaktionstypen gezeigt werden. Desweiteren wurde der Relief-Algorithmus genutzt um eine funktionale Verbindung zwischen den hyperspektralen Reflexionssignaturen und den beobachteten Genexpressionen während der frühen Gersten-*Bgh* Interaktionen zu analysieren. Hierdurch war eine Interpretation der relevanten Wellenlängen zu den biologischen Funktionen der Gentranskripte möglich.

Die Ergebnisse dieser Arbeit tragen zu einem besseren Verständnis der optischen Eigenschaften von erkrankten Pflanzen bei und fördern die Phänotypisierung in der Resistenzzüchtung. Die Erkenntnisse können in Hochdurchsatz-Anlagen zur Phänotypisierung eingebracht werden um die Leistung von mehrfachen Genotypen zu bewerten. Weitere Untersuchungen von funktionalen Zusammenhängen zwischen der hyperspektralen Reflexion und zu Enzymaktivitäten, Änderungen in sekundär Metaboliten und Hormonhaushalt während Gersten-*Bgh* Interaktionen werden eine direkte Phänotypisierung der Genotypen-Pathogen Interaktionen durch hyperspektrale bildgebende Verfahren ermöglichen.

Publications included in this thesis

Chapter 3 has been published:
Kuska, Matheus, Wahabzada, Mirwaes, Leucker, Marlene, Dehne, Heinz-Wilhelm, Kersting, Kristian, Oerke, Erich-Christian, Steiner, Ulrike, and Mahlein, Anne-Katrin. 2015. Hyperspectral phenotyping on the microscopic scale: Towards automated characterization of plant-pathogen interactions. *Plant Methods*, 11:28.

Chapter 4 has been published:
Kuska, Matheus Thomas, Brugger, Aanna, Thomas, Stefan, Wahabzada, Mirwaes, Kersting, Kristian, Oerke, Erich-Christian, Steiner, Ulrike, and Mahlein, Anne-Katrin, 2017. Spectral patterns reveal early resistance reactions of barley against *Blumeria graminis* f. sp. *hordei*. *Phytopathology*, 107:1388-1398.

List of Abbreviations

2D	two dimensional
3D	three dimensional
AVR	avirulence factor
BC	before christ
BGH	*Blumeria graminis* f.sp. *hordei*
BP	base pairs
CBB	coomassie brilliant blue R-250
CC	coiled coil
CCD	charge coupled devices
CD	candela
CHL	chlorophyll
CMOS	complementary metal-oxid-semiconductors
CSLD2	cellulose synthase like d2
CV	cultivar
CWA	cell wall appositions
DA	dalton
DAI	day after inoculation
DAB	3,3'-diaminobenzidine
DRF	dehydration responsive factor
FAO	food and agriculture organization of the United Nations
FSP	forma specialis
GLB	globulin
GS	growth stage
H	hours
HAI	hours after inoculation
HR	hypersensitive response
HS	hyperspectral
HV	*Hordeum vulgare*
HSI	hyperspectral imaging
JIP	jasmonate induced protein
LDA	linear discriminant analysis
LED	light emitting diode
LLR	likelihood ratio
LLR	leucin rich repeat
LN	liquid nitrogen
MLA	mildew locus a
MLO	mildew locus o
NB	nuclear binding site
NDVI	normalized difference vegetation index
NIR	near infrared
PR	pathogen related
RAR	required for mla resistance
RGB	red, green and blue color image

RH	relative humidity
RUBISCO	ribulose-1,5-bisphosphate carboxylase small subunit
ROI	region of interest
ROR	required for mlo resistance
ROS	reactive oxygen species
RSD	relative standard deviation
SD	standard deviation
SIVM	simplex volume maximization
SVM	support vector machine
SWIR	short wave infrared
VIS	visible range
WT	wild type

Contents

Abstract i

Kurzfassung ii

Publications included in this thesis iii

List of Abbreviations iv

1 Introduction 1
- 1.1 Barley as a model crop plant . . . 3
- 1.2 *Blumeria graminis* f.sp. *hordei*: The obligate biotrophic plant pathogen . . . 5
  - 1.2.1 The broad-spectrum *mlo* resistance of barley against *Blumeria graminis* f.sp. *hordei* . . . 7
  - 1.2.2 Race specific *Mla* resistance of barley against *Blumeria graminis* f.sp. *hordei* 8
- 1.3 Hyperspectral imaging of plants . . . 10
  - 1.3.1 Status quo: Interpretations of reflectance signatures during plant - pathogen interactions . . . 13
  - 1.3.2 Analysis of hyperspectral data: Manual and data driven approaches . . . 14

2 Objectives of this thesis 17

3 Hyperspectral phenotyping on the microscopic scale 19
- 3.1 Abstract . . . 20
- 3.2 Introduction . . . 20
- 3.3 Materials and Methods . . . 22
  - 3.3.1 Plant cultivation and inoculation of *Blumeria graminis* f.sp. *hordei* . . . 22
  - 3.3.2 Hyperspectral time series imaging and data preprocessing . . . 23
  - 3.3.3 Pre-processing of hyperspectral images . . . 23
  - 3.3.4 Spectral signature extraction, analysis and characterization . . . 24
  - 3.3.5 Data driven approach for fast analysis of hyperspectral dynamics . . . 24
- 3.4 Results . . . 26
  - 3.4.1 Phenotypic development of healthy and inoculated barley leaves . . . 28
  - 3.4.2 Spectral similarity of non-inoculated near-isogenic barley lines over time . 30

3.4.3 Spectral signatures of near-isogenic barley lines during powdery mildew pathogenesis . . . 30
3.4.4 *mlo3* inoculated leaves showed no powdery mildew infestation over time . 31
3.4.5 Automated analysis of hyperspectral images for plant phenotyping 31
3.4.6 Extraction of spectral dynamics of healthy and *Blumeria graminis* f.sp. *hordei* inoculated barley leaves . . . 35
3.5 Discussion . . . 37
3.5.1 Leaf senescence influence hyperspectral reflectance . . . 37
3.5.2 Hyperspectral dynamic in powdery mildew infestation . . . 37
3.5.3 *Mlo3* resistant barley only indicate by decelerate senescence . . . 38

4 Spectral patterns reveal early resistance reactions of barley against *Blumeria graminis* f. sp. *hordei* 39
4.1 Abstract . . . 40
4.2 Introduction . . . 41
4.3 Materials and Methods . . . 42
4.3.1 Plant material and cultivation . . . 42
4.3.2 Pathogen inoculation . . . 42
4.3.3 Histological observation and quantification . . . 42
4.3.4 HSI and manual data extraction . . . 42
4.3.5 Automated data mining of spectral dynamics by HR . . . 44
4.4 Results . . . 46
4.4.1 Microscopic analysis of the interaction phenotypes . . . 46
4.4.2 Hyperspectral signatures of powdery mildew, HR, and papilla . . . 52
4.4.3 Automatic detection of HR on *Mla1* leaves against *Blumeria graminis* f.sp. *hordei* . . . 56
4.5 Discussion . . . 58
4.5.1 Powdery mildew pathogenesis-related processes influence the VIS-NIR spectrum of barley . . . 58
4.5.2 *Mla*-resistance uncovered by HSI . . . 58
4.5.3 Formation of *mlo3* papilla transiently influence spectral signature . . . 59
4.5.4 Objective and accurate resistance phenotyping by HSI . . . 59

5 Functional link of gene expression and optical properties of barley genotypes 61
5.1 Abstract . . . 62
5.2 Introduction . . . 62
5.3 Materials and Methods . . . 64
5.3.1 Plant material and cultivation . . . 64
5.3.2 Pathogen and inoculation . . . 64
5.3.3 Total RNA extraction, reverse transcription-polymerase chain reaction and real time qPCR . . . 64
5.3.4 Hyperspectral image acquisition, reflectance extraction and histological observation . . . 67
5.3.5 Linear Discriminant Analysis for the visualization of synergistic effects . . 67
5.3.6 RELIEF algorithm for feature selection . . . 68
5.4 Results . . . 70
5.4.1 Relevance of spectral wavelengths for discrimination of non-inoculated and inoculated barley . . . 70

5.4.2 Early hyperspectral reflectance differences between powdery mildew susceptible, *mlo* and *Mla* resistant barley 73
5.4.3 Gene expression profiles during barley-powdery mildew interactions . . . 75
5.4.4 Interrelations between hyperspectral signatures and gene expression profiles 77
5.4.5 Relevant wavelength bands for the individual gene expression profiles . . 79
5.5 Discussion 81
5.5.1 *Blumeria graminis* f.sp. *hordei* influence early spectral characteristics of barley 81
5.5.2 Gene expression profiles and their link to spectral reflectance 82
5.5.3 HSI reveals the metabolism during incompatible barley-powdery mildew interactions 83

6 Summary and outlook **85**

References **89**

Danksagung **109**

Erklärung **111**

CHAPTER 1

Introduction

Recent cultivation techniques have result in higher plant pathogen incidence and susceptibility of plants in agriculture (Oerke and Dehne, 2004). Besides the import of new diseases by human activities and favorable conditions due to climate changes, factors which increase the susceptibility of plants to fungal pathogens are the use of non-local adapated high yield varieties, unbalanced fertilisation, large-scale cultivation of genetically uniform plants, reduced crop rotation and tillage cultivation (Oerke and Dehne, 2004). Plant pathogens reduce the quality and products from crop plants and increase the costs in agriculture, due to the application of plant protection measures. One of the most sustainable measures of crop protection is breeding of resistant plant varieties. The cultivation of resistant crops can also reduce the impact of agriculture on the environment, due to less applications of plant protections. A continuous research and plant breeding is in favor necessary which includes the increase of genetic resistance repertory, respectively (Borlaug, 2002). This is because of several limitations of resistant crop varieties. Occasionaly plant pathogens overcome effective plant resistances, like *Puccinia graminis* f.sp *tritici* isolate Ug99 the causal agent of wheat stem rust during the last years (Pretorius et al., 2000). An anticipating plant resistant breeding is challenging, because of high and fast reproduction rates of fungal crop diseases which lead to many spontaneous mutations differing in the impact on common crop varieties.

In contrast, the average development time for a single new resistant crop is at least 12 years before it launches the market (Shimelis and Laing, 2012). A couple of steps make the breeding process time and labor intensive and therefore it is not possible to react to new situations in short time (reviewed in Wenzel (1985)). Several sophisticated methods are available for plant breeding. Marker-assisted selection, bi-parental recombinant inbred lines, or the increasing number of completely sequenced species in genomic databases accelerate and improve first breeding steps (reviewed in Schaart et al. (2016)). These methods enable a fast screening to detect relevant traits such as resistance (reviewed in Wenzel (2006)).

However, after several hybridizations and generations, the set of genotypes of interest must be investigated in different environments and under different conditions. Hereby qualitative characterization of the genome expression to plant function in a given environment is done by the visual estimation of human raters. This step is defined as the phenotyping process (Fiorani and Schurr, 2013). Phenotyping is the visual description and assessment of plants from single

organs to the canopy during all growth stages (Fiorani and Schurr, 2013). This includes the plant growth rate, the architecture, the leaf color, the health status and the detection of abiotic and biotic stress symptoms and their severity. Depending on the testing property, this phenotyping process is necessary in the vegetative and generative phase of a plant. However, it requires a high human effort and the testing of certain environments limits the throughput and is described as the phenotyping bottleneck (Furbank and Tester, 2011). In addition, the traditional visual estimation of plant disease severity is prone to errors, because plant-pathogen interactions sites are on the cellular and leaf level and the assessment is subjectively influenced by the rater (Bock et al., 2010; Nutter et al., 2006, 1993).

To overcome these circumstances, objective methods are required. Highly sensitive sensors are developed and investigated to increase the breeding throughput and standardized rating methods (reviewed in Simko et al. (2017); Mahlein (2016); Fiorani and Schurr (2013)).

For the improvement of plant phenotyping, various optical sensors and methods could accelerate the assessment of parameters of interest. In contrast to destructive 'omic methods, sensors are non-invasive measurement systems and can be performed on the same individuals over time. Different optical sensors such as RGB, 3D, fluorescence, thermography and hyperspectral imaging (HSI) enable the characterization of relevant plant parameters (Paulus et al., 2014; Ustin and Gamon, 2010; Chaerle et al., 2007; Oerke et al., 2006).

Among these optical sensors and methods, hyperspectral sensing has shown promising results to objectively assess different plant parameters and diseases (West et al., 2003; Gamon and Surfus, 1999). Hyperspectral sensing enable the detection of abiotic and biotic stresses, which open new opportunities for field phenotyping and field management (Mahlein et al., 2010; Strachan et al., 2002). Hyperspectral close range imaging characterized plant pathogenesis in space and time and improved the hyperspectral analysis by considering the spatial resolution (Mahlein et al., 2012). Early plant-pathogen interactions are in the submilimeter size which limit the early observation using hyperspectral imaging (HSI) (Mahlein et al., 2012). An increased spatial resolution of hyperspectral cameras can be obtained by hyperspectral microscope setups. With this approach, small and subtle pathogenesis and resistance related reactions of plants against pathogens can be investigated. This enables new possibilities for basic research studies and can be implemented in breeding routines. Nevertheless, the acquired hyperspectral images must be linked to biologic processes during plant-pathogen interactions. These findings can be then used to improve and calibrate resistance-screening systems by HSI. A positive consequence will be an accelerated and objective plant phenotyping process with a reduced human effort as well as a reduced amount of plant material.

The current thesis will present the development of a state-of-the-art hyperspectral imaging microscope and the determination and characterization of plant resistance reactions against a fungal pathogen. One main focus was the biologic interpretation of specific spectral signatures during plant-pathogen interactions. Experiments were carried out on barley plants and the pathogen *Blumeria graminis* f.sp. *hordei*, the causal agent of powdery mildew on barley. To characterize specific spectral signatures of the pathogenesis and the specific barley resistance response, the susceptible barley cultivar (cv.) Ingrid and resistant near-isogenic lines containing 'mildew locus o' and 'Mildew locus a' gene based resistances have been investigated and compared during their plant-pathogen interaction. The acquired hyperspectral images were manually analyzed. For a deeper understanding of complex sensor data, data driven approaches were developed and applied. With this comprehensive approach, hyperspectral data could be biologically interpreted and linked to histological observations and gene activities.

1.1 Barley as a model crop plant

Barley (*Hordeum vulgare* L.) is an ancient feeding grain which cultivated already ~8.000 B.C. in the Fertile Crescent which was the beginning of grain-crop cultivation (Saisho and Purugganan, 2007). It is a therophyte and anemophil plant belonging to the family of *Poaceae*. Barley is a diploid crop with n = 7 chromosoms, which are all mapped (Kleinhofs et al., 1993). Nowadays, the high albuminous winter barley is mainly used as animal feed and summer barley as brewing barley. The world average production from 2000-2014 was ~140 million t/year (FAOSTAT 2014). In this timespan, Germany was the second greatest producer with an average yield of ~113 million t/year (FAOSTAT 2014).

Despite all agronomic cultivation strategies, barley is threatened by different biotic stresses. Foliar diseases reduce the assimilation during vegetative growth and during flowering. Relevant fungal pathogens causing foliar diseases on barley are *Drechslera graminea* (stripe disease), *Drechslera teres* (net blotch), *Ramularia collo-cygni* (Ramularia leaf spot), *Rhynchosporium commune* (scald), *Puccinia hordei* (leaf rust), *Puccinia striiformis* f.sp. *hordei* (stripe rust) and *Blumeria graminis* f.sp. *hordei* (powdery mildew) (reviewed in Walters et al. (2012)). The selection of an adapted variety for specific conditions is very important to avoid plant diseases and to receive high quality and quantity.

In Germany 135 powdery mildew resistant cultivars are available (54x distichous summer barley; 35x distichous winter barley; 45 multiline winter barley; 1x nude barley) (Beschreibende Sortenliste 2016, Federal Plant Variety Office). These resistances are based on 22 different resistance genes, whereof seven are not effective anymore against powdery mildew in Germany (Table 1.1). All listed non-effective powdery mildew resistance genes in Table 1.1, were activated by specific avirulence factors derived from *B. graminis* f.sp. *hordei* during infestation (Schulze-Lefert and Vogel, 2000). A loss of an efficient resistance can be explained by the plant-pathogen arms race, which is a rotated adaptation and counter-adaptation between plants and pathogens (Maor and Shirasu, 2005). Spontaneous mutations during the asexual reproduction of fungal spores enable feasible adaptations against resistant plant varieties and can lead to a lose of avirulence factors, respectively. According to the Red Queen Hypothesis, specialized plant pathogens are selected due to new applied plant resistance mechanisms (Clay et al., 2008). This reduce the species diversity in microbial communities to adapted pathogens which can parasite the crop (Clay et al., 2008). Barley can be fast reproduced and different compatible and incompatible interactions with powdery mildew are described on the histological and molecular level which make barley a feasible model crop plant for plant resistance breeding studies.

Table 1.1: Non-effective barley resistance genes against powdery mildew in Germany (adapted from Beschreibende Sortenliste 2016, Federal Plant Variety Office).

Resistance name	**Gene(s)**	**Response**
Spontaneum	*Mla6*	local hypersensitive reaction
Lyallpur	*Mla7*-(*Mlk*)	hypersensitive reaction
Arabische	*Mla12*	local hypersensitive reaction
Weihenstephan	*Mlg*-(Ml(CP))	hypersensitive reaction
Hauters	*Mlh*	cell wall apposition, local hypersensitive reaction
Borwina	*Ml*(Bw)	hypersensitive reaction
Laevigatum	*MlLa*	intermediate type of hypersensitive reaction

1.2 *Blumeria graminis* f.sp. *hordei*: The obligate biotrophic plant pathogen

The ascomycota *Blumeria graminis* f.sp. *hordei* (*Bgh*) is an obligate biotroph organism and the causal agent of barley's powdery mildew. It mainly infests leaves of young barley plants but can grow on other green organs as well. To control the disease, the main strategies are fungicide applications during the growth stages (GS) 31-39, 41-55 and 55-69, as well as the cultivation of resistant cultivars (Walters et al., 2012). Despite the use of crop protection, powdery mildew can provide barley yield losses of 3.3-11 % in Germany and up to 15 % in Europe (Oerke and Dehne, 2004; Wolfe, 1984; Kolbe, 1982; Lutze et al., 1982).

The disease infestation starts from an air born conidium on the leaf surface (Fig. 1a). Within ~30 minutes the conidium germinates and develop the primary germ tube (pre-penetration). A secondary germ tube will be grown four hours later and develop an appressorium eight hours after inoculation (hai). Underneath the appressorium, a penetration peg will be formed and the epidermal cell wall will be penetrated using high turgor pressure from the appressorium and cell wall-break down enzymes at the penetration peg tip 15 hai (Pryce et al., 1999; Francis et al., 1996).

The post-penetration stage starts with the invagination of the fungus, which develops a haustorium in the periplasmatic space 24 hai (Fig. 1b). Haustoria are the feeding organs of *Bgh* and they deliver nutrients and necessary compounds (Green et al., 2002). A missing ATPase activity in *Bgh* is predicted to cause a loss of solute retention capacity of the host cell, which enable *Bgh* to take up nutrients (Gay et al., 1987). To make necessary carbohydrates available, *Bgh* reduce the activity of Ribulose-1,5-bisphosphate carboxylase/oxygenase (RuBisCO) and further enzymes of the calvin cycle (Wright et al., 1995a; Scholes et al., 1994). Studies with powdery mildew of wheat (*B. graminis* f.sp. *tritici*) indicates that powdery mildew triggers the accumulation of acid invertases to change the source-sink relation in cereals (Wright et al., 1995b). However, with the assured nutrient income, *Bgh* is able to develop secondary mycelium on the leaf surface. Close to the area of the primary haustorium, conidiophores are grown and produce new conidia 5 days after inoculation (dai). This is the final step in the asexual reproduction of *Bgh* (Fig. 1 and 2). The disease is then macroscopically visible as white pustules and the conidiophores produce ~6000 conidia per millimeter per day (Blumer, 1967). Depending on the environmental conditions, the conidia are vital for ~30 hours and spread over by wind (Mühle, 1971).

At the end of the vegetation period, the diseased leaves become senescent and necrotic. Sexual reproduction starts due to fusion of hyphae (one ascogonium and one antheridium) forming cleistothecia with one nucleus(reviewed in Glawe (2008)). These cleistothecia are black-brown fruit bodys, which produces asci with including eight haploid ascospores. These will be released in autumn after a hot and dry summer period (Wolfe, 1984). The cleistothecium absorbs water and crack open. The ascus is protruded from the opening and bursts to release the ascospores, which will spread by the wind (Wolfe, 1984).

Despite a broad host spectrum of powdery mildew, the fungus is host specific with pathotypes (forma specialis). As an example, *B. graminis* f.sp. *tritici* can not infest other monocots (e.g. barley, rice and maiz) or dicots (e.g. sugar beet, apple and grapevine). Nevertheless, the sexual and asexual life cycle of powdery mildews are histological and cytological similar. In addition with the brief ontogenesis, powdery mildew is an obligate biotrophic model to study compatible and incompatible plant-pathogen interactions. Incompatible interactions, based on different modes of plant resistances against powdery mildew are well described for barley-*Bgh* (Schulze-Lefert and Vogel, 2000; Jørgensen, 1992a,b).

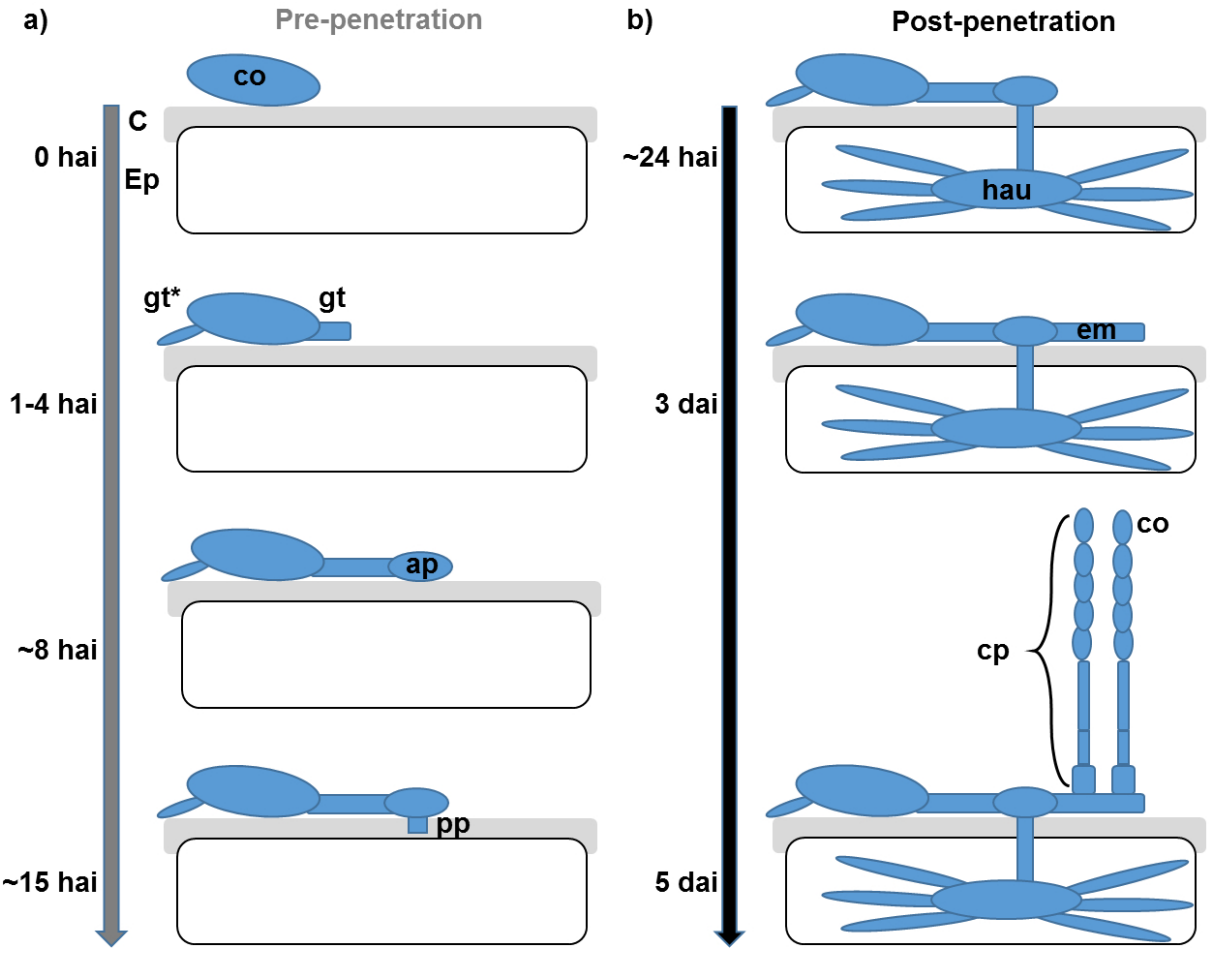

Figure 1: Asexual life cycle of *Blumeria graminis* f.sp. *hordei* (*Bgh*). Pre-penetration starts with a conidium (co) germinating on a barley leaf. An appressorium (ap) is developed by the second germination tube (gt). Via a penetration peg (pp) *Bgh* invaginates the epidermal cell (Ep) and initiate the post-penetration phase. A primary haustorium (hau) develops, which is the feeding organ of *Bgh*. Following, secondary mycelia overgrow as epiphytic mycelia (em) the leaf surface and conidiophores (cp) are grown, which produce new conidia. (C, cuticula; dai, days after inoculation; gt*, primary germ tube; hai, hours after inoculation).

1.2.1 The broad-spectrum *mlo* resistance of barley against *Blumeria graminis* f.sp. *hordei*

A broad-spectrum powdery mildew resistance of barley is based on the dysfunction of *Mildew locus o* (*Mlo*) gene (Jørgensen, 1992a). It was first described 1942 in an X-ray induced *mlo1* mutant (Mutante 66) of the German cultivar Haisa. Following investigations described further *mlo* loci, correlated with *Bgh* resistances. In the following 50 years, 150 *mlo* mutant alleles have been reported (Jørgensen, 1992a). After the second world war, 250 survived barley accession from German expeditions to Ethiopia (1937 and 1938) could be listed by (Giessen et al., 1956). Among these accessions, powdery mildew resistant lines were found and two of them could be allocated to *mlo* genes (Jørgensen and Mortensen, 1977; Nover, 1972).

The *mlo* resistance response was described as "large cell wall appositions" (papillae), due to callose formations directly below the penetration spots of *Bgh* (Skou et al., 1984) (Fig. 2). These papillae inhibit the *Bgh* penetration and have a layered structure (Chowdhury et al., 2014). The inner core consists of callose and arabinoxylan (Chowdhury et al., 2014). The outer layer mainly contain cellulose and arabinoxylan (Chowdhury et al., 2014). During the formation of the outer layer, a callose layer is disposed to prevent cell wall hydrolysis and penetration by *Bgh* (Eggert et al., 2014). As a result, *Bgh* cannot infest the epidermal cell and cannot complete its life cycle. In addition to the polysaccharides, several compounds are necessary for successful papilla development such as cell wall-bound phenolics and reactive oxygen species (ROS), but it is independent from salicylic acid, jasmonic acid and ethylene (Consonni et al., 2006; Hückelhoven et al., 1999; Röpenack et al., 1998; Kogel et al., 1995).

The *Mlo* loci have been mapped on the long arm of chromosome 4 (4H) (Büschges et al., 1997). The transcripted Mlo protein is a 60 kDa plant-specific, integral membrane protein, which works as a negative regulator of "required for *mlo*-specified resistance" (*Ror1* and *Ror2*) genes (Bhat et al., 2005; Devoto et al., 1999; Peterhänsel et al., 1997; Freialdenhoven et al., 1996). Polimerized Mlo is redistributed in the plasmamembran and accumulated underneath the fungal appressoria during *Bgh* infestation (Bhat et al., 2005). For a successfully papilla formation, *Ror2* encodes a syntaxin with high similarity to *Arabidopsis thaliana* syntaxin SYB121 (PEN1) (Collins et al., 2003). In addition, the resistance response requires "synaptosome-associated protein, molecular mass 25" (SNAP-25), which forms a SNAP receptor (SNARE) complex with Ror2 in *H. vulgare*, as well as PEN1 in *A. thaliana* (Collins et al., 2003). This complex is in addition with a glycosyl hydrolase and an ABC transporter involved in vesicle trafficking of papilla formation against powdery mildew (Stein et al., 2006; Lipka and Panstruga, 2005; Assaad et al., 2004). A current report indicates a key role of *cellulose synthase-like D2* gene (*HvCslD2*) during successful *Bgh* resistant papilla formation, respectively (Douchkov et al., 2016).

However, all different *mlo* loci and their responsible, proteomically complex and poorly understood formation of papillae, confer essentially the same barley broad-spectrum resistant phenotype against *Bgh*.

1.2.2 Race specific *Mla* resistance of barley against *Blumeria graminis* f.sp. *hordei*

After a *Bgh* recognition, the *Mla* resistance reaction is a rapidly induced necrosis of the epidermal cell at the site of infection, referred as a hypersensitive response (HR) (Hückelhoven et al., 1999)(Fig. 2). This host-cell death usually begins within 24 hai in the penetrated epidermal cell and expands sometimes into the adjacent mesophyll layer. An important signalling molecule in this cell-death program is H_2O_2 at low concentrations. High concentrations of H_2O_2 has a direct effect on pathogens (reviewed in Lamb and Dixon (1997)). During the HR, H_2O_2 is accumulated subcellulary, several hours before the cell death directly under the appressorium and fills then the entire penetrated cell (Hückelhoven et al., 1999; Thordal-Christensen et al., 1997).

R-gene *Mildew locus a* (*Mla*) loci have been all mapped on barleys chromosom 5 (1H) (Jørgensen, 1994; Wei et al., 1999). This *Bgh* race-specific immunity encodes intracellular coiled-coil (CC) domain, nucleotide-binding site (NB) and leucine-rich repeat (LRR) containing receptor proteins ((CC)-NB-LRR proteins) (reviewed in: Shen and Schulze-Lefert (2007)). NB-LRR proteins of plants are predicted to be localized to 80 % nuclear, 8.4 % chloroplastic and 8.4 % cytoplasmic (Caplan et al., 2008; Nair and Rost, 2005). These proteins act as receptors for pathogen specific compounds, described as avirulence (Avr) effectors to recognize pathogen infestations (Lu et al., 2016; Stergiopoulos and Wit, 2009; Ellis et al., 1999; Ellingboe, 1980). This imply a *Bgh* race-specific resistance, because a specific *Mla* can detect a specific avirulence factor of *Bgh* (Lu et al., 2016; Caldo et al., 2004).

The transcriptional regulation of the *Mla* based response is complex, but can be separated into two different pathways (Moscou et al., 2011; Shen et al., 2003; Hückelhoven et al., 2000). Most *Mla* triggered HRs need a signal pathway over Zn^2+ binding proteins described as "required for *Mla12*- specified disease resistance" (Rar1 and Rar2) (Hückelhoven et al., 2000). *Mla1* and -*7* are Rar independent, but provide the same HR against *Bgh* (reviewed in Schulze-Lefert and Vogel (2000)). Interestingly, yeast two-hybrid experiments indicated that the regulation of the *Mla* genes in both pathways are realized by the *Mla* CC domain interactor *MYB6*, which interact directly with the barley *WRKY1* repressor (Chang et al., 2013). Several investigations indicated that the *Mla* based resistance response is linked with different cell cycle regulators, respectively (Haltermann and Wise, 2004; Liu et al., 2004; Hubert et al., 2003; Shen et al., 2003; Takahashi et al., 2003; Azevedo et al., 2002). Currently, investigations also proposed a novel *Rar3* gene with a function in the *Rar1* dependent *Mla* pathway (Chapman et al., 2016). Nevertheless, the derived interactions during *Mla* response need further investigation to identify the whole transcriptional pathways.

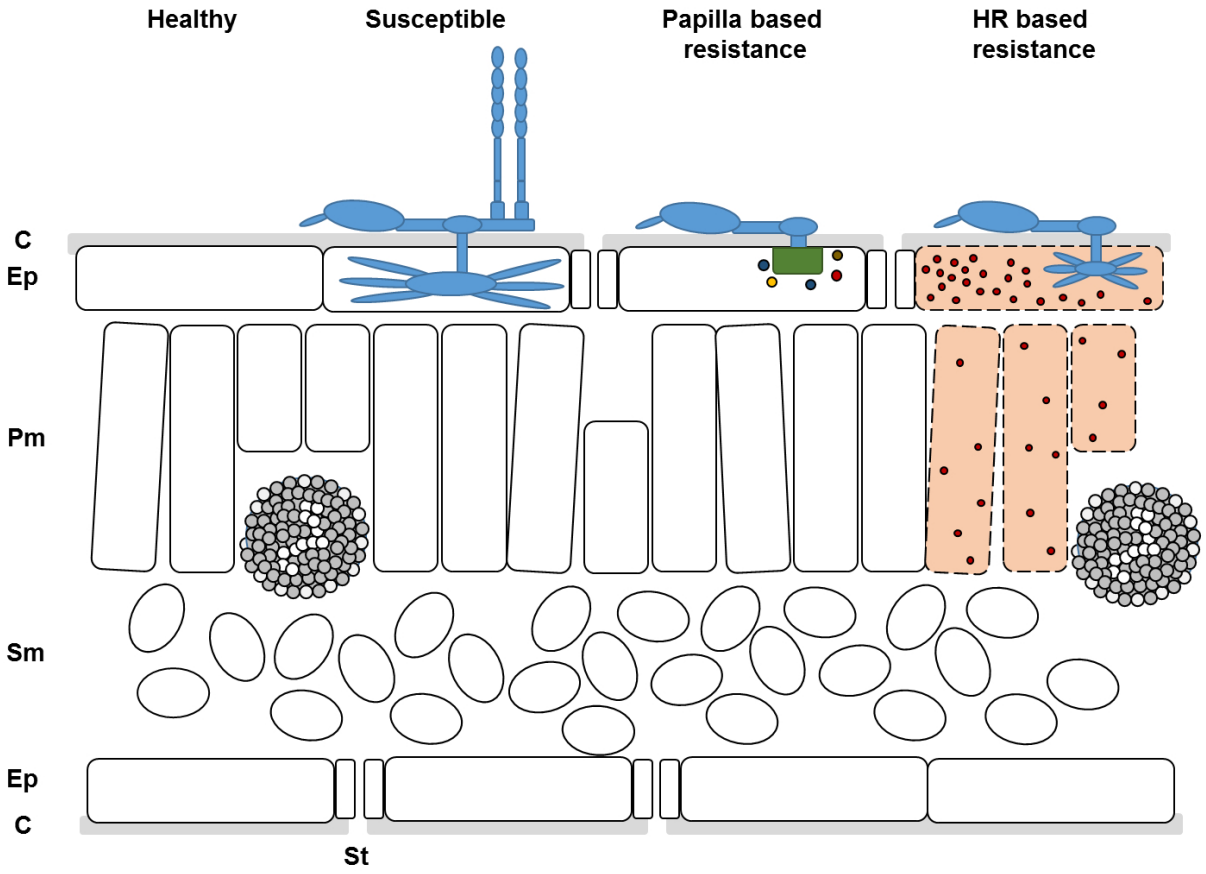

Figure 2: Schematic cross section through a barley leaf and interaction types with *Blumeria graminis* f.sp. *hordei* (*Bgh*). From left to right: healthy cell tissue, *Bgh* infested epidermal cell (Ep), papilla resistance, hypersensitive response (HR) after penetration. (C, cuticula; Pm, palisade mesophyll; Sm, spongy mesophyll; St, stomata).

1.3 Hyperspectral imaging of plants

Hyperspectral imaging (HSI) is a non-invasive method, which can provide detailed and highly resolved reflectance characteristics of plants on different scales. Therefore, HSI is a promising method to accelerate plant phenotyping processes in plant resistance breeding (reviewed in Simko et al. (2017); Mahlein (2016)).

HSI includes high resolution optical techniques similar to conventional RGB cameras with an increased spectral resolution. In addition to red, green and blue wavebands, HSI can assess narrow wavebands in the visual light from 400-700 nm (VIS), in the near-infrared from 700-1000 nm (NIR) and in the shortwave infrared from 1000-2500 nm (SWIR). The VIS reflectance of plants is mainly characterized by absorption of the leaf pigments like chlorophyll, carotenoids and xanthophylls (Gay et al., 2008). The NIR and SWIR stimulate molecular motion that induce a strong absorption or reflection by compounds that show characteristic spectral pattern (reviewed in Burns (2008)). Due to the interaction with matter, NIR reflectance of plants is mainly influenced by the leaf and cell structure (Slaton et al., 2001; Gates et al., 1965). Atmospheric water absorbs characteristic wavelength bands in the SWIR. Nevertheless, it is possible to determine plant water content using the SWIR reflected light from plants (Seelig et al., 2008). Therefore, a deeper knowledge about the interaction of light with a plant is essential for hyperspectral image analysis and interpretation of the electromagnetic spectrum (Fig. 3). One part of the radiated light on a leaf will be directly reflected by the leaf surface due to the waxy cuticula and the cell wall (Heim et al., 2015; Lillesaeter, 1982; Gates et al., 1965). Plant pigments and further compounds will absorb specific wavebands of the light (reviewed in Blackburn (2007); Curran (1989)). In addition, after internal scattering processes in the leaf, a part of the radiated light will be reflected, respectively (Gates et al., 1965). The portion of light permitting the leaf is defined as the transmission (Gates et al., 1965). HSI can determine the reflected and transmitted light (Thomas et al., 2017). Different applications have been developed e.g. the PROSPECT model (Jacquemoud and Baret, 1990), which use the reflected and transmitted light to assess leaf compounds. The application of transmittance sensing is limited in the throughput, due to the handling and complex measuring setups. Consequently, the focus of HSI is on sensing the reflected light.

In contrast to measurements of reflectance averages by hyperspectral non-imaging sensors, the spatial resolution in HSI has enabled an exact allocation of a hyperspectral pixel (Mahlein et al., 2012). Studies on HSI provide new developments in materials, detectors and software, as well as new application- and research fields for hyperspectral imaging e.g. in medicine, agriculture and food production during the last decades (reviewed in Cheng et al. (2017); Mahlein (2016); Muselimyan et al. (2016); Sendin et al. (2016)). In precision agriculture, HSI can be used for abiotic and biotic stress screening and monitoring, which will improve sustainable agriculture by site-specific and selective field management (reviewed in Simko et al. (2017); Mahlein (2016); West et al. (2003)).

The detector selection depends on the demanded wavelength range and object of interest. Silicon made charge coupled devices (CCD) and complementary metal-oxide-semiconductors (CMOS) are the most common detectors for the visible and near infrared range (reviewed in Fischer and Kakoulli (2006); Bogaerts et al. (2005)). These are implemented in different sensing types such as whisk broom scanners, push broom and full-frame cameras. The received data from HSI is a hyperspectral data cube (Fig. 4). The data cube contains the spatial information in a 2D image. Figure 4 shows in this example a powdery mildew pustule on a barley leaf with a dense pustule center and disperse border as well as healthy leaf tissue. Every pixel in this hyperspectral image contains the reflectance properties from 400-1000 nm. Various investigations characterized

the optical properties of plants and assessed the different plant compounds on their maximum absorption or reflectance of the electromagnetic spectrum (Merzlyak et al., 2008; Le Maire et al., 2004; Gamon and Surfus, 1999; Jacquemoud and Baret, 1990; Curran, 1989). This enabled a detailed characterization of the leaf efficiency and health status.

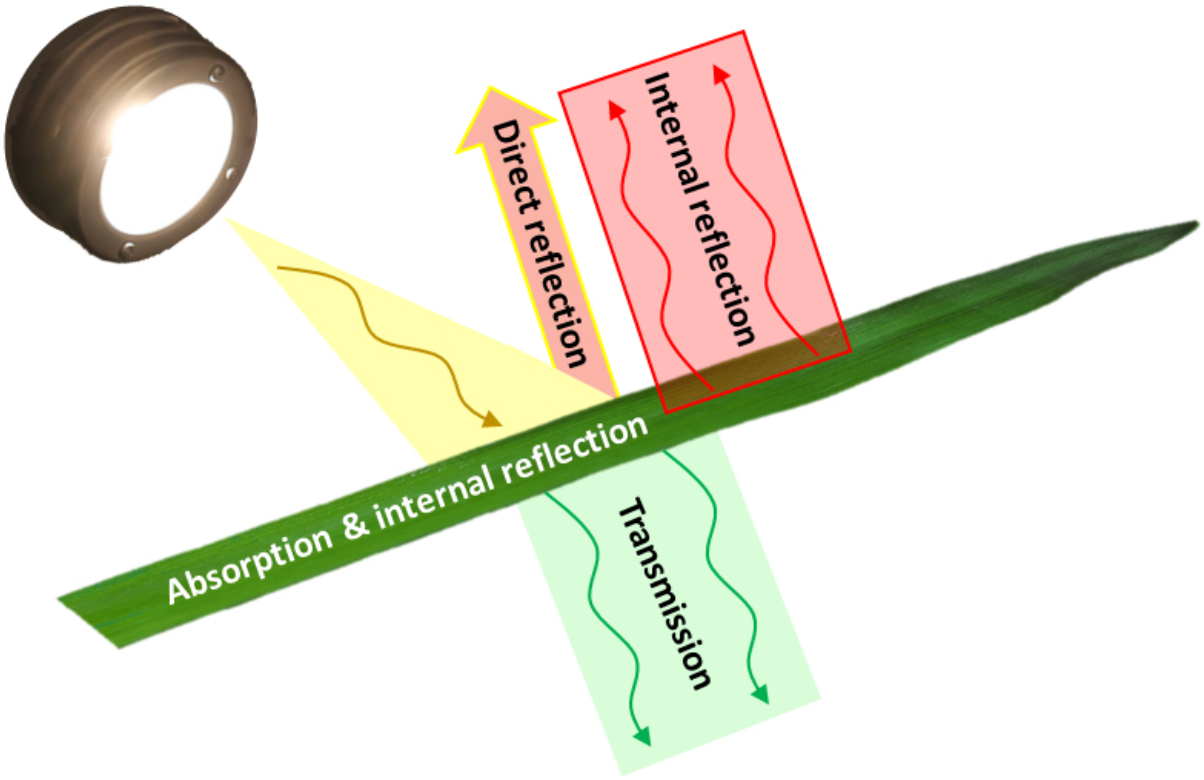

Figure 3: Route of light in a barley leaf. Incoming radiation is directly reflected by the leaf surface. One part of the light is absorbed by photo-pigments. Additional part of the light is reflected after internal scattering processes. Light, which is going through the leaf is define as the transmission.

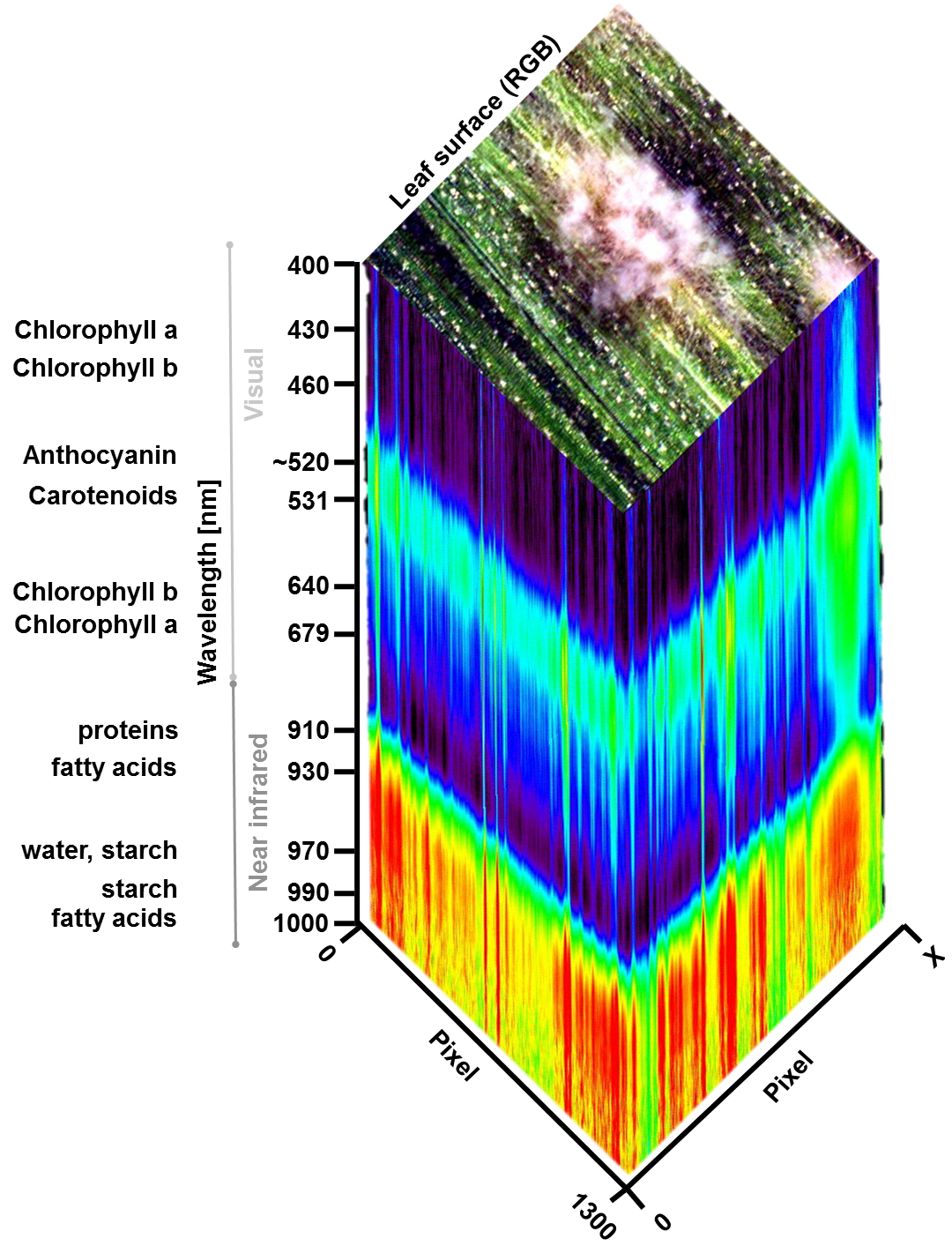

Figure 4: A hyperspectral data cube which contains the spatial information in a 2-dimensional pseudo- RGB image and the spectral reflectance properties for every pixel in this image of a powdery mildew pustule on a barley leaf. The data cube shows the visual spectral reflectance from 400-700 nm and the near infrared from 700-1000 nm. Wavelength with maximal absorption of different photo pigments and leaf compounds are indicated.

1.3.1 Status quo: Interpretations of reflectance signatures during plant - pathogen interactions

Plant pathogens influence the characteristic reflectance spectrum of healthy plants (Mahlein et al., 2010). Changes in the reflectance spectrum are specific for individual pathogens (Mahlein et al., 2012). This is based on the different ontogenesis, nutrition and structure of fungal diseases. The pathogenesis has a spatial and temporal dynamic, influencing different wavelength ranges during different pathogenesis stages (Wahabzada et al., 2015a; Mahlein et al., 2012).

A characteristic reflectance spectrum of a healthy plant show low reflectance around 450 nm and 600-700 nm, due to absorption of photo pigments (Fig. 5, 0 dai). Furthermore, it shows a green peak around 550 nm and an inflection point at 690 nm with a high reflectance in the NIR. During *Bgh* pustule development, the reflectance intensity from 560-700 nm increased and further overgrowing of the leaf surface by mycelia influence the blue range around 400-450 nm (Fig. 5). These changes are explained by pigment degradation and the ectoparasitic development of powdery mildew. As a different example, brown rust influences the visual range 550-650 nm after pustule development and provide a decreased reflectance intensity in the NIR range 700-1000 nm when the epidermis is ruptured and uredospores are released.

In addition, the absorption activities of leaf chemicals and compounds can be characterized by remote hyperspectral sensing (reviewed in Blackburn (2007); Curran (1989)). Characterization and interpretation of spectral changes during plant pathogenesis were also enabled by biochemical and histological analysis (Zhao et al., 2016; Mahlein et al., 2012; Gay et al., 2008; Gates et al., 1965). Similar to plant pathogenesis, occur incompatible interactions, due to plant resistance reactions based on transcriptional signal pathways as well as biochemical and histological changes against the fungal invader. However, type, amount and temporal development of the spectral properties during a plant resistance reaction are completely unknown. The spectral characterization of plant resistance reactions would improve plant phenotyping by HSI.

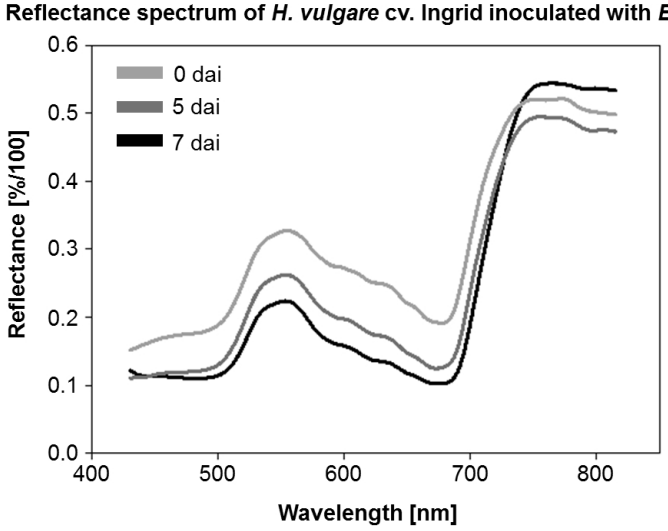

Figure 5: Spectral reflectance of barley leaves inoculated with *Blumeria graminis* f.sp. *hordei* (*Bgh*) 0, 5 and 7 days after inoculation (dai). Reflectance signature at 0 dai represents a characteristic healthy plant reflectance signature. With ongoing *Bgh* pathogenesis reflectance intensity from 400-700 nm increase and changes in NIR indicate structural changes due to the powdery mildew development.

1.3.2 Analysis of hyperspectral data: Manual and data driven approaches

HSI is promoted to provide multiple of information about different plant parameters. In fact, HSI records the electromagnetic spectrum which is reflected from plants. The optical information summarizes the plant compartments, type of leaf, the surface texture, the leaf age, et cetera. To extract relevant information on the plant status, the reflectance signature need to be analyzed and characterized. This can be done manually. But the extraction of the reflectance signatures pixel by pixel is labor intensive, because hyperspectral images can consist of millions of pixels. The selection of regions of interest (ROI) pixels is non-objective and limited if no visible changes on the spatial hyperspectral images occurred. In addition, HSI data sets of time series experiments can contain several gigabytes or even terabytes (Kersting et al., 2016).

The combination and calculation of narrow or broad wavelengths ratios were developed to establish relationships of hyperspectral reflectance signatures to plants and their biophysical variables in remote sensing (Thenkabail et al., 2000). These are described as spectral vegetation indices and result in a reduction of data dimension. The Normalized Difference Vegetation Index (NDVI) is a common spectral index to assess plant vitality by the green biomass and chlorophyll content from remote sensing (Gamon and Surfus, 1999; Jackson, 1983; Rouse et al., 1974). The NDVI is a normalized difference calculation of reflectance from the NIR and from the red range (NDVI = (NIR-Red) / (NIR+Red)) (Jackson, 1983; Rouse et al., 1974). During the last decades, further spectral vegetation indices were developed and adapted for proximal plant sensing approaches. Spectral vegetation indices for plant disease detection were developed and evaluated (Mahlein et al., 2013; Delalieux et al., 2007; Steddom et al., 2005). The development of spectral vegetation indices requires the connection of the spectrum with biochemical and biophysical properties, which depends intensive investigation and validation.

However, for the interpretation of the spectrum, signatures (e.g. Fig. 5) must be extracted from pixels of interest of the hyperspectral image. Changes or differences in the extracted spectral signatures during plant-pathogen interactions, can be assessed by calculations of the spectral differences, ratios or derivations (Mahlein et al., 2010; Pietrzykowski et al., 2006; Carter and Knapp, 2001). To improve the analysis of hyperspectral imaging data, data driven approaches can be developed and adapted.

Data driven and machine learning approaches can reduce the labor intensity and could enable the detection of attributes on hyperspectral images such as pre-detection and allocation of plant diseases (reviewed in Behmann et al. (2015)). Among machine learning approaches, unsupervised and supervised methods for classification and clustering can be applied. Unsupervised machine learning tries to find key pattern in the data without additional manual input. In contrast, supervised machine learning requires a set of labelled training data, which consists of described examples e.g. image annotations and pixel allocations. However, pre-labelled plant data are difficult to obtain for early compatible and incompatible plant-pathogen interactions. Common classification and clustering methods for crop hyperspectral image analysis are: k-means (unsupervised), IsoData (unsupervised), self-organizing maps, support vector machines, spectral angle mapper and artificial neural networks (Kersting et al., 2016; Mahlein, 2016; Behmann et al., 2015). In Fig. 6 unsupervised and supervised clustering methods, as well as NDVI were used on a multispectral image of *Bgh* infested barley plants. Pixels are classified as healthy (green) or powdery mildew infested pixels (red) by supervised methods. For unsupervised classification, different clusters were interpreted and manually labelled as healthy (green) or powdery mildew infested (red) pixel. The image visualization of the clustering results indicate that all algorithms classified several pixels different (Fig. 6e).

For interpretable unsupervised clustering, hyperspectral data sets can be preprocessed by

matrix factorization techniques e.g. simplex volume maximization (SiVM). SiVM is a linear time algorithm, which decompose a hyperspectral image into extreme data vectors (archetypes) and represent each spectral signature by a linear combination of them (Römer et al., 2012; Thurau et al., 2010). This application results in a reduction of the data dimension and enable following statistical analysis e.g. likelihood ratios, without information loss (Römer et al., 2012).

Combinations of different data driven methods can be used for interpretable classifications. Summarized by Behmann et al. (2015), a classification process to detect *Cercospora beticola* on sugar beet leaves was applied using: I) feature extraction from reflectance spectra, which is an specific property of this spectral data, II) learning a classification model on training data (e.g. a supervised method from Fig. 6) and III) applying the model on new unknown data to detect the diseased pixels.

Using machine learning approaches it was also possible to wordify the hyperspectral reflectance signature during three different barley pathogenesis, which simplified the interpretation of hyperspectral signatures of plant diseases for non-experts (Wahabzada et al., 2016). This could enable a modern art of spectral libraries, which contains spectral features of plant diseases and the plant health status, respectively. Thereby, machine learning approaches on hyperspectral images are promising applications for the detection, classification and characterization of subtle plant resistance reactions during incompatible plant-pathogen interactions. But until now, fusion of hyperspectral reflectance and 'omic data for the interpretation of spectral signatures of plants is not available.

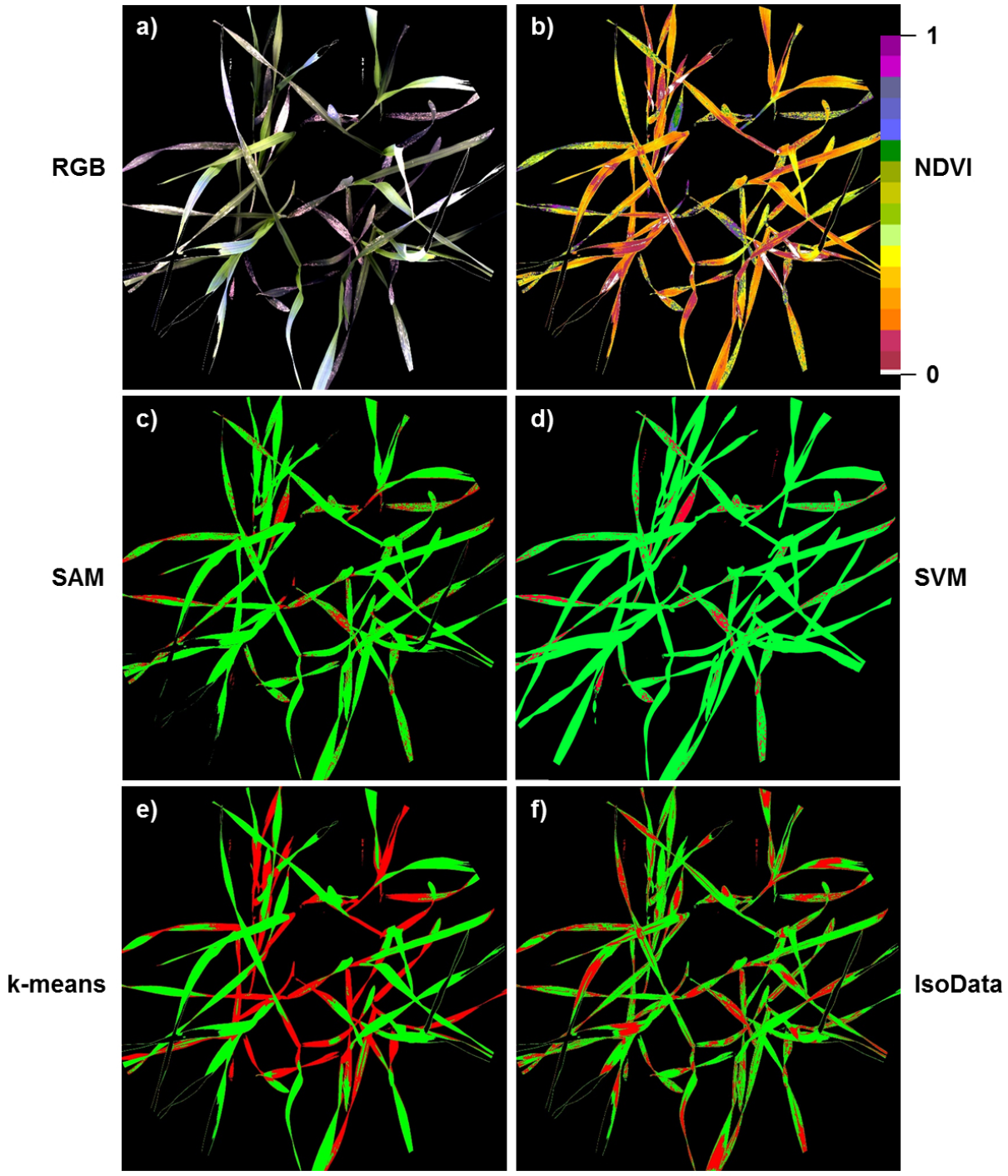

Figure 6: Different clustering and classification approaches on a multispectral image of *Blumeria graminis* f.sp. *hordei* susceptible barley plants. In addition, the NDVI was computed using reflectance intensities at 680 nm and 780 nm. Higher values indicate higher biomass/relative chlorophyll content per pixel (0-1 NDVI). Supervised classification via spectral angle mapper (SAM) and support vector machine (SVM) accurately differentiate healthy (green) from diseased (red) pixels (c, d). Unsupervised k-means clustering shows weak discrimination, in contrast to IsoData (f) clustering.

CHAPTER 2

Objectives of this thesis

The overall aim of this study was to characterize compatible and incompatible *Hordeum vulgare* - *Blumeria graminis* f.sp. *hordei* interactions using hyperspectral imaging and efficient data analysis methods. Until now changes in the spectral reflectance due to resistance reactions are unknown, because of the limited spatial resolution of hyperspectral cameras.

To realize a non-invasive analysis of barley-powdery mildew interactions, a hyperspectral imaging microscope and measuring protocol have been established. Furthermore, the biological meaning of the spectral signatures of plants have to be explained to evaluate hyperspectral imaging as a high efficient research tool in plant sciences.

Therefore, spectral changes were linked to biological processes on the cellular and molecular level. The assessed data were correlated with hyperspectral reflectance pattern of barley-powdery mildew interactions. This establish for the first time a direct link among 'omic data and hyperspectral reflectance.

The main objectives were to:

- establish a hyperspectral imaging microscope system for the assessment of subtle changes during plant-pathogen interactions (Chapter 3).
- develop a methodological protocol for hyperspectral investigation of powdery mildew pathogenesis, *mlo* based resistance and *Mla* based resistance (Chapter 3).
- discriminate barley-powdery mildew interactions using manual and data driven analysis on hyperspectral images (Chapter 3 and 4).
- determine characteristic spectral reflectance signatures of pathogenesis and resistance in space and time (Chapter 3, 4 and 5).
- link spectral changes during barley-powdery mildew interactions with biological processes (Chapter 3, 4 and 5).
- evaluate the coherency of plant reflectance and barley gene expression profiles of different interaction types (Chapter 5).

CHAPTER 3

Hyperspectral phenotyping on the microscopic scale: Towards automated characterization of plant-pathogen interactions

Chapter 3 has been published:
Kuska, Matheus[1], Wahabzada, Mirwaes[1], Leucker, Marlene[1], Dehne, Heinz-Wilhelm[1], Kersting, Kristian[2], Oerke, Erich-Christian[1], Steiner, Ulrike[1], and Mahlein, Anne-Katrin[1] 2015. Hyperspectral phenotyping on the microscopic scale: Towards automated characterization of plant-pathogen interactions. *Plant Methods*, 11:28.

[1]Institute for Crop Science and Resource Conservation (INRES) - Phytomedicine, University of Bonn, Nussallee 9, 53115 Bonn, Germany.
[2]Department of Computer Science, TU Dortmund, Otto-Hahn-Str. 14, 44227 Dortmund, Germany.

Changes made in the thesis chapter compared to the original publication. Additional text to the original research publication is underlined:
The Result and Discussion part of Kuska et al., 2015 is separated and rearranged into 3.4 Results and 3.5 Discussion. The Conclusion part and Figure 8 of the original research publication are not included in this dissertation. Table 3.1 is not included in the original research paper. Table 3.2 in Results 3.4 is originally a supplementary file of the publication Kuska et al., 2017 Phytopathology, 107:1388-1398 which is used as chapter 4 in this dissertation. This publication is only used in the dissertation of Matheus Kuska and in no other dissertation.

Authors' contributions
Matheus Kuska, M. Wahabzada, H-W. Dehne, K. Kersting, E-C. Oerke, U. Steiner, and A-K. Mahlein designed the study, interpreted the data and drafted the manuscript. M. Leucker, U. Steiner, E-C. Oerke and A-K. Mahlein constructed the hyperspectral microscope. **Matheus Kuska** and A-K. Mahlein developed the measuring procedure and the assessment of hyperspectral images of detached barley leaves on phyto agar. **Matheus Kuska** carried out all hyperspectral measurements, manual and statistical analysis. M. Wahabzada and K. Kersting developed and applied data mining methods for the automated spectral data analysis.

3.1 Abstract

The detection and characterization of resistance reactions of crop plants against fungal pathogens are essential to select resistant genotypes. In breeding practice phenotyping of plant genotypes is realized by time consuming and expensive visual rating. In this context hyperspectral imaging (HSI) is a promising non-invasive sensor technique in order to accelerate and to automate classical phenotyping methods.

A hyperspectral microscope was established to determine spectral changes on the leaf and cellular level of barley (*Hordeum vulgare* L.) during resistance reactions against powdery mildew (*Blumeria graminis* f.sp. *hordei*) (*Bgh*). Experiments were conducted with near isogenic barley lines of cv. Ingrid, including the susceptible wild type (WT), mildew locus a 12 (*Mla12*) and the resistant mildew locus o 3 (*mlo3* based resistance), respectively. The reflection of inoculated and non-inoculated leaves was recorded daily with a hyperspectral linescanner in the visual (400-700 nm) and near infrared (700-1000 nm) range 3 to 14 dai.

Data analysis showed no significant differences in spectral signatures between non-inoculated genotypes. Barley leaves of the near-isogenic genotypes, inoculated with *B. graminis* f.sp. *hordei* differed in the spectral reflectance over time, respectively. The susceptible genotypes (WT and *Mla12*) showed an increase in reflectance in the visible range according to symptom development. However, the spectral signature of the resistant *mlo3*-genotype did not show significant changes over the experimental period. In addition, a recent data driven approach for automated discovery of disease specific signatures, which is based on a new representation of the data using Simplex Volume Maximization (SiVM) was applied. The automated approach revealed only in a fraction of time similar results comparing to the time and labor intensive manually assessed hyperspectral signatures. The new representation determined by SiVM was also used to generate intuitive and easily interpretable summaries, e.g. fingerprints or traces of hyperspectral dynamics of the different barley-*Bgh* interactions.

With this HSI based and data driven phenotyping approach an evaluation of host-pathogen interactions over time and a discrimination of barley genotypes differing in susceptibility to powdery mildew is possible.

3.2 Introduction

In agricultural production the demands on efficient crop plants are manifold. Improved quantitative and qualitative plant traits are desired, along with enhanced stress resistance, especially against plant pathogens. The development of resistant cultivars is a challenging task in plant breeding. Fungal plant pathogens affect almost all relevant crops in different stages of their development and impair the yield and product quality. In barley production powdery mildew is one of the main damaging diseases in Europe and other temperate regions (Lyngkjaer et al., 2000). The disease is caused by the biotroph ascomycete *Blumeria graminis* f.sp. *hordei* (*Bgh*) and is spread during the vegetation period by wind with conidiospores. *Bgh* is able to colonize barley plants within 24 hours after the first contact. A haustorium -the feeding organ of *Bgh*- develops within penetrated epidermal cells, which remain vital. The new epiphytic mycelium grows over the leaf surface to penetrate other epidermal cells and develops new haustoria. Finally, *Bgh* produces conidiophores bearing new conidia. This asexual life cycle is completed in approximately five days and is repeated by multiple generations per season. The application of fungicides and the cultivation of resistant barley varieties are the main methods to control powdery mildew on barley (Walters et al., 2012). Unfortunately, the farmers face fungicide

resistances developed by *Bgh* (Ma and Michailides, 2005). This emphasises the importance of resistant barley genotypes generated in breeding programs.

A well-known resistance mechanism of barley against *Bgh* is the non-race specific mildew locus o (*mlo*) based resistance (Jørgensen, 1992a). In all *mlo* mutants, *Bgh* cannot penetrate the epidermal cell because a cell wall apposition (papilla) is developed under the penetration point (Jørgensen and Mortensen, 1977). This possesses a high electron density (Hippe-Sanwald et al., 1992). The basic components of this cell wall apposition are a complex of lignin, cellulose, callose, peroxidases, phenols, proteins and further cell-wall materials (Schulze-Lefert and Vogel, 2000). The mildew locus a (*Mla*) gene based resistance is an another resistance reaction of barley against *Bgh* and is associated with a hypersensitive reaction of epidermal cells attacked by *Bgh* (Schulze-Lefert and Vogel, 2000; Hückelhoven et al., 1999; Jørgensen, 1994). These resistance properties are used in plant breeding programs to improve the resistance of barley plants to powdery mildew. However, one main drawback of recent breeding programs is their time consuming and labor intensive nature.

The traditional breeding procedure of common crop plants still takes 7 to 17 years and requires a high amount of plant material and human effort on the way to a desired cultivar (Shimelis and Laing, 2012). In this complex breeding process, manifold steps in different environments - under controlled and under field conditions - at different plant levels - from single organs to the canopy - are executed. Hereby the selection process of predominant genotypes and relevant crop traits by genotyping and phenotyping methods is crucial and determines the time span and the success of the breeding process. In recent years the genotyping of plants has been significantly accelerated by advances in molecular profiling and sequencing technologies (reviewed in Fiorani and Schurr (2013)). Marker-assisted selection, bi-parental recombinant inbred lines or the increasing number of completely sequenced species in genomic databases provides solutions to current breeding challenges (reviewed in Furbank and Tester (2011)). To bridge the gap from genomic characterization to plant function and agricultural traits, the expression of the genome in a given environment has to be tested carefully. This step is defined as the phenotyping process. Several authors have addressed the labor-intensive and costly nature of conventional phenotyping processes as the limiting and time-consuming factor in plant breeding. This challenge has been identified as the phenotyping bottleneck (reviewed in Cobb et al. (2013); Fiorani and Schurr (2013); Furbank and Tester (2011)).

Innovative technologies, e.g. optical and non-invasive sensors, have been characterized as new phenotyping methods with potential to overcome this bottleneck and to improve the breeding process. Various optical imaging methods using e.g. RGB (Hartmann et al., 2011), 3D (Paulus et al., 2014), fluorescence (Chaerle et al., 2007), thermography (Oerke et al., 2006) and HSI (Ustin and Gamon, 2010) sensors are able to characterize different plant parameters and could potentially be implemented in automated, high-throughput phenotyping pipelines. Among these methods, hyperspectral imaging (HSI) is one of the most promising techniques to assess functional plant traits (Mahlein et al., 2012; Rascher et al., 2011; Ustin and Gamon, 2010). Using HSI, the spectral characteristics of plants can be visualised non-invasively over time and on different scales. The sensitivity of sensors enable a high spectral and spatial resolution and the reflectance per pixel can be analyzed in narrow wavelengths. Characteristic spectral signatures provide information about the physiological status of plants and for plant breeding on the reaction of different genotypes to biotic or abiotic stress factors (reviewed in Behmann et al. (2015)). Leaf pigments, like chlorophylls and carotenoids are the main factors influencing the spectral information in the visual range (VIS, 400-700 nm) (Curran, 1989). The near infrared range (NIR, 700-1000 nm) is mainly affected by scattering processes in the spongy mesophyll,

and additionally by absorptions due to proteins, fatty acids, starch, water and cellulose with different specific absorption wavelengths. The leaf water content, including further chemical compounds, can be derived from the short wave infrared range (SWIR, 1000-2500 nm).

Various researchers have demonstrated that plant diseases and processes during pathogenesis can be detected by hyperspectral sensors (Mahlein et al., 2010; Delalieux et al., 2007; West et al., 2003). Plants diseased by fungal pathogens could be distinguished from healthy plants at different stages of the pathogenesis and at different disease severities. Since first interaction sites and primary symptoms of fungal plant diseases are in the range of sub-millimeters, highly sensitive sensor systems and powerful subsequent data analysis routines are required for a reliable evaluation of plants under biotic stress. Few researchers postulate that early modifications of the cellular leaf structure occur due to fungal toxins or plant resistance reactions and that these subtle changes are detectable via HSI (**?**Rumpf et al., 2010).They focused on small-scale studies with HSI or on the detection and identification of plant diseases before visible symptoms appear. Based on these insights the development of a HSI routine to estimate the susceptibility of plants and to characterize defence mechanisms against fungal pathogens is a desirable task. However, it requires methodological adaptions and technical advances to exploit the potential of hyperspectral sensors for the implementation in resistance screenings.

The hypothesis of this chapter is that subtle processes during compatible and incompatible plant-pathogen interactions have an effect on optical properties of plants. It is expected that specific regions of the electromagnetic spectrum are influenced depending on the type of interaction. The detection of these changes demands specific sensor setups with a high spatial and spectral resolution combined with sophisticated, data analysis methods. To proof this hypothesis a HSI microscope, a measuring protocol for detached barley leaves and an automated data analysis approach were established. This approach can be used in resistance screening for the differentiation of barley genotypes and for a characterization of their interaction with *Bgh*, the causal agent of powdery mildew. As an application model susceptible and resistant genotypes with different, well known genetic backgrounds were monitored visually and by hyperspectral imaging in time-series experiments at small-scale level. To uncover the full information from high-dimensional HSI data, characteristic spectra were extracted both manually and using data mining techniques. A qualitative and automated analysis of reflectance data was realized using a data driven approach based on the matrix factorisation technique Simplex Volume Maximisation (SiVM) (Thurau et al., 2012). With this methodological approach, (I) processes during pathogenesis on the different genotypes could be characterized, (II) stages of pathogenesis were automatically visualized and (III) spectral dynamics were evaluated over time.

3.3 Materials and Methods

3.3.1 Plant cultivation and inoculation of *Blumeria graminis* f.sp. *hordei*

Near-isogenic barley (*Hordeum vulgare* L.) lines cv. Ingrid wild type (WT), Ingrid I10 containing resistant mildew locus a 12 (*Mla12*) (Shen et al., 2003) and Ingrid M.C. 20 containing dysfunction in mildew locus o 3 (*mlo3*) (Hinze et al., 1991) were grown in a commercial substrate (Klasmann-Deilmann GmbH, Germany) in plastic pots (10x10x20 cm) in a greenhouse at 23/20 °C (day/night), 60% relative humidity (RH) and a photoperiod of 16 h. One week after sowing, the primary leaves (with an approx. length of 10 cm) were detached and transferred on to aseptic phyto agar (Duchefa Biochemie, Haarlem, Netherlands) containing 0.34 mM benzimidazole.

For each genotype, three leaves were inoculated with fresh spores of *Blumeria graminis* f.sp.

hordei isolate K1 (*Bgh*-K1) (Hacquard et al., 2013), and four leaves were kept untreated as healthy control. *Bgh*-K1 is virulent to cv. Ingrid WT and Ingrid I10 (Shen et al., 2003) and avirulent to Ingrid M.C. 20 (Hinze et al., 1991). Fresh conidia were obtained from heavily infected barley cv. Leibniz (KWS, Einbeck, Germnay). Twenty-four hours before plant inoculation, the conidia of *Bgh*-K1 infested plants were shaken off and discarded in order to assure homogenous and vital conidia for the inoculation. Conidia of a recently formed powdery mildew pustule (7 dai) were transferred to the prepared leaves on phyto agar using an aseptic inoculation loop. The agar plates were sealed with Parafilm M® (Bemis, Oshkosh, USA) and incubated in a controlled environment at 19 °C, 1100 $m^{-2} \cdot cd$ illuminance and a photoperiod of 16 h per day.

3.3.2 Hyperspectral time series imaging and data preprocessing

Spectral reflectance was measured with an hyperspectral imaging line scanner (spectral camera PFD V10E, Specim, Oulu, Finland) mounted on a stereo microscope foreoptic (Z6 APO, Leica, Wetzlar, Germany) with a magnification up to 7.3x. The line scanning spectrograph has a spectral range from 400-1000 nm and a spectral resolution of up to 2.73 nm. The maximum image size of the 30 µm sensor slot results in 1300 pixels per line with a sensor pixel size of 0.0074 mm. Depending on this measurement setup and the magnification, a maximum spatial resolution of 7.5 µm per pixel was obtained.

For image recording the leaf samples were placed nadir on a XY-moving stage (H105/2/0 ProScan Upright Stage, Prior Scientific, Jena, Germany), controlled with a joystick and Oasis software (Oasis Controller, Objective Imaging Ltd., Cambridge, England). The samples were illuminated by two linear light emitters (Dual line Lightlines, Schott, Mainz, Germany) with a vertical orientation of 30° and a distance of 20 cm to the sample besides the foreoptic. As a light source a 150 watt halogen tungsten lamp connected to the line lights via a non-absorbing fiber was used (DCR® Light Source EKE, Polytec, Waldbronn, Germany). Hyperspectral measurements were performed in a dark room after 60 minutes pre-heating of the light source in order to realize constant and reproducible illumination conditions. The software SpectralCube (Spectral Imaging Ltd., Oulu, Finland) was used for controlling the HSI line scanner and for acquiring the hyperspectral images. Images on the leaf surface level were taken with spectral binning 1 and spatial binning 1. Frame rate and exposure time were adjusted to the object. The reflection in the range from 400-1000 nm was measured daily 3 to 14 dai with a magnification of 7.3x. Additionally, RGB images of each leaf were taken daily with a digital camera (EOS 6D, Canon, Tokio, Japan) and a 100 mm object lens (EF Lens Ultrasonic EF 100 mm 1:2.8 L Macro IS USM, Canon, Tokio, Japan).

3.3.3 Pre-processing of hyperspectral images

Because reflection data was noisy at the extremes, only data values between 420-830 nm were analyzed. For image normalization four hyperspectral images per sample were taken. First, a white reference bar (SphereOptics GmbH, Uhldingen-Mühlhofen, Germany) was recorded (W), followed the dark current image (B_1). Subsequently, the leaf sample (I_0) and a corresponding dark current image (B_2) were recorded. Calculation of reflectance was according to Formula 1 using the software ENVI 5.1 + IDL 8.3 (ITT Visual Information Solutions, Boulder, USA). Furthermore, the spectral signals are smoothed by employing the Savitzky-Golay filter (Savitzky and Golay, 1964). Parameters for the smoothing process were 12 supporting points to the left and right, respectively, and a third degree polynomial. The pre-processed images were used for further analysis using ENVI 5.1 + IDL 8.3 and data mining methods.

$$I = \frac{I_0 - B_2}{W - B_1}$$

Formula 1: Normalization of hyperspectral images to a white reference (100 % reflectance) and dark current images (sensor noise).

3.3.4 Spectral signature extraction, analysis and characterization

In a first step, spectral signatures of pixels from healthy and diseased regions were extracted manually. Therefore ≥ 300 pixel were extracted daily from the same area by an ellipsoid region of interest from each non-inoculated leaf. When powdery mildew pustules became visible the symptomatic area was extracted as region of interest. Thus, the amount of pixels extracted increased depending on symptom development.

3.3.5 Data driven approach for fast analysis of hyperspectral dynamics

Following the method of Wahabzada et al. (2015a), a data driven approach was applied, allowing an automated analysis of hyperspectral data. Simplex Volume Maximization (SiVM) applied for fast and interpretable factorization (Thurau et al., 2012), used a Python™ implementation based on the Python™ Matrix Factorization Module (PyMF) library (http://pymf.googlecode.com). SiVM represents the hyperspectral data in terms of only few extreme components determined across all images considered. The resulting coefficients are proportions describing the relative contribution of each of the extremes to a hyperspectral signature. The columns in the coefficient matrix can be considered as data points from a simplex spanned by the extreme basis vectors. This allows statistical analysis on massive scales (Wahabzada et al., 2015a). Since the components are real extreme signatures, they are easily interpretable and uncover the variations existing in the data (Fig. 7). The signatures within all hyperspectral images were then represented as combination of these extreme components. Given the new representation opens door to statistical data mining on a massive scale. That is, the representation can be used to discover disease specific signatures within diseased leaves. This procedure avoids the risk of losing valuable information when selecting disease specific signatures manually at some diseased spots only.

Following Wahabzada et al. (2015a), the differences for each particular signature was computed using likelihood ratios LLR(s) together with the distributions computed using simplex representation of the data. That is, the LLR(s) for a signature s of a diseased leaf at day d were computed in terms of the distributions of non-inoculated healthy leaf at day d and of a subsequent day r (r=d+2 was used) of the diseased leaf as the reference. For the later days (d $\geq$ 8 dai) the distribution determined from the image 10 dai was used for the diseased leaf as reference, because it was assumed to observe the most diseased specific hyperspectral characteristics at this day. For the binary maps of the location of disease spots a Gaussian filter was placed on the computed differences LLR(s) and set all positive values to 1 and 0 otherwise.

The leaf traces were computed by applying the Dirichlet aggregation regression on the representation determined by SiVM (Kersting et al., 2012a). For interpolated mean signatures a 2D map was computed by the followed simplex traces approach (Kersting et al., 2012b). This uncovers hyperspectral dynamics of diseased and non-inoculated (healthy) leaves of the different genotypes over time.

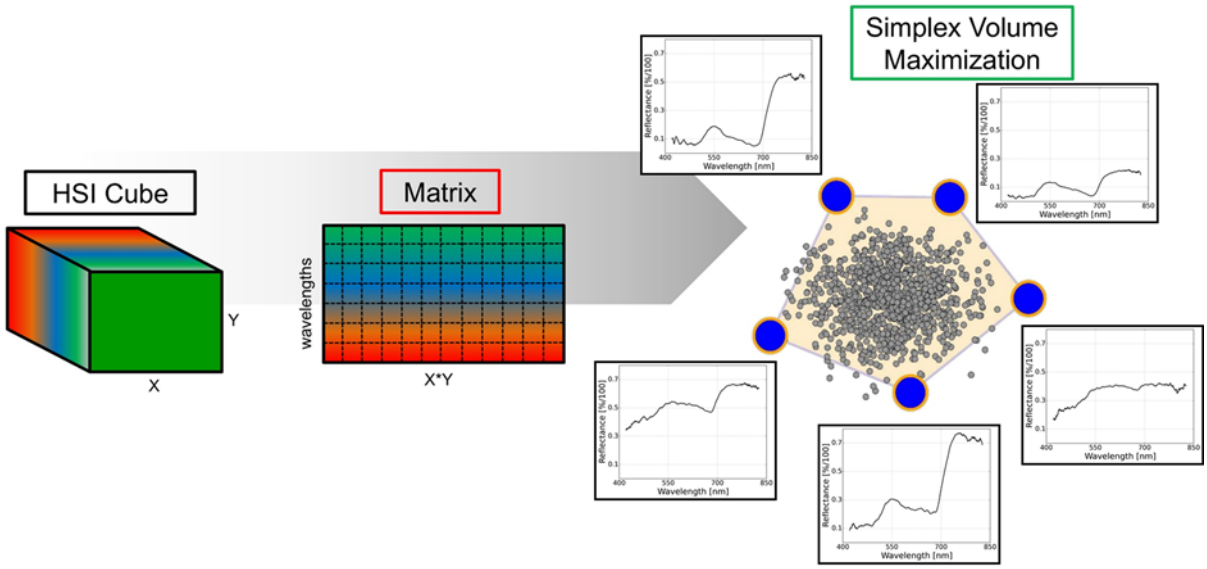

Figure 7: Interpretable matrix factorization for hyperspectral images. Each hyperspectral data cube is transformed into a dense matrix. Then, extreme components/signatures on all matrices are computed, using Simplex Volume Maximization. The final step includes the computation of the new representation of all signatures in a space spanned by the extremes.

3.4 Results

The pathogenesis of powdery mildew and early interactions on different barley genotypes was characterized on the leaf and tissue level using the novel hyperspectral microscope (Fig. 8). A high spatial resolution of a pixel size as low as 7.5 µm allowed the detection of subtle processes (table 3.1). This results in a plain of 56 µm^2 per pixel. The amount of pixels covering structures of interest in HSI data are mentioned in (table 3.2).

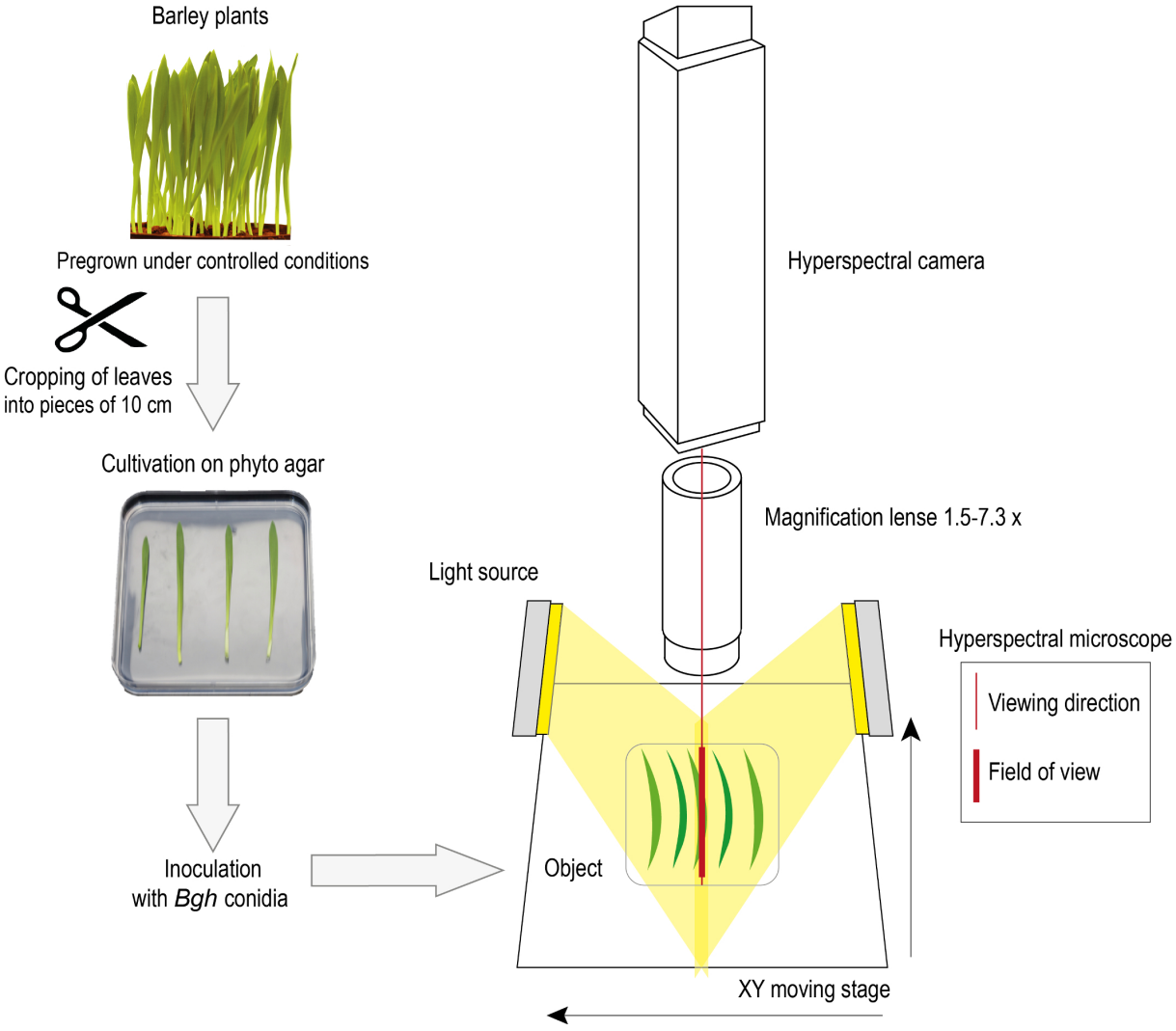

Figure 8: Hyperspectral imaging microscope setup for small-scale image analysis. The spectral reflectance of detached barley leaves on phyto agar was measured with a hyperspectral camera, which was mounted on a magnification lens to enable a magnification up to 7.3x. Two linear light emitters with a vertical orientation of 30° illuminated the samples in a distance of 20 cm. The samples were moveable due to a XY moving stage. A spectral resolution of up to 2.73 nm and a maximum spatial resolution of 7.5 µm per pixel was obtained. The field of view ranged from 4.1 to 0.95 cm, dependent on the magnification.

Table 3.1: Magnification parameters of the novel hyperspectral microscope.

Magnification	Field of vision	Pixel size
1.15x	4.1 cm	47.62 µm
1.6x	3.4 cm	33.33 µm
2.0x	2.9 cm	26.32 µm
2.5x	2.5 cm	21.28 µm
3.2x	2.0 cm	16.67 µm
4.0x	1.6 cm	12.20 µm
5.0x	1.35 cm	10.64 µm
6.5x	1.05 cm	8.26 µm
7.3x	0.95 cm	7.5 µm

Table 3.2: Size of barley epidermal cells, papillae aggregations as well as papillae and *Blumeria graminis* f.sp. *hordei* conidia and amount of pixels covering these structures in HSI data, assessed with the highest magnification, resulting in a pixel size of 7.5 µm (~56µm^2).

Object	Dimension (µm)	Plain (µm^2)	Associated pixels
epidermal cells	150-280 x 25	3750-7000	67-125
papillae aggregations	10-30 x π	79-707	1.4-12.6
papillae	10-15 x π	79-177	1.4-3.2
conidia	20-33 x 10	200-330	3.6-5.0

3.4.1 Phenotypic development of healthy and inoculated barley leaves

The phenotypes of detached, healthy and *Bgh* inoculated leaves of barley genotypes WT, *Mla12* and *mlo3* were assessed visually on phyto agar (Fig. 9). *Mla12* leaves were included as an additional susceptible genotype to analyze differences during the pathogenesis between near-isogenic lines.

Non-inoculated leaves of the three genotypes did not show any visible symptoms during the first 6 dai. Symptoms of senescence occurred 6 dai on healthy *mlo3* leaves, indicated by yellowing of the leaves. The WT and *Mla12* started to became chlorotic 10 dai. This senescence process developed further until 14 dai. The relative long life span and vitality of detached leaves in this investigations indicated consistent conditions for HSI of the plant system in a controlled environment for a period of 14 days.

Bgh inoculated leaves showed no visible symptoms during the first 5 dai. Characteristic powdery mildew pustules occurred 6 dai on the susceptible WT and the near-isogenic *Mla12* line. On *Mla12* leaves the pustules were distributed homogeneously on the leaf surface compared to clustered pustules on WT leaves. Pustules expanded and covered nearly the complete leaf surface of the susceptible WT and *Mla12* leaves 10 dai. Furthermore, the leaves became light-green and chlorotic in areas without powdery mildew pustules 10 dai. Necrotic tissue occurred with the exception of powdery mildew dominated leaf areas, which showed light-green to yellow discoloration 14 dai. The resistant *mlo3* leaves did not show any powdery mildew symptoms during the experiment. The leaves were healthy and green with a delayed senescence. First signs of senescence of inoculated *mlo3* leaves appeared only 14 dai.

Figure 9: Phenotypes of detached barley leaves non-inoculated (healthy) and inoculated with *Blumeria graminis* f.sp. *hordei* (*Bgh*) of near-isogenic lines cv. Ingrid (WT, *Mla12* and *mlo3*) 0, 3, 6, 10 and 14 dai on phyto agar. Non-inoculated leaves of the genotypes showed natural senescence over the experimental period. First characteristic powdery mildew pustules became visible 6 dai on inoculated leaves of the susceptible WT and the near-isogenic line *Mla12*. The resistant near-isogenic *mlo3* leaves did not show any powdery mildew symptoms. Senescence of inoculated near-isogenic *mlo3* leaves was delayed until 14 dai. Images were taken with a digital camera (EOS 6D, Canon, Tokio, Japan) and a 100 mm object lens (EF Lens Ultrasonic EF 100 mm 1:2.8 L Macro IS USM, Canon, Tokio, Japan).

3.4.2 Spectral similarity of non-inoculated near-isogenic barley lines over time

Detached non-inoculated (healthy) and inoculated leaves of the near-isogenic lines cv. Ingrid WT, *Mla12* and *mlo3* were measured daily 3 to 14 dai in order to assess changes in the spectral signatures. Healthy leaves of the different near-isogenic lines exhibited a typical spectral pattern of healthy plants with low reflectance from 400-700 nm, a characteristic green peak at 500-570 nm, a steep reflectance increase at the red edge inflection point and a high reflectance plateau in the NIR 3 days after detachment (Fig. 10a). This pattern slightly changed over time but other ranges of the spectrum were not affected. However, differences in the development of individual leaves were reflected by the relative standard deviation (RSD) of 0.6-6.8 % over time and measured wavelength range. The highest RSD was calculated in the NIR range for WT 10 dai, for *Mla12* 13 dai, and for *mlo3* 13 dai.

3.4.3 Spectral signatures of near-isogenic barley lines during powdery mildew pathogenesis

The susceptible near-isogenic genotypes cv. Ingrid WT and *Mla12* and the *Bgh* isolate K1 were used to evaluate the progress of powdery mildew pathogenesis and to identify spectral fingerprints of the barley-*Bgh* system.

Inoculated WT leaves showed minor differences to healthy WT leaves 3 dai (Fig. 10b). The reflectance of inoculated WT leaves increased between 534-563 nm. An overall increase of reflectance in the entire range was observed already 4 dai and the shift to higher reflectance, continued the following days. Reflectance in the NIR from 743-830 nm decreased 5 dai. This NIR response turned to an increased reflectance again 6 dai, when first powdery mildew pustules occurred on the WT leaf surface. Subsequently, the reflectance in the NIR from 743-830 nm decreased stepwise until 14 dai. Symptoms were accompanied by significant reflectance changes over the full range. This gradual increase of reflectance was prominent from 400-680 nm and from 700-740 nm. The reflectance in the VIS increased daily according to the growth of powdery mildew mycelium until 9 dai. The course of the spectral pattern changed from 10 to 14 dai and the reflectance from 420-500 nm decreased again due to the occurrence of first necrosis and tissue collapse below powdery mildew pustules. Increased green reflectance was in accordance with senescence chloroses, associated to a reduction and breakdown of chlorophyll (Fig. 9). The reflectance spectrum 14 dai represented a necrotic leaf tissue covered with powdery mildew. The RSD among the inoculated WT leaves was 1-14.7 % over time and wavelengths. The highest RSD was calculated 14 dai over the full spectral range.

The hyperspectral reflectance pattern of *Bgh* pathogenesis described for WT was also monitored for the near-isogenic line *Mla12* (Fig. 10d). The appearance of first tiny powdery mildew pustules 4 dai was associated to first increase of leaf reflectance between 420-680 nm. In contrast to inoculated WT leaves, reflectance did not decrease in the blue range 10 dai and later. Reflectance of *Mla12* leaves in the range 500-742 nm increased day by day in contrast to the WT leaves. This effect can be explained by a faster development of *Bgh* on *Mla12* leaves compared to WT leaves. In addition, the diseased area and the density of mycelium and conidia on the leaves was higher than on the WT leaves. Similar to inoculated WT leaves, reflectance increased stepwise until 14 dai, except from 743-830 nm the reflectance did not change significantly over time. Interestingly, the reflectance between 743-830 nm 5 dai was lower compared to the other days. This phenomenon was also observed for inoculated WT leaves 5 dai. The RSD of reflectance among inoculated *Mla12* leaves was 3-14 % over time and wavelengths. The highest RSD was calculated between 500-680 nm 14 dai. Also the range 420-500 nm showed high RSD

among the inoculated *Mla12* leaves from 6 dai until 14 dai.

3.4.4 *mlo3* inoculated leaves showed no powdery mildew infestation over time

The spectral reflectance of *Bgh* inoculated *mlo3* leaves (Fig. 10f), differed from that of inoculated, susceptible WT and *Mla12* leaves. Resistant *mlo3* leaves showed a spectral pattern similar to non-inoculated leaves of all genotypes until 9 dai. No visible symptoms were assessed on the inoculated *mlo3* leaves. Interestingly, inoculated *mlo3* leaves showed no effects of natural senescence on reflectance until 13 dai. The reflectance was constant over time with low RSD of 5-7 % in the full spectral range. A first increase in reflectance was observed from 540-680 nm 13 dai when also first symptoms of senescence occurred.

3.4.5 Automated analysis of hyperspectral images for plant phenotyping

The effective analysis and interpretation of HSI data are limiting factors for an implementation into plant phenotyping. The 3-dimensional complexity of HSI data requires high input of human intervention and labelling of disease specific image pixels. Automated analysis pipelines are required to optimize the use of HSI for phenotyping or precision agriculture. Within this study an automated analysis cascade using Simplex Volume Maximization was adopted (Fig. 7).

Reflectance spectra of inoculated WT leaves assessed by this automatic approach showed patterns similar to the manually assessed reflectance spectra (Fig. 11a, c). Differences between manually and automatically extracted reflectance were calculated to highlight the similarity of the results (Fig. 11b, d). According to both methods of data analysis, no differences between healthy and diseased leaves were observed 3 dai. An increase of reflectance between 420 and 742 nm was detected in the automated approach already 4 dai. Further differences were detected in the NIR range 4 and 5 dai (Fig. 11b). The next days showed a spectral trend similar to the manual analysis. The differences between automated and manually assessed reflectance values were low and reached only -0.04 [%/100] at 680 nm. Based on the automatically assessed reflectance spectra a binary map system of *Bgh* inoculated susceptible leaves was established (Fig. 12). The binary maps visualize *Bgh* diseased leaf tissue over time. Black pixels indicate healthy leaf tissue, while white pixels indicate sites with powdery mildew. This allows the observation of disease development on susceptible plant genotypes with rapid visual identification of relevant pixels. Powdery mildew symptoms were absent on RGB images 3 dai. The corresponding binary map was almost completely black, however some white pixels appeared before visible symptoms occurred. First tiny powdery mildew pustules became visible on RGB images 4 dai and were accurately detected in the binary map. Senescent leaf tissue was not included in the binary maps due to the consideration of natural senescence of detached, healthy leaves.

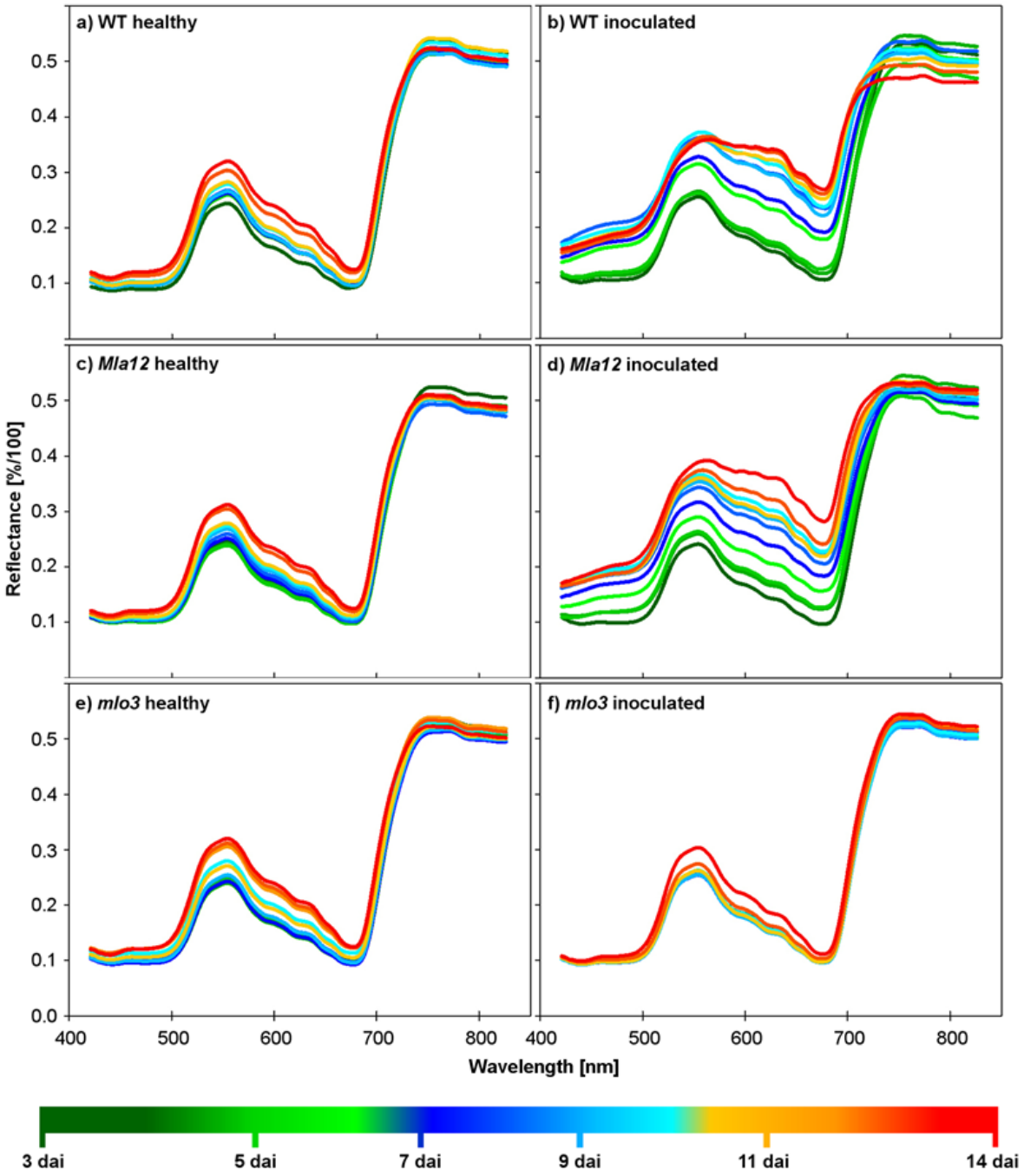

Figure 10: Spectral signatures of non-inoculated (healthy) barley leaves cv. Ingrid WT (a), *Mla12* (c), *mlo3* (e) and barley leaves inoculated with *Blumeria graminis* f.sp. *hordei* (*Bgh*) (b, d, f) from 3 to 14 dai. Reflectance spectra of healthy leaves of the near-isogenic lines are similar. During the measuring period, the reflectance of healthy leaves increased in the visible range. Reflectance of inoculated, susceptible genotypes (WT and *Mla12*) increased in the VIS and WT had decreased reflectance in the NIR. The inoculated, resistant *mlo3*-genotype showed significant differences to healthy leaves in the reflection from 530-680 nm only 14 dai. (n = 3 biological replicates).

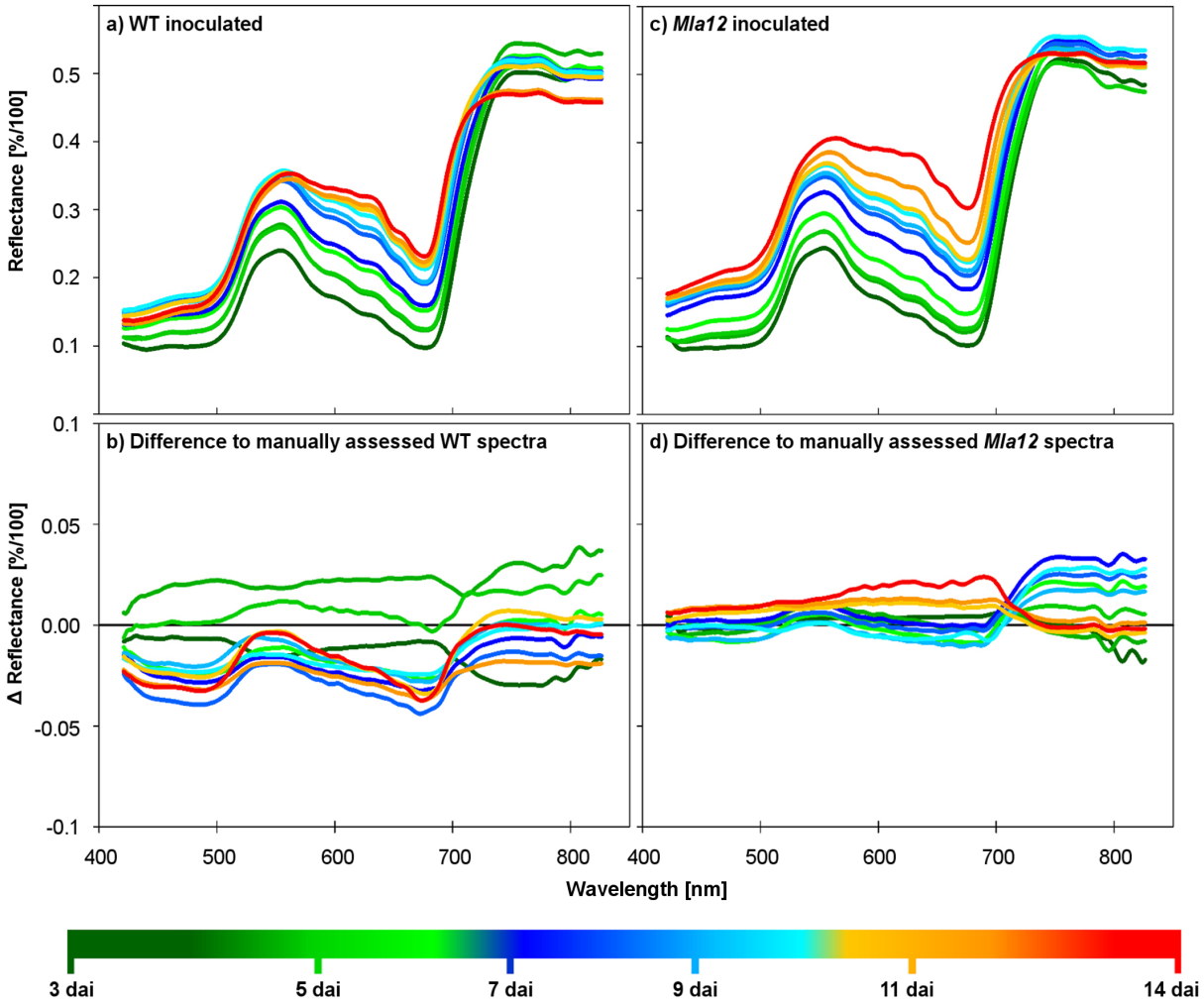

Figure 11: Automatically determined mean signatures of barley leaves cv. Ingrid WT (a) and *Mla12* (c) inoculated with *Blumeria graminis* f.sp. *hordei* from 3 to 14 dai. The automatically assessed spectra were similar to signatures assessed manually. The differences between automatically and manually analyzed data for WT were -0.04 - 0.04 [%/100] (b), -0.02 - 0.03 [%/100] for *Mla12* (d) over the wavelengths and time, respectively.

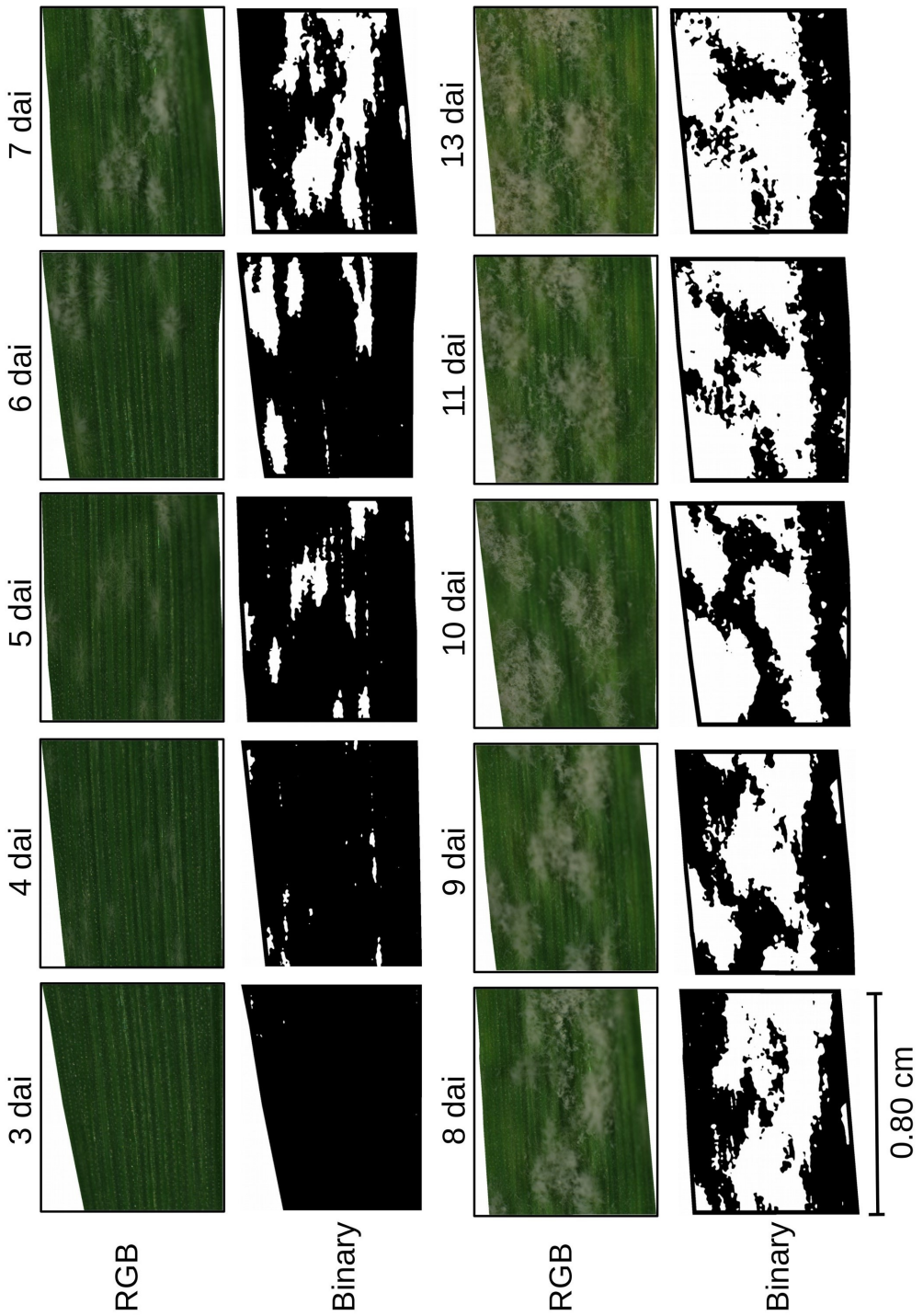

Figure 12: RGB images and binary infestation maps for automatic localization of barley tissue diseased by *Blumeria graminis* f.sp. *hordei* (*Bgh*) 3 to 10 dai. Black color indicates *Bgh* free tissue, white color highlights *Bgh* diseased barley tissue. Image section varies from day to day. No powdery mildew symptoms were visible 3 dai on RGB images. The binary map was almost completely black with small exceptions. First tiny powdery mildew pustules occurred in the RGB image 4 dai, which were detected and illustrated as white areas on the binary map.

3.4.6 Extraction of spectral dynamics of healthy and *Blumeria graminis* f.sp. *hordei* inoculated barley leaves

The spectral dynamics of healthy and inoculated near-isogenic lines over time were used to elucidate differences among the near-isogenic lines illustrated as traces (Fig. 13) according to Kersting et al. (2012a). Figure 13a illustrates the mean traces of healthy and inoculated WT, *Mla12* and *mlo3* genotypes.

Each line describes the spectral trace of three leaves 3 to 13 dai. The similarity among healthy leaves is indicated by the close trends of the traces. They developed in the same direction and had similar dynamics in time, indicated by short traces. Differences in the spectral traces of diseased WT and *Mla12* leaves were apparent. A variation in symptom development and time can be concluded from slightly different traces of the inoculated genotypes. During the experimental time, the mean trace of resistant *mlo3* overlapped with the traces for all healthy leaves and finally differed from them. The traces in Figure 13a allowed for an overall overview of the disease development over time. In order to reach this global view, the averaged mean signatures over all images of the leaves of the same type and treatment was used. To visualize specific details (Fig. 13b, c, d), traces for each particular leave are provided for each genotype (WT, *Mla12* and *mlo3*) and treatment (healthy and inoculated) separately. Differences in the spectral traces in direction and length between the healthy and diseased genotypes are indicated (Fig. 13b, c). For inoculated, susceptible genotypes WT and *Mla12*, differences within genotype and treatment resulted from different disease severities and development stages of powdery mildew over time. Likewise, inoculated *mlo3* leaves gave different spectral traces (Fig. 13d).

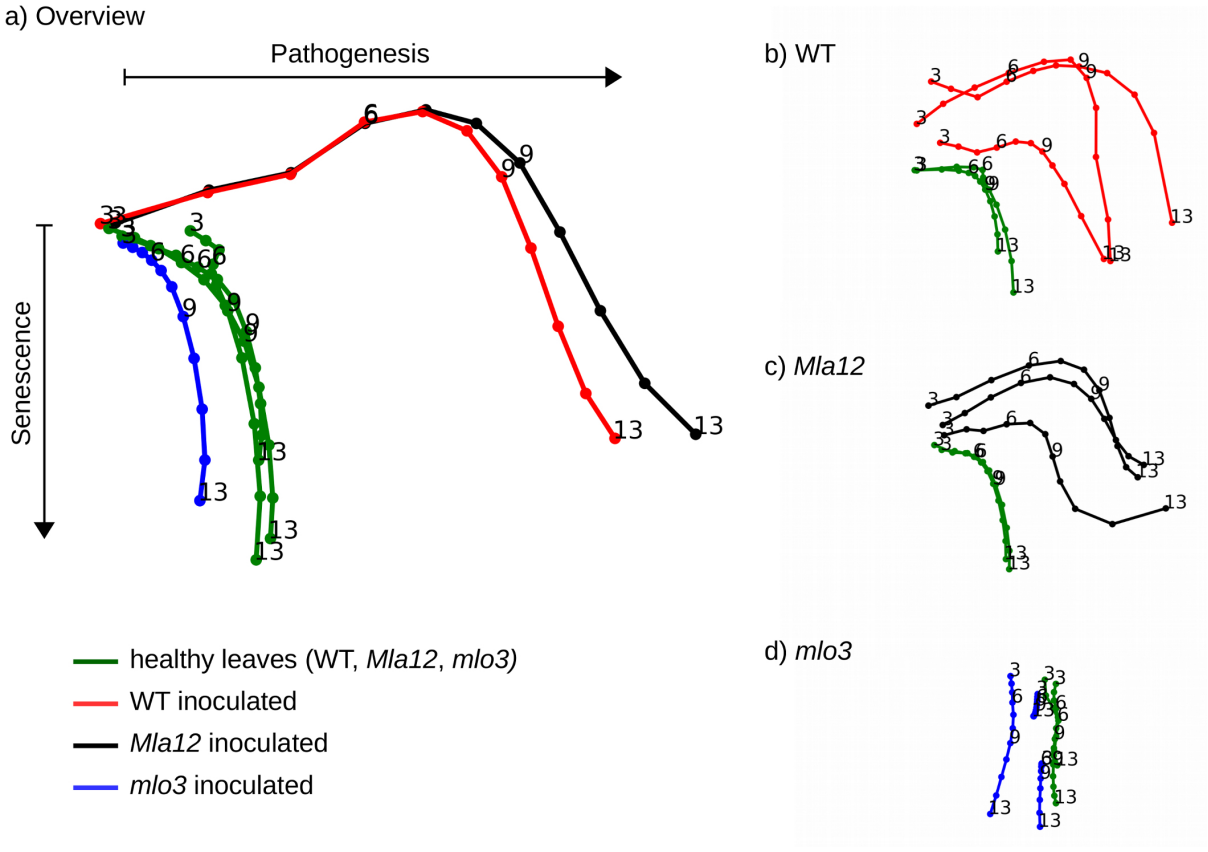

Figure 13: Leaf traces to uncover hyperspectral dynamics of healthy and *Blumeria graminis* f.sp. *hordei* inoculated near-isogenic lines of cv. Ingrid leaves (WT, *Mla12*, *mlo3*) over time. Healthy leaves had a similar spectral pattern and trend, indicated by a minor distance among their traces (a). This is shown also for inoculated WT and *Mla12* leaves (a). Between the individual leaves, hyperspectral dynamics are illustrated by their spectral traces (b, c). The traces of inoculated, resistant *mlo3* leaves differed from healthy and inoculated, susceptible (WT and *Mla12*) leaves over the measuring period (a). Inoculated *mlo3* leaves, showed differences (d).

3.5 Discussion

Hyperspectral imaging can improve disease detection through a better examination of host pathogen interactions (Bock et al., 2010). This has been demonstrated by researchers, using a diversity of hyperspectral sensors with different crops and their relevant diseases on different scales ranging from remote to proximal sensing (Oerke et al., 2014; West et al., 2003). Since imaging sensors allow for a pixel-wise attribution of disease-specific symptoms, primary infection sites can be identified and analyzed spectrally (Mahlein et al., 2012). In contrast to the new plant phenotyping approach in this thesis, existing HSI microscopes are prohibited due to destructive nature (Leavesley et al., 2012; Schultz et al., 2001).

3.5.1 Leaf senescence influence hyperspectral reflectance

Spectral changes indicated senescence processes of non-inoculated, healthy leaves over time, which were in accordance to the leaf phenotype. The reflectance between 420-680 nm increased every day due to changes in the pigment composition (Carter and Knapp, 2001; Gamon and Surfus, 1999; Gamon et al., 1997). The absorption features in this range are related to chlorophyll and other pigments linked to photosynthesis (Gamon and Surfus, 1999; Gamon et al., 1997; Curran, 1989). Increased hyperspectral reflectance indicated then a reduction to the chlorophyll activity and content. This effect is well described as one main process during plant senescence (reviewed in Krupinska (2007); Scheumann et al. (1999)).

Nevertheless, the low RSD of hyperspectral reflectance between the barley genotypes indicate the practicability and robustness of a detached leaf system for the assessment of phenotypic differences due to resistance reactions. The similarity between reflectance spectra of healthy *Mla12* and *mlo3* leaves to healthy WT leaves was due to the identical genomic background of the near-isogenic lines. Consequently, healthy leaves of the near-isogenic lines cv. Ingrid WT, *Mla12* and *mlo3* showed a high spectral similarity and a similar performance on the phyto agar plates. The assessed barley spectra were characteristic reflectance patterns of healthy plant tissue (Wahabzada et al., 2015a; Mahlein et al., 2012; Rumpf et al., 2010; Jacquemoud and Ustin, 2001).

3.5.2 Hyperspectral dynamic in powdery mildew infestation

Reflectance alterations in the VIS of inoculated WT leaves indicated changes in photochemical processes and pigment content, which are associated to the photosynthetic activity (Carter and Knapp, 2001; Gamon and Surfus, 1999; Gamon et al., 1997). Furthermore, the increased reflectance was in accordance with the *Bgh* ontogenesis on barley leaves. The spatial distribution of the *Bgh* mycelium and the vitality of the individual leaves influenced the leaf phenotypes, which explained the higher RSD of the hyperspectral reflectance compared to non-inoculated leaves.

Susceptible near-isogenic lines WT and *Mla12* showed slightly differences in the spectral reflectance during the pathogenesis. Nevertheless, reflectance patterns of *Bgh* pathogenesis on the susceptible genotypes were characterized by a reflectance increase between 400-700 nm over time. This increase is likewise due to white powdery epiphytic mycelium and conidia. Similar patterns were observed for mildew diseased leaves of sugar beet and winter wheat on different scales (Mahlein et al., 2012; Zhang et al., 2012). Furthermore, the automatically assessed reflectance spectra of inoculated *Mla12* leaves in this thesis were in accordance to those assessed manually. The present results highlight a standardized system with detached leaves for

a HSI microscopy and automated data mining suitable for plant phenotyping. Interestingly, the automatically assessed reflectance spectra showed more details among days as all image pixels were considered, whereas the manually assessed spectra are only from a few selected pixels.

In addition, binary maps illustrates disease specific pixels and allows the operator to control the automated results by comparing the binary maps with the corresponding RGB images. In complex biological systems and for resistance screenings, it will be an advantage to take spatial properties of spectral dynamics into account (Fiorani et al., 2012; Mahlein et al., 2012). Overall, the results demonstrate a similarity of spectral patterns and dynamics during powdery mildew pathogenesis independently of the scale of investigations, but with a higher sensitivity of the HSI microscope because of the higher spatial resolution.

3.5.3 *Mlo3* resistant barley only indicate by decelerate senescence

Swarbrick et al. (2006) reported an induced cell-death and a reduction of the photosynthetic activity during the resistance reaction of *mlo5* leaves inoculated with *Bgh* isolate A6. In contrast, *Bgh* isolate K1 inoculated *mlo3* leaves in this study did not change the chlorophyll content until 13 dai. This is indicated by constant low reflectance from 420-680 nm (Carter and Knapp, 2001; Gamon and Surfus, 1999; Gamon et al., 1997). Moreover, the constant reflectance over time, especially at 680-700 nm, allowed to distinguish between susceptible and resistant leaves already 4 dai. The applied spectral traces indicated the resistant barley from the susceptible and healthy leaves, respectively. It highlighted the phenotypic evolution and processes during the barley-*Bgh* interaction. However, specific reflectance patterns of the barley *mlo3* resistance reaction were not assessed in this experiment. Maybe specific resistance reactions of barley genotypes, such as lignification, controlled cell death, or formation of papilla can be assessed only by using a HSI system with higher spatial resolution (Mahlein et al., 2012). Papilla aggregations have a 10-30 µm size in diameter and the remaining functional papilla only 10-15 µm (Bushnell and Bergquist, 1974).

The hyperspectral microscope is an important methodological innovation to elucidate subtle responses of plants to biotic stress, but further investigations of the first 48 hours after inoculation are required. Since most defense mechanisms of plants against fungal pathogens take place within the first hours after plant-pathogen contact, attempted penetration and early infection (reviewed in Bell (1981)). In addition, to improve the results from the HSI microscope, exact spatial referencing of images from subsequent days is necessary. A better spatial orientation within the image could be realized by placing localization plates beside the leaf area of interest.

CHAPTER 4

Spectral patterns reveal early resistance reactions of barley against *Blumeria graminis* f. sp. *hordei*

Chapter 4 has been published:
Kuska, Matheus Thomas[1], Brugger, Anna[1], Thomas, Stefan[1], Wahabzada, Mirwaes[1], Kersting, Kristian[2], Oerke, Erich-Christian[1], Steiner, Ulrike[1], and Mahlein, Anne-Katrin[1,3] 2017. Spectral patterns reveal early resistance reactions of barley against *Blumeria graminis* f. sp. *hordei*. *Phytopathology*, 107:1388-1398.

[1]Institute for Crop Science and Resource Conservation (INRES) - Phytomedicine, University of Bonn, Nussallee 9, 53115 Bonn, Germany.
[2]CS Department and Centre for Cognitive Science, TU Darmstadt, Hochschulstrasse 1, 64289 Darmstadt, Germany.
[3]Institute of Sugar Beet Research (IfZ), Holtenser Landstraße 77, 37079 Göttingen, Germany.

Changes made in the thesis chapter compared to the original publication. Additional text to the original research publication is underlined:
Figures 16, 17 and 19 in chapter 4.4 Results were used as supplementary data in the original publication. In addition, supplementary Figure S4 is not included in this dissertation and supplementary Table S1 is included in chapter 3.4 as Table 3.2. This publication is only used in the dissertation of Matheus Kuska and in no other dissertation.

Authors' contributions
Matheus Kuska and A-K. Mahlein designed the study and interpreted the data. **Matheus Kuska** and A-K. Mahlein developed the hyperspectral measuring procedure of detached barley leaves on phyto agar. **Matheus Kuska** carried out all hyperspectral measurements, manual and statistical analysis. **Matheus Kuska** and A. Brugger performed microscopic investigations. M. Wahabzada and K. Kersting developed and applied data mining methods for the automated spectral data analysis. **Matheus Kuska**, E-C. Oerke, U. Steiner and A-K. Mahlein drafted the manuscript.

4.1 Abstract

Differences in early plant-pathogen interactions types are mainly characterized by using destructive methods. Optical sensors are advanced techniques for phenotyping host-pathogen interactions on different scales and for detecting subtle plant resistance responses against pathogens.

A microscope with a hyperspectral camera was used to study interactions between *Blumeria graminis* f.sp. *hordei* (*Bgh*) and barley (*Hordeum vulgare* L.) genotypes with high susceptibility or resistance due to hypersensitive response (HR) and papilla formation. Qualitative and quantitative assessment of pathogen development was used to explain changes in hyperspectral signatures.

Within 48 hai, genotype specific changes in the green and red range (500-690 nm) and a blue shift of the red edge inflection point were observed. Manual analysis indicated resistance-specific reflectance patterns from one to three dai. These changes could be linked to host plant modifications depending on individual host-pathogen interactions, respectively. Retrospective analysis of hyperspectral images revealed spectral characteristics of HR against *Bgh*. For early HR detection, an advanced data mining approach localized HR spots before they became visible on the RGB images derived from hyperspectral imaging.

The link among processes during pathogenesis and host resistance to changes in hyperspectral signatures provides evidence that sensor based phenotyping is suitable to advance time-consuming and cost-expensive visual rating of plant disease resistances.

4.2 Introduction

Physical and chemical barriers, like waxy cuticle, cell wall, and constitutive anti-microbial compounds are the first defense of plants against fungal pathogens (reviewed in Dangl and Jones (2001). Even when a potential pathogen overcomes these preformed defense mechanisms, the pathogen is confronted with the inducible immune system (reviewed in Jones and Dangl (2006)). Two resistance mechanisms of *H. vulgare* against *B. graminis* f.sp. *hordei* (*Bgh*), the causal agent of powdery mildew on barley are based on different processes and are operative at different stages of pathogenesis. Dysfunction of *H. vulgare* mildew locus o (*mlo*) gene triggers the formation of effective cell wall appositions (papillae) at sites of *Bgh* penetration during the first ~40 hai and inhibit penetration (Röpenack et al., 1998; Jørgensen, 1992a). This papilla formation is based on fast and high local accumulations of callose, arabinoxylan, polysaccharides, ferulic acid and cellulose (Chowdhury et al., 2014). Plasma membrane associated callose synthases are transported in vesicle-like bodies to (*Bgh*) penetration sites after conidia get in contact with the leaf (Eggert et al., 2014; Bayles et al., 1990). The following deposition of (1,3)-ß-glucan polymers and callose synthesis establish a polymer network between the plasma membrane and the cellulosic cell wall, which acts as a penetration barrier (Chowdhury et al., 2014; Eggert et al., 2014; Bayles et al., 1990; Skou, 1985). Barley lines and cultivars with a *Bgh* race-specific resistance mildew locus a (*Mla*) gene are characterized by fast single-cell hypersensitive response (HR) to *Bgh* penetration (Hückelhoven et al., 1999). The barley *Mla* locus encodes a high number of leucine-rich repeat proteins for different *Bgh* isolate-specific resistances (Seeholzer et al., 2010). *Mla* resistance is activated by avirulence locus a effectors from *Bgh* during leaf penetration (Bieri et al., 2004), which lead to an WRKY1 based signal cascade (Chang et al., 2013). Finally, the penetrated cell undergoes a programmed cell death (Hückelhoven and Kogel, 1998).

The identification and characterization of processes during plant resistance reactions against fungal pathogens are essential for plant breeding to select new resistant genotypes. In breeding practice, phenotyping of genotypes is realized by time-consuming, subjective and expensive visual plant ratings. Non-invasive sensors could improve and accelerate plant phenotyping in breeding for disease resistance (Mahlein, 2016; Fiorani and Schurr, 2013; Chaerle et al., 2004). Hyperspectral imaging has shown the potential to determine different plant parameters and to identify plant diseases (Simko et al., 2017; Wahabzada et al., 2016; Mahlein et al., 2012). Recently, there are a few examples that plant resistance reactions influence the spectral properties of plants (Leucker et al., 2017; Arens et al., 2016; Leucker et al., 2016; Oerke et al., 2016; Iori et al., 2015; Kuska et al., 2015). The aforementioned resistance reactions of *H. vulgare* against *Bgh* change the leaf physiology and require several chemical compounds, which can have specific optical properties. Papillae produce an autofluorescence resulting from the accumulation of cell wall-bound phenolic compounds (Röpenack et al., 1998). The local induced cell death by HR is a regulated complex process with multiple compounds involved in different types of cell collapsing (reviewed in Greenberg (1997)), which include pigment degradation of e.g. chlorophyll (Chl) (reviewed in Matile and Hörtensteiner (1999). Changes in the Chl content and photosynthetic activity as well as further leaf compounds can be measured non-invasively using hyperspectral reflectance (Yendrek et al., 2016; Gay et al., 2008; Gitelson et al., 2003; Curran, 1989).

The present study identified specific hyperspectral reflectance pattern in the visual (VIS, 400-700 nm) and near infrared (NIR, 700-1000 nm) range of HR- and papillae- based resistance by elucidating optical properties of different types of plant-pathogen interactions. Linking reflectance spectra to histological observations revealed events and relevant time points in pathogenesis.

4.3 Materials and Methods

4.3.1 Plant material and cultivation

H. vulgare cv. Ingrid wild type (WT) and the corresponding near-isogenic line Ingrid M.C. 20, containing resistant mildew locus o 3 (*mlo3*) (Hinze et al., 1991), as well as cv. Pallas 01, containing resistant mildew locus a 1 and a 12 (*Mla1*; *Mla12*) were used (Boyd et al., 1995; Kølster et al., 1986). Experimental plants were grown in commercial substrate (Klasmann-Deilmann GmbH, Germany) for 10 days in the greenhouse at 23/20 °C and a photoperiod of 16 hours. The primary leaves were then transferred on phyto agar plates containing 0.34 mM benzimidazole.

4.3.2 Pathogen inoculation

B. graminis f. sp. *hordei* isolate K1 (Hacquard et al., 2013) was used to analyze the *mlo3* and *Mla1* resistance response (Shen et al., 2003; Zhou et al., 2001). Preliminary investigations showed that *Mla12* is not effective in this interaction (Shen et al., 2003). *Bgh* K1 was maintained on *H. vulgare* cv. Tocada (KWS, Einbeck, Germnay) in a controlled environment. Twenty-four hours before plant inoculation, the conidia of heavily infested plants were shaken off and discarded to assure homogenous and vital conidia for inoculation. Detached leaves on phyto agar were inoculated with a density of $\overline{X} = 329$ ($\pm$ 107) conidia/cm^2 from a young powdery mildew pustule (7-10 dai) using an aseptic brush. For each barley genotype, four leaves were inoculated with *Bgh*, four leaves were kept non-infected as control. The agar plates were sealed with Parafilm M® (Bemis, Oshkosh, USA) and incubated in a growth chamber at 19 °C, 1100 m^{-2}·*cd* and a photoperiod of 16 h per day.

4.3.3 Histological observation and quantification

For histological analysis of *Bgh* development on different genotypes, further plant sets were prepared in parallel. Leaf discs harvested daily 0 until 4 dai were fixed 15 hours at ~23 °C in ethanol-chloroform (75:25 v/v) mixture containing 0.15 % trichloroacetic acid (Wolf and Frič, 1981). Probes were stained in a dye solution of 1:1 volume of 15 % trichloroacetic acid and 0.6 % Coomassie Brilliant Blue R-250 (CBB) (dissolved in 99 % methanol) for 12 minutes before microscopic analysis. Total amount of conidia as well as conidia, which were able to germinate, to form appressoria, to develop a penetration peg and to develop mycelium were quantified daily until 4 dai.

H_2O_2 generation was investigated by an endogenous peroxidase-dependent staining in 1 mg/ml 3,3'-diaminobenzidine (DAB) for 15 hours at ~23 °C (Thordal-Christensen et al., 1997). DAB polymerizes instantly and locally as soon as it come into contact with H_2O_2 and has then a brownish color. Epidermal cells and mesophyll cells as well as anticline cell walls stained by polymerized DAB were quantified daily until 4 dai. Specimens were examined under a Leica DMR 6000B photomicroscope (Leica, Wetzlar, Germany).

4.3.4 HSI and manual data extraction

The previously described hyperspectral microscope (Kuska et al., 2015) was used for time series imaging. Hyperspectral images were acquired with a line scanner (ImSpector PFD V10E, Spectral Imaging Ltd., Oulu, Finland) with a spectral range of 400-1000 nm and a spectral resolution of 2.73 nm. Hyperspectral measurements were performed in the dark. Magnification was ad-

justed to 7.3x (spatial resolution ~7.5 µm per pixel). Spectral binning and spatial binning were set to 1. Frame rate and exposure time were adjusted to the object. *For* detailed description of the measuring setup *see Chapter 3.3.*

Hyperspectral data cubes were acquired daily until 8 dai. To receive the relative reflectance a white reference bar (SphereOptics GmbH, Uhldingen-MÃijhlhofen, Germany) was recorded (W), followed by a dark current image (B_1). Subsequently, the leaf sample (I_0) and a corresponding dark current image (B_2) was recorded. Calculation of relative reflectance was according to the Formula 1 (chapter 3.3.3), using the software ENVI 5.1 + IDL 8.3 (ITT Visual Information Solutions, Boulder, USA). Following, spectral signals are smoothed by employs the Savitzky-Golay filter (Savitzky and Golay, 1964) and cut below 420 nm and above 830 nm, because of data noise. Parameters for the smoothing process were 12 supporting points to the left and right and a third degree polynomial.

Spectral signatures of pixels from healthy and diseased regions were extracted manually and retrospectively from the last experimental day (Fig. 14). Depending on the development of symptomatic areas, an ellipsoid region of interest of about 300-127000 (WT), 300-70000 (*mlo3*) and 880-5100 (*Mla1*) pixels was extracted per day and specimen, retrospectively. This retrospective signature extraction was used to determine individual interaction spots accurately over the experimental period, because symptoms and resistance responses are visible on the last day of the experiment. For *mlo* genotypes, the region of interest in the leaf center was chosen on empirical values of pre-experiments with the hyperspectral microscope. The extracted reflectance was averaged for ellipsoid areas of interest. These were used to calculate the arithmetic average as well as the standard deviation between the biological replicates. Differences in hyperspectral reflectance among genotypes and over time were calculated according to Carter and Knapp (2001). To enable significant thresholds for spectral differences, a variance propagation with a level of significance of 90% was applied by using Formula 2 for every wavelength. Afterwards the arithmetic mean was calculated of the variance propagation from every wavelength per genotype and dai. The mean variance propagation per genotype and dai were subsequently averaged and used as the threshold of significance. To consider the biological dynamic, a variance propagation was calculated according to formula 2 and were used as standard deviation.

$$\left(\left(\frac{(\sigma_{\text{healthy}})}{2}\right)^2 + \left(\frac{(\sigma_{\text{inoculated}})}{2}\right)^2\right) \times 1.64$$

Formula 2: Calculation of the mean variance propagation for the reflectance intensity per wavelength.

4.3.5 Automated data mining of spectral dynamics by HR

A data mining approach following Kuska et al. (2015) was adapted to efficiently analyze the incompatible barley *Mla1-Bgh* system (Fig. 14). Simplex Volume Maximization (SiVM), which establishes a fast archetypal analysis, was introduced (Thurau et al., 2012). It computes a low-dimensional representation where each hyperspectral signature is represented by a convex combination of only few extreme signatures. The resulting coefficients are proportions adding up to 1 describing the relative contribution of each of the extremes to a hyperspectral signature. The columns in the coefficient matrix can be considered as data points from a simplex spanned by the extreme basis vectors. This allows for a statistical analysis at massive scale (Wahabzada et al., 2015a). Using this regions, the signatures that characterize the specific measurements for the resistance reactions could be automatically extracted.

To determine cells undergoing a HR, the method was further modified using pre-clustering, which compiles similar signatures of all measured leaves per day and considers the groups of signatures instead of only single observations in further processing. In addition, it also captured the spectral differences of diseased leaves. Overall, the approach consists of the following steps: It first employs SiVM to determine few extremes from hyperspectral images of all leaves and time points. Then it represents all signatures as a combination of selected extremes. Thirdly, measurements of all leaves per day were clustered using the new representation, where each data point is considered as a sample from the simplex, spanned by the extremes (Leucker et al., 2017; Wahabzada et al., 2015b). Finally, for each cluster a simplex distribution such as Dirichlet was computed using the coefficients obtained by SiVM. In terms of the Bhattacharyya distance (Kailath, 1967), clusters with the highest differences to the distributions of healthy leaves were chosen for further consideration. In this experiments, the number of extremes computed by SiVM were set to k=25 and the number of clusters to c=16. Three clusters with the highest differences in terms of Bhattacharyya distance were selected. It should be noted that prior to computing the factorization, the signatures were normalized by their Euclidean norm to mitigate the effects of varying reflectance intensities due to specular or uneven surface.

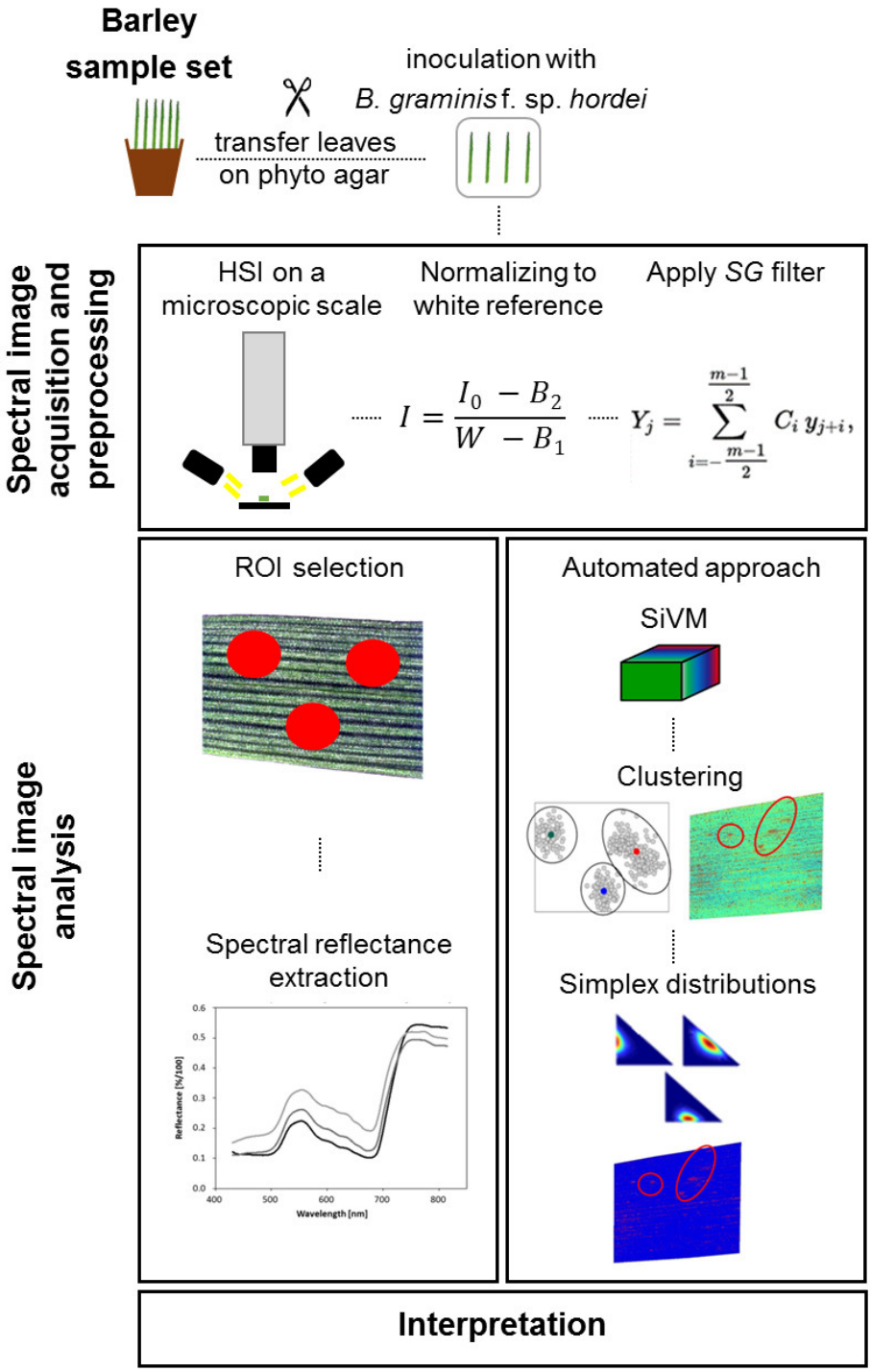

Figure 14: Detection and analysis of plant-pathogen interactions using hyperspectral imaging. Primary leaves of young barley plants were transferred on phyto agar and were inoculated with *B. graminis* f.sp. *hordei*. After hyperspectral image acquisition and normalization, the Savitzky-Golay-filter was applied to reduce data noise. Reflectance values were manually and retrospectively extracted from regions of interest. For the automated detection of hypersensitive response spots (HR-maps), Simplex Volume Maximization was applied to compute a low-dimensional representation of all hyperspectral signatures per image and pixel. Hyperspectral images were clustered using the new representation. For each cluster a simplex distribution was computed. Finally, spectral signatures and HR-maps were displayed and interpreted.

4.4 Results

4.4.1 Microscopic analysis of the interaction phenotypes

The *Bgh* ontogenesis on leaves of susceptible barley cv. Ingrid WT was in accordance with the typical asexual lifecycle described, which includes pre-penetration stages (conidia germination, development of functional appressoria and penetration pegs) and post-penetration stages (fully developed haustoria, epiphytic mycelium and conidiophores). The transition from pre-penetration to post-penetration stage started ~10 hai, indicated by fully developed appressoria (Fig. 15) and first functional haustoria (~24 hai) (Fig. 16a). Epiphytic hyphae were formed 2 dai, increased in number and length during the next days. First conidiophores with conidia appeared 4 dai. Powdery mildew pustules were visible for the human eye 4 dai (Fig. 17). On *Mla1* and *mlo3* resistant leaves the *Bgh* conidia successfully developed primary and secondary germ tubes as well as appressoria (Fig. 15). Epidermal cells with functional haustoria were not present on inoculated *mlo3* leaves, even though ~75% conidia were germinated. The *Bgh* development stopped on the epidermal cell wall and conidia were shriveled on *mlo3* leaves 4 dai. On *Mla1* resistant leaves, ~1% of the conidia penetrated epidermal cells and successfully formed haustoria 3 dai (Fig. 16b). Further development stopped and the asexual life cycle could not be completed by the pathogen (Fig. 16b).

Generation of H_2O_2 was observed as an indicator for barley reactions related to HR response and papilla development (Fig. 18). Susceptible WT leaves generated H_2O_2 in ~20 epidermal cells per cm^2 1 dai (Fig. 18). Epidermal cells with haustoria did not show H_2O_2 generation 2 dai (Fig. 18).

In *mlo3* resistant leaves, H_2O_2 was generated around the *Bgh* penetration site 1-2 dai, indicating the role of H_2O_2 in papilla formation. H_2O_2 generation decreased in these leaves 3 and 4 dai and was observed mainly in the anticline cell walls.

Mla1 resistant leaves showed H_2O_2 generation in ~26 epidermal cells per cm^2 1 dai, which increased to ~45 epidermal cells per cm^2 4 dai (Fig. 18). In addition, H_2O_2 generation was detected in the anticline walls of epidermal cells (Fig. 18). Mesophyll cells generating H_2O_2 were detected only in *Mla1* leaves 4 dai. H_2O_2 generation in *Mla1* leaves increased in epidermal and mesophyll cells until 5-6 dai (Fig. 19a, b). These became macroscopically visible as necrotic spots between 5-7 dai (Fig. 19c). The cellular quantification of H_2O_2 indicated three barley-powdery mildew interaction phenotypes.

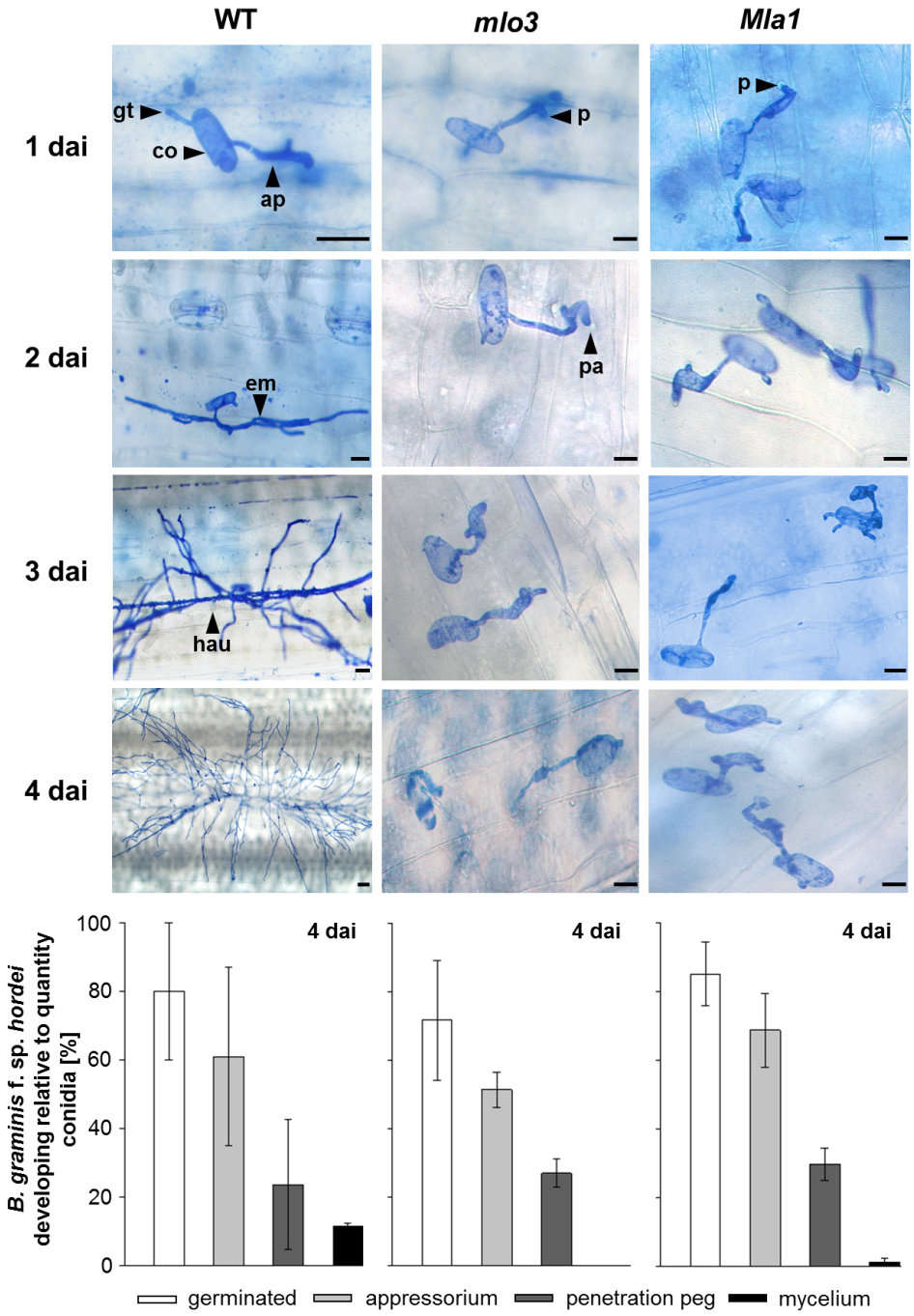

Figure 15: Development of *Blumeria graminis* f.sp. *hordei* (*Bgh*) on cv. Ingrid wild type (WT), *mlo3* and cv. Pallas 01 (*Mla1*) 1 to 4 dai, stained with coomassie brilliant blue R-250. Frequency of *Bgh* developmental stages was quantified 4 dai. Pre-penetration of conidia (co) was present on all host genotypes, indicated by fully developed germination tubes (gt) and appressoria (ap). The *Bgh* life cycle was only completed on susceptible WT leaves. On both resistant genotypes, the post-penetration development was stopped. *Mlo3* leaves showed papillae (pa). On *Mla1* leaves, only few mycelia were quantified, with absent conidiophore development. dai, days after inoculation; em, epiphytic mycelia; hau, haustorium; p, penetration peg. (n = 5 replicates. Scale bars correspond to 20 µm. Quantitative mean of inoculated conidia per cm^2: WT = 223; *mlo3* = 406; *Mla1* = 330; error bars indicate relative standard deviation).

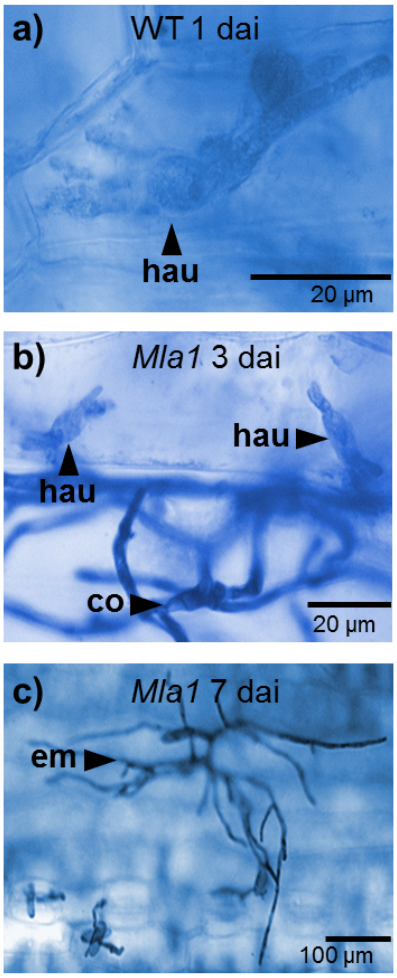

Figure 16: Histological observation of *Blumeria graminis* f.sp. *hordei* development on cv. Ingrid (WT) 2 dai (a) and cv. Pallas 01 (*Mla1*) 3 and 7 days after inoculation (dai) (b, c) using coomassie brilliant blue R-250. (co, conidium; em, epiphytic mycelium; hau, haustorium).

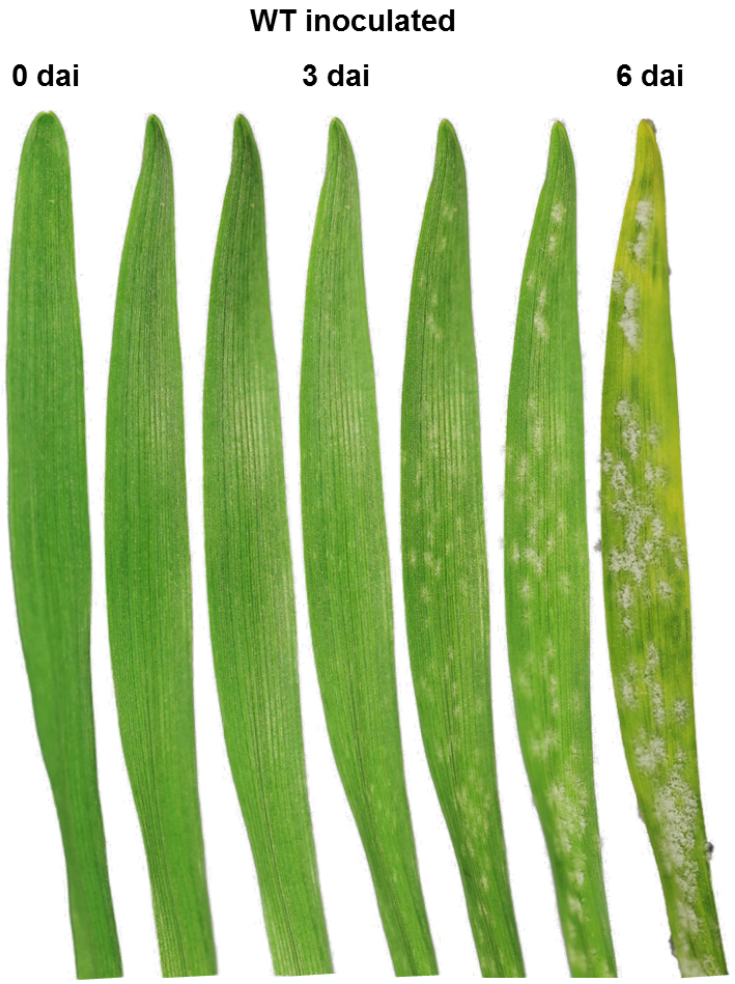

Figure 17: Phenotypes of detached barley leaves cv. Ingrid WT inoculated with *Blumeria graminis* f.sp. *hordei*, 0 to 6 days after inoculation (dai). Typical powdery mildew symptoms appeared from 4 dai.

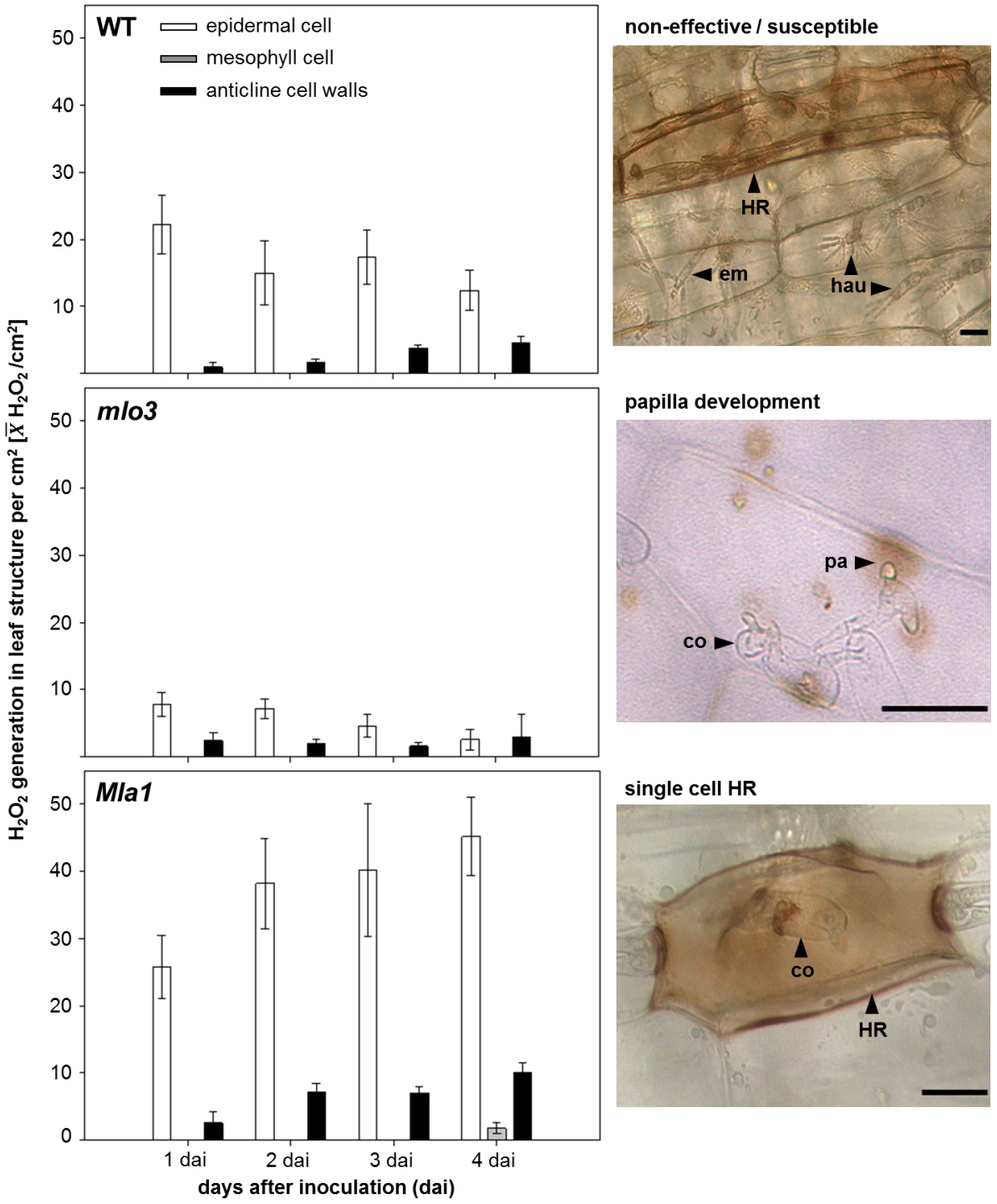

Figure 18: Generation of H_2O_2 at interaction sites on cv. Ingrid wild type (WT), *mlo3* and cv. Pallas 01 (*Mla1*) after inoculation with *Blumeria graminis* f. sp. *hordei* (*Bgh*), stained with 3,3'-diaminobenzidine according to Thordal-Christensen et al. (1997). All genotypes showed H_2O_2 generation in epidermal cells and anticline cell walls, which was only increased in *Mla1* leaves 1 to 4 dai. In addition, in *Mla1* H_2O_2 was generated in mesophyll cells 4 dai. In *mlo3* leaves, H_2O_2 was generated around the penetration point, where papillae developed. Images were taken 2 dai. (n = 5 biological replicates; error bars indicate standard deviation; em, epiphytic mycelium; hau, haustorium; HR, hypersensitive reaction; co, *Bgh* conidium; pa, papilla. Scale bars correspond to 20 µm).

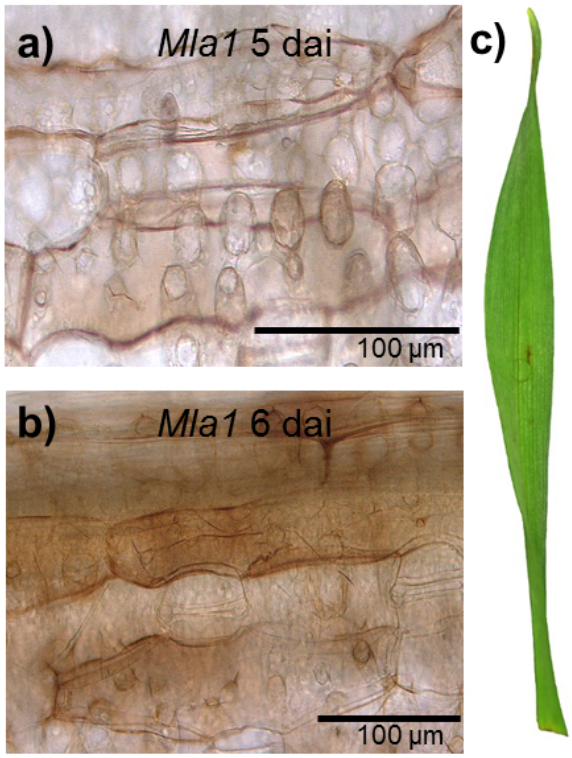

Figure 19: Generation of H_2O_2 at interaction sites on *Mla1* leaves 5 days after inoculation (dai) (a) and 6 dai (b) stained with 3,3'-diaminobenzidine according to Thordal-Christensen et al. (1997). In addition, the corresponding phenotype is illustrated 6 dai (c) and reveals brownish spots, which are associated to strong hypersensitive responses.

4.4.2 Hyperspectral signatures of powdery mildew, HR, and papilla

Hyperspectral reflection changed over time specifically for each genotype during disease progression (Fig. 20). Spectral differences were calculated between reflectance of healthy and *Bgh* inoculated leaves to consider effects of the host genotype and the influence of leaf senescence (Fig. 21). After inoculation, all genotypes showed similar reflectance in the VIS (400-700 nm) and NIR range (700-830 nm), without significant spectral differences to the corresponding non-inoculated leaves (Fig. 20). First spectral changes appeared 2 dai on *Mla1* resistant leaves in reflectance from 400-690 nm and from 720-830 nm. Differences spectra indicated significant differences around ~680 nm and from 720-830 nm (Fig. 21). Reflectance from 400-480 nm, 510-580 nm and from 610-690 nm increased gradually 3 dai (Fig. 20c). Spectral difference were also visible in the NIR range, here inoculated *Mla1* resistant leaves showed the lowest reflectance intensity among all three genotypes (Fig. 21).

Non-inoculated WT leaves had a decreased reflectance at 500-660 nm and around ~710 nm. Later, these leaves had an increased reflectance 400-680 nm, in the red edge and a slightly decreased reflectance in NIR 7 dai (Fig. 20d). The spectral reflectance of inoculated *mlo3* resistant leaves increased from 480-670 nm 2 dai (Fig. 20b). This phenomenon changed to the opposite from 3 dai (Fig. 21). Important spectral changes during the barley-powdery mildew interactions are summarized in Table 4.1.

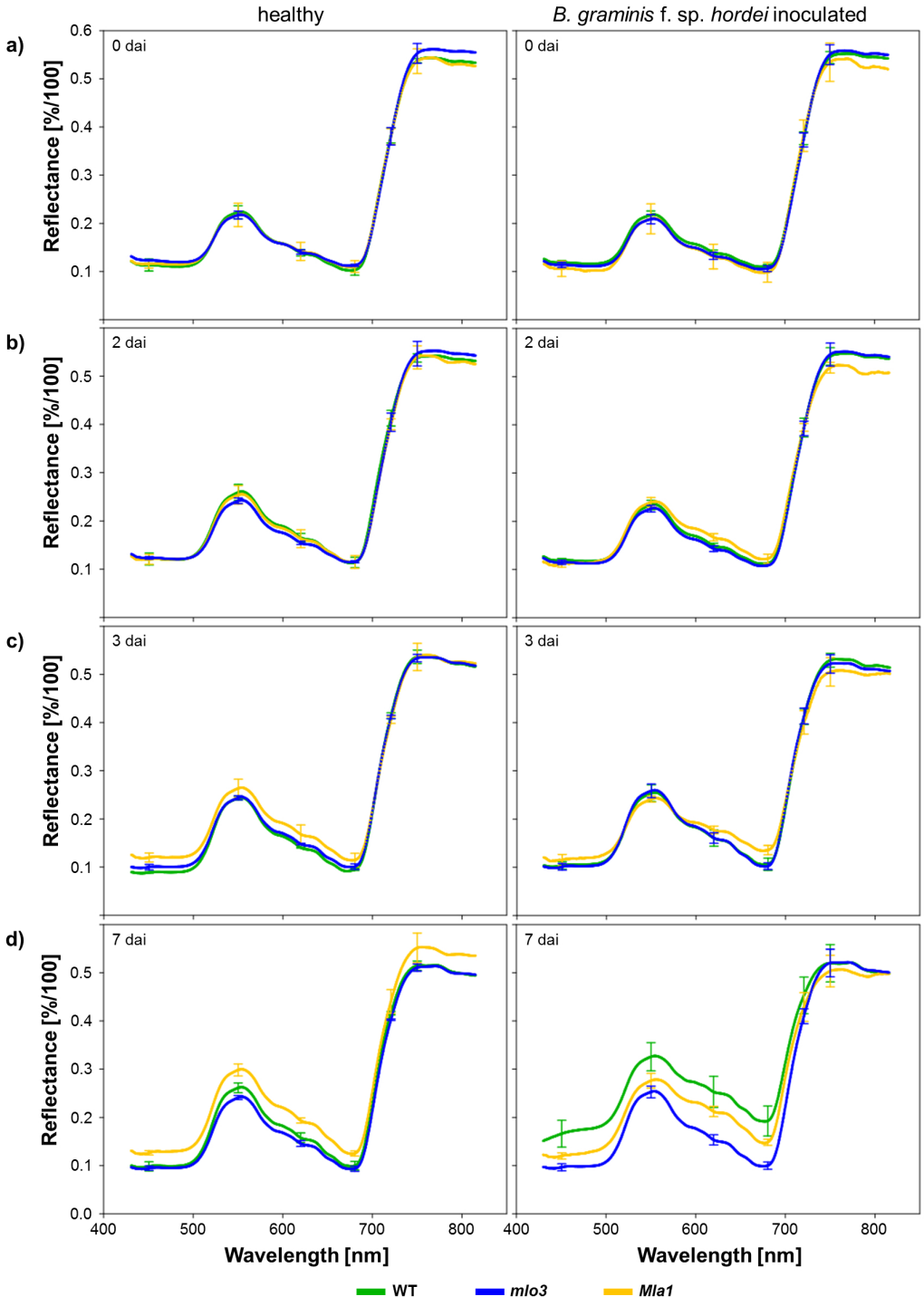

Figure 20: Spectral signatures of healthy barley leaves and inoculated with *Blumeria graminis* f.sp. *hordei*, cv. Ingrid (WT, *mlo3*) and cv. Pallas 01 (*Mla1*), 0 (a), 2 (b) 3 (c) and 7 (d) dai. Reflectance spectra of inoculated genotypes were similar 0 dai, without significant differences to the corresponding spectrum of the healthy leaf. *Mla1* reflectance intensity increased in the green range, around 680 nm and decreased in the near infrared 2 dai (b). These changes became more prominent 3 dai (c). Susceptible WT leaves showed increased reflectance over the entire spectrum 7 dai. (n = 4x($\geq$ 300) biological replicates x technical replicates, relative standard deviation per near-isogenic line over time and measured wavelength range: 0.8-20 % (a); 1-8 % (b); 1-13 % (c); 2-17 % (d)).

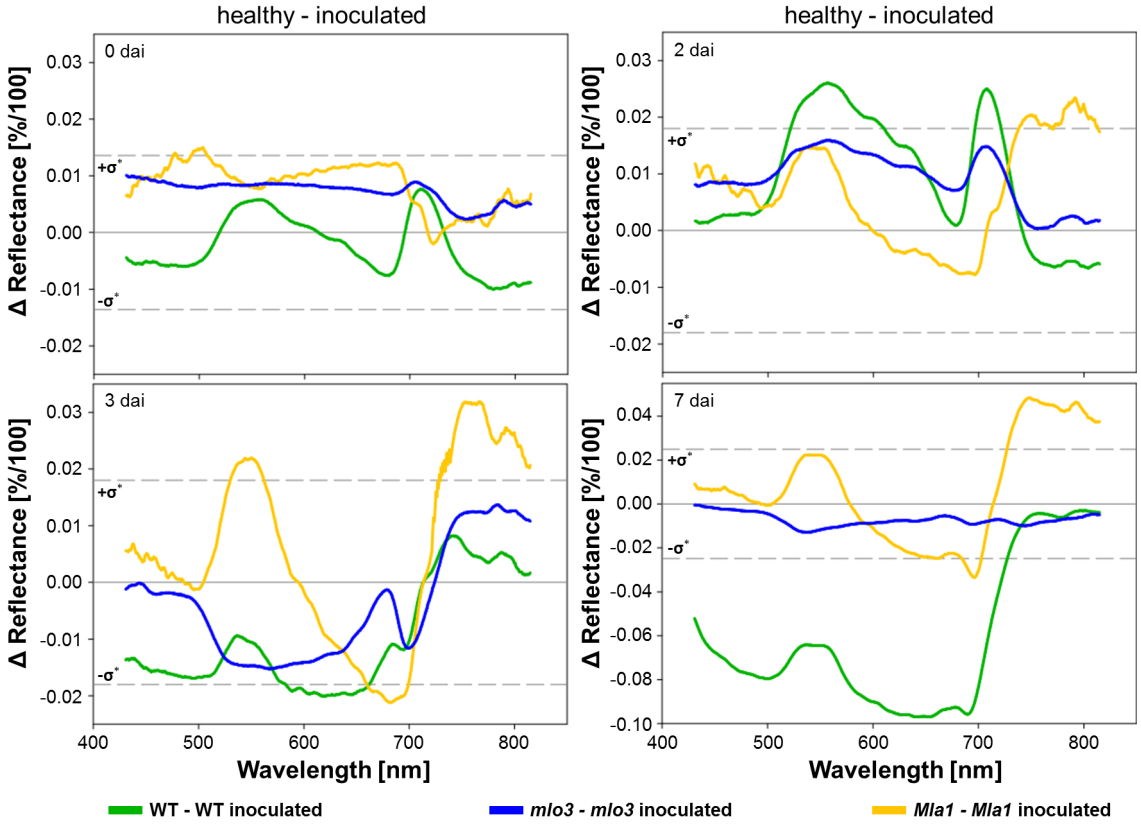

Figure 21: Differences in the spectral reflectance of healthy and with *Blumeria graminis* f.sp. *hordei* inoculated barley leaves, cv. Ingrid (WT, *mlo3*) and cv. Pallas 01 (*Mla1*), 0, 2, 3 and 7 dai. Positive values in the difference plot demonstrate higher reflectance intensity of healthy leaves, negative values higher reflectance intensity of inoculated leaves. The highest measure of dispersion over the whole difference spectrum of all barley genotypes per dai is indicated by $\pm\sigma^*$ and is used as the threshold of significance. Measure of dispersion were calculated as a variance propagation with a 90 % level of significance. (n = 4x($\geq$ 300) biological replicates x technical replicates).

Table 4.1: Influence of individual interaction types of barley near isogenic lines on spectral reflectance during powdery mildew infestation, papilla formation and hypersensitive response. Relevant spectral ranges were selected on the basis of spectral differences between healthy and inoculated genotypes. Relevant wavelength ranges with the highest significance are indicated.

Interaction type	Interaction time frame	Relevant functional spectral ranges	Description
Powdery mildew (wild type)	early	500-660 nm	decelerated senescence
	established, non-visible	400-680 nm ∼690 nm ∼710 nm	structural and physiological changes
	late	400-730 nm	collapsing and chlorotic tissue
Papilla formation (*mlo3*)	early	400-690 nm ∼700 nm	decelerated senescence
	formation	480-670 nm ∼700 nm 730-830 nm	putative cell wall apposition
	established	/	/
Hypersensitive response (*Mla1*)	early	600-680 nm 720-830 nm	structural and physiological changes
	established	∼550 nm ∼680 nm 720-830 nm	necrotized single cells
	late	550-690 nm 720-830 nm	necrotized cell tissue

4.4.3 Automatic detection of HR on *Mla1* leaves against *Blumeria graminis* f.sp. *hordei*

In order to assess the influence of the HRs of *Mla1* resistance, changes in spectral characteristics of inoculated *Mla1* leaves which have shown necrotic spots 8 dai were analyzed over time (Fig. 22). The hyperspectral signature of HR spots had an increased reflectance 8 dai. Reflectance was increased in the range from green to red and caused a blue shift in the red inflection point (Fig. 22). Necrotic spots on *Mla1* leaves appeared 5-6 dai.

For earlier detection of these necrotic spots, corresponding to HR regions, an unsupervised clustering approach was adapted. Binary maps from hyperspectral data visualized pixel indicating healthy leaf tissue in black and HR spots in yellow (Fig. 23). On corresponding pseudo RGB images, HR spots were visible for the first time 5 dai. These HR spots were absent on earlier days. Binary maps indicate HR spots already 2 dai.

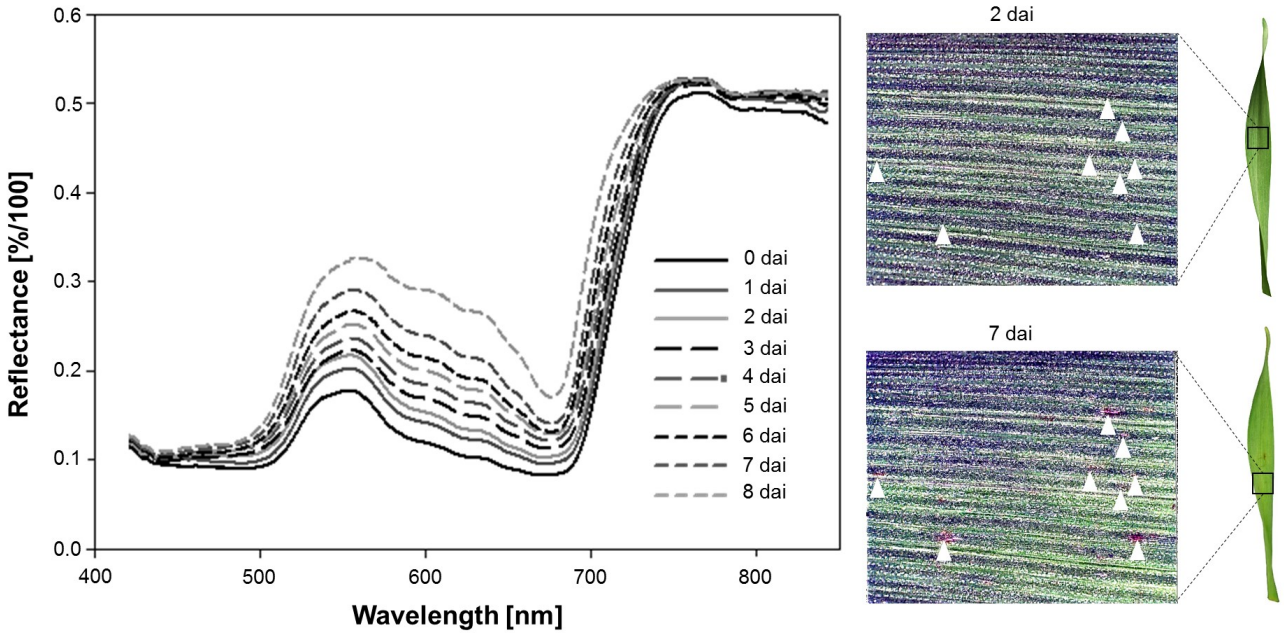

Figure 22: Spectral characteristics of hypersensitive response (HR) spots on near-isogenic barley cv. Pallas 01 (*Mla1*) 0 to 8 days after inoculation (dai) and the corresponding hyperspectral- and RGB- (taken with a digital camera, EOS 6 D, Canon, Tokio, Japan) images 2 and 7 dai. Spectral properties of HR were manually extracted and spots were monitored retrospectively. First HR sites became visible to the human eye 5-8 dai. Reflectance pattern changed over time by increased intensity in the blue and green range, around 680 nm and a blue shift in the red edge.

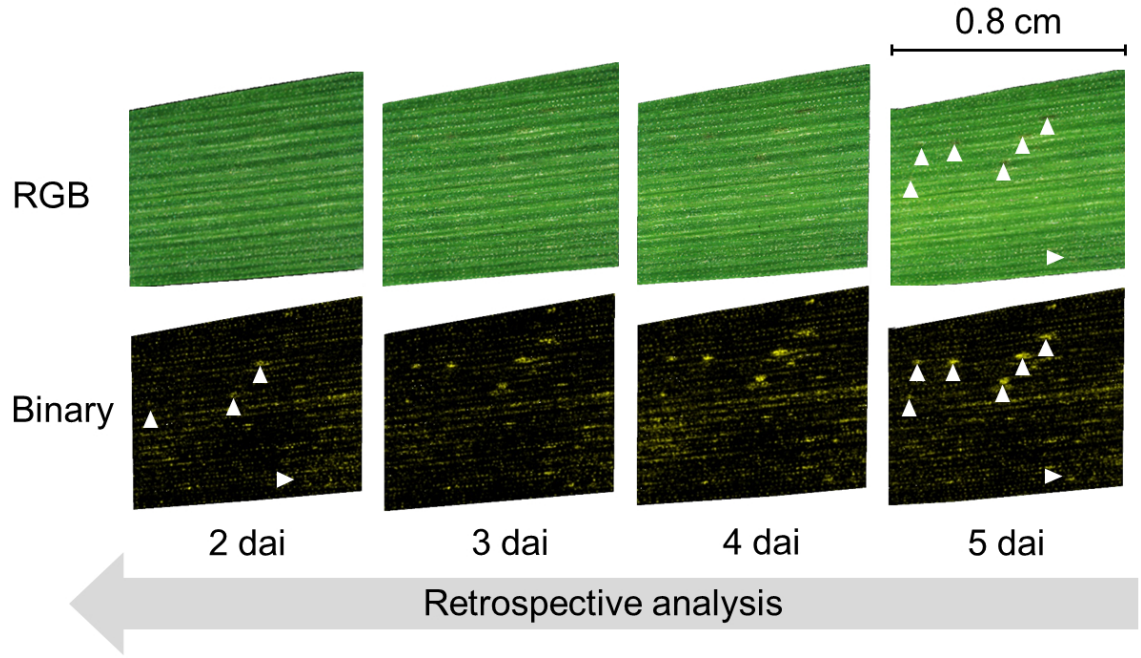

Figure 23: Automatically determined hypersensitive response (HR) spots of near-isogenic barley cv. Pallas 01 (*Mla1*) 2 to 5 dai by retrospective analysis. Black pixels indicate healthy leaf tissue; accumulated yellow pixels HR spots. Detected HR spots matched with brownish HR spots on the RGB images from HS measurements 5 dai. These HR spots were also detected at earlier time points on the binary maps, which were not visible on the corresponding RGB image.

4.5 Discussion

4.5.1 Powdery mildew pathogenesis-related processes influence the VIS-NIR spectrum of barley

Typical *Bgh* pathogenesis on detached WT leaves was associated with dynamics in hyperspectral reflectance of susceptible barley leaves and whole plants (Thomas et al., 2017; Kuska et al., 2015; Wahabzada et al., 2015a). First spectral differences between healthy and *Bgh* inoculated WT leaves appeared 2 dai around 500-650 nm and 710 nm, when primary haustoria developed and first epiphytical mycelium grows. The spectral differences indicate a temporary inhibited senescence of inoculated WT leaves. This phenomenon may be initiated by *Bgh*, inhibiting the senescence which is linked to *PR* gene expressions (Robatzek and Somssich, 2002). Senescence is described as a resistance mechanism against biotrophic fungal pathogens, which the fungal invader try to impede (Häffner et al., 2015). After haustorium development, effector proteins are secreted by *Bgh* to successfully infest the plant and to overcome plant immunity (Ahmed et al., 2015; Robatzek and Somssich, 2002, 2001).

Nevertheless, the reflectance of inoculated WT increased in the VIS range from 3 dai. This reflectance increase is due to the pathogen overgrowing the leaf surface with dense mycelia and conidiophores, where new conidia were produced (Thomas et al., 2017; Kuska et al., 2015; Wahabzada et al., 2015a). This optical effect is also visible around 710 nm, which is correlated to structural parameters and resulting scattering processes (Thomas et al., 2017; Wahabzada et al., 2015a; Green et al., 2002). Later stages of powdery mildew pustules showed increased reflectance from 560-700 nm, which correspond to chlorotic plant tissue (Kuska et al., 2015). This spectral pattern is linked to the reduction of chlorophyll content and a reduced rate of photosynthesis during powdery mildew infestation (Swarbrick et al., 2006; Scholes et al., 1994).

4.5.2 *Mla*-resistance uncovered by HSI

The *Mla* trigger is necessary to start a transcriptional reprogramming of the infested cell (Blanvillain et al., 2011; Hückelhoven et al., 2000). The programmed cell death induces a collapsing of the infested cell, which involves also the reduction of plant pigments (reviewed in Matile and Hörtensteiner (1999). Increased reflectance from 600-700 nm indicated a reduction of the photosynthetic activity already 2 dai in inoculated *Mla1* leaves, which became significant from 3 dai. Several investigations could not confirm the supposed reduction of chloroplasts during cell death (reviewed in Aken and Breusegem (2015)). This is in accordance with lower reflectance in the green peak of inoculated *Mla1* leaves from 2 dai. Studies by Melis and Harvey (1981), showed also that the photosynthesis rate can be different from the chlorophyll content, due to the chloroplast ultrastructure.

However, structural changes indicate a decreased reflectance of *Mla1* leaves in the NIR. This corresponds to collapsing cells, during HR. At time points of spectral changes, collapsing cells could be observed microscopically by increased H_2O_2 generations in inoculated *Mla1* leaves 1-4 dai. This H_2O_2 generation takes place before the cell death (Hückelhoven et al., 1999; Thordal-Christensen et al., 1997). Local necrotized tissue in inoculated *Mla1* leaves showed H_2O_2 generation also in the beneath mesophyll tissue. This is in accordance with mildew loci study by Kogel and Hückelhoven (1999), observing superoxide generation in mesophyll cells as well as necrotic mesophyll tissue in incompatible *Mla12* (HR) barley-powdery mildew system. The necrotized tissue in *Mla1* leaves were spectrally indicated in decreased reflectance of the NIR 7 dai. The influences on spectral signatures in the VIS-NIR by HR could be transferred

to other host-pathogen systems. This could be hypothesized because the oxidative burst by a hypersensitive response induce the cell death with a complex but organize cell collapsing (reviewed in Baxter et al. (2014); Greenberg and Yao (2004).

4.5.3 Formation of *mlo3* papilla transiently influence spectral signature

During *mlo3* mediated cell-wall appositions, a complex of lignin, cellulose, callose, arabinoxylan, ferulic acid peroxidases, phenols, proteins and divers cell-wall materials are accumulated (Chowdhury et al., 2014). Studies on foliar chemistry of healthy plants and spectral properties from remote sensing demonstrated correlations of compounds, such as lignin, cellulose, callose and proteins to spectral reflectance of plants (Curran, 1989; Gates et al., 1965).

Papilla formation presumes local and early reflectance changes in the blue range and NIR. First significant changes occurred with an increased reflectance from 490-660 nm and around 710 nm 2 dai. This spectral pattern was transient and turned back to be normal within a few days. Temporal processes during papilla formation are indicated by cytoplasmic streaming in attacked epidermal cells (Bushnell and Bergquist, 1974). This aggregation has 10-30 µm in diameter and the remaining functional papilla only 10-15 µm (Bushnell and Bergquist, 1974). The used hyperspectral microscope has a spectral resolution of 7.5 µm per pixel, which translates in 1.4 to 12.3 pixels for the aggregation and 1.4 to 3.2 pixels for the remaining papilla *(Chapter 3, Table 3.2)*. An epidermal cell is about 15 times larger and is imaged by 67 to 125 pixels, by this a higher influence of early stages on spectral signature can be assumed. These cytoplasmic streams are filled with several compounds e.g. vesicles and proteins relevant for plant defense responses, especially during papilla aggregations (Schmelzer, 2002; Kobayashi et al., 1997; Freytag et al., 1994). After papilla formation, the nuclei of the epidermal cells are repositioned and cytoplasmic streaming is reduced to normal levels (Schmelzer, 2002; Bushnell and Bergquist, 1974). This is in accordance with the transient increase of spectral reflectance of inoculated *mlo3* leaves 2 dai, which is not detectable on later days because the resistance response has been completed and is restricted to a tiny portion of leaf surface compared to HR of total cells in *Mla*-mediated resistance.

4.5.4 Objective and accurate resistance phenotyping by HSI

Visual assessment and symptom quantification has a variable error rate and is strongly influenced by the human rater (Nutter et al., 2006, 1993). To overcome these unfavorable circumstances on different levels, a large number of highly sensitive sensors and multiple data analysis approaches has been investigated (reviewed in Simko et al. (2017); Mahlein (2016); Großkinsky et al. (2015); Bock et al. (2010)). To date, early detection and assessment of plant-pathogen interaction types was only realized by destructive analysis. The microscopic phenotyping system "HyphArea" by Seiffert and Schweizer (2005) allows an objective quantification of *Bgh* hyphal growth rate 30 hai. In addition, the detection of *Mla9* (HR) resistance was established between 50-54 hai by the invasive HyphArea system. In a previous HSI study, an HSI analysis pipeline allowed early detection of *Bgh* infestation already 3 dai (Kuska et al., 2015). The HSI microscope enables to monitor the development of the same individual e.g. pustule or HR over time. HR maps indicated non-invasively all HR spots 2-3 dai, which could be visible by the human eye on RGB images 5-6 dai.

Alongside the reduced labor intensity, HSI enabled the determination between different barley-*Bgh* interactions. Susceptible and resistant HR or papilla genotypes can be distinguished 2-3 dai using the HSI data. In a next step, these results will be evaluated on different scales

to analyze the scalability of spectral patterns of resistance responses. In future research, the assessed spectral range will be increased to the shortwave infrared range to analyze physiological parameters and changes in e.g. proteins, cellulose, sugars and fatty acids based on hyperspectral images (Curran, 1989). The presented approach can expand studies like the determination of *Arabidopsis thaliana* mutant phenotypes in powdery mildew interactions by molecular methods and histological quantifications (Weißling and Panstruga, 2012). Recently, reactions of grapevine genotypes with different resistances to *Plasmopara viticola* were characterized by using HSI (Oerke et al., 2016). HSI also showed promising results in investigating two quantitative trait loci of sugar beet resistance against *Cercospora* leaf spot using the same hyperspectral microscope (Leucker et al., 2017).

New insights for a biological interpretation of spectral signatures enable the development of spectral models characterizing specific plant-pathogen interactions. Therefore, correlations between subtle biochemical and physiological processes with hyperspectral signatures must be investigated. Furthermore, identification of scale-independent traits is required, to utilize new insights across different scales, from the lab to the field. These studies can be enhanced using further sensors to analyze different physiological parameters and link them to hyperspectral imaging e.g. chlorophyll fluorescence (Zhao et al., 2016; Pan et al., 2015). This will improve common and state-of-art technologies in plant sciences and will enable a fast and accurate plant resistance screening.

CHAPTER 5

Discovering coherency of gene expression and optical reflectance properties of barley genotypes with differing resistance reaction against powdery mildew

Chapter 5 will be submitted as a research article:
Kuska, Matheus Thomas[1], Behmann, Jan[1], Namini, Mahsa[1], Oerke, Erich-Christian[1], Steiner, Ulrike[1], and Mahlein, Anne-Katrin[1,2]. Discovering coherency of gene expression and optical reflectance properties of barley genotypes with differing resistance reaction against powdery mildew.

[1]Institute for Crop Science and Resource Conservation (INRES) - Plant Diseases and Plant Protection, University of Bonn, Nussallee 9, 53115 Bonn, Germany.
[2]Institute of Sugar Beet Research (IfZ), Holtenser Landstraße 77, 37079 Göttingen, Germany.

It should be noticed: This manuscript has not yet been reviewed or accepted for publication. The final published version may differ. This manuscript is only used in the dissertation of Matheus Kuska and in no other dissertation.

Authors' contributions
Matheus Kuska, J. Behmann, and A-K. Mahlein designed the study. **Matheus Kuska** carried out all hyperspectral measurements, manual and statistical analysis. **Matheus Kuska** and M. Namini determined and assessed gene expression profiles. J. Behmann adapted and applied the Relief algorithm, Welchs t'test and LDA to determine relationships between hyperspectral signatures and gene expression profiles. **Matheus Kuska**, J. Behmann, E-C. Oerke, U. Steiner and A-K. Mahlein interpreted the data. **Matheus Kuska**, J. Behmann and A-K. Mahlein drafted the manuscript.

5.1 Abstract

Plant phenotyping is a constraint in plant resistance breeding, described as the phenotyping bottleneck. Hyperspectral imaging has proved its potential for evaluating complex plant-pathogen interactions and phenotyping in several studies. Different steps in pathogenesis have been linked by histological and physiological analysis to spectral profiles. However, a closer link of the spectral signatures and genotypic characteristics remains elusive.

In this chapter a relation between gene expression profiles and specific waveband ranges from hyperspectral reflectance imaging during three barley (*Hordeum vulgare* L.) – powdery mildew (*Blumeria graminis* f.sp. *hordei* (*Bgh*)) interactions is shown. For the investigation of very early and subtle processes of interactions, hyperspectral imaging data were acquired every 3 hours until 48 hai followed by daily measurements until 5 dai. Relevant wavelength bands to characterize barley-*Bgh* interactions were determined by applying the Relief algorithm, a filter algorithm which assess the relevance of features in a specific scenario.

Significant changes in the relevance occurred 12, 24, 48 and 72 hai, indicating genotype specific spectral pattern. Gene expression profiling of seven genes related to cell metabolism, signaling and resistance response was used to determine the powdery mildew pathogenesis and barley resistance stages. Susceptible barley upregulated pathogenesis-related (*PR*) genes 12 hai. In contrast, a papilla based resistant barley genotype (*mlo3*) revealed a stable cell metabolism and upregulated *PR* genes. Resistant genotypes based on hypersensitive responses (*Mla1*) showed a downregulation of all genes proved from 12 hai. For linking gene expression profiles with spectral profiles the Relief algorithm was applied. According to the function of the genes during barley-*Bgh* interactions, relevant wavelengths were identified from 0 until 72 hai. Based on relevant spectral wavelengths and their individual intensities, *RuBisCO* expression profile elucidating the coherency to the photosynthesis apparatus.

These findings outline for the first time a link between gene expression and spectral reflectance during barley-*Bgh* interactions, which can be used for efficient non-invasive phenotyping of the plant resistance. In addition, relevant wavelength bands for specific gene expression profiles were interpreted by the corresponding transcripts. This enables new insights into early plant-pathogen interactions.

5.2 Introduction

Molecular analysis entered as a rapid and advanced method for pre-selection and resistance screenings in plant breeding processes (Tenenboim and Brotman, 2016; Poland and Rife, 2012). However, it is necessary to test the function of the genome of the breeding material in greenhouse and field trials to assess their stability in different environments (reviewed in Fiorani and Schurr (2013); Furbank and Tester (2011)). This phenotyping process by visual estimation is labor and cost-intensive (Shimelis and Laing, 2012). To overcome this phenotyping bottleneck, many recent investigations deal with optical sensor approaches for a non-invasive and efficient evaluation of plant properties (Kirchgessner et al., 2017; Virlet et al., 2017; Friedli et al., 2016). Within this context, hyperspectral imaging is a promising tool to assess different plant parameters with high accuracy (Mahlein, 2016). The plant physiology, chemistry and health status can be derived from the electromagnetic spectrum (Gay et al., 2008; Seelig et al., 2008; Curran, 1989). This enables non-invasive detection and characterization of fungal plant pathogens as well as plant resistance reactions by hyperspectral imaging (Leucker et al., 2017; Oerke et al., 2016; Mahlein et al., 2012). Hyperspectral imaging data are often analyzed and interpreted with histological

and physiological observations as well as information from established sensors such as chlorophyll fluorescence (Leucker et al., 2016; Mahlein et al., 2012; Gay et al., 2008). The correlation of genes or proteins to spectral reflectance patterns has not yet proven, despite the fact that many plant resistance reactions and the plant immunity pathways are known on the 'omic level (Jones and Dangl, 2006; Schulze-Lefert and Vogel, 2000).

Within this context, salicylic acid is identified as the key hormone to activate systemic acquired resistance and to induce pathogenesis-related (PR) proteins (Fu and Dong, 2013). Several families of small PR proteins (5-75 kDa) were analyzed and show different encodings as well as a salicylic acid independent pathway (Fu and Dong, 2013). The *PR2* transcript encodes a ß-1,3-glucanase, which has high similarity to a putative, extracellular localized ß-1,3-endo-glucosidase (Molitor et al., 2011; Roulin et al., 1997; Xu et al., 1992). This enzyme hydrolyzes (1-3, 1-6) branched ß-glucans of fungal cell walls. A second protein encoder against fungal pathogens is the *PR3* expressed transcript, encoding a chitinase class 2 (EC 3.2.1.14) (Kirubakaran and Sakthivel, 2007). This chitinase class is generally described as acidic and extracellular, but detectable in the apoplast and protoplast, respectively (Dore et al., 1991; Benhamou et al., 1990). Further important stress correlated genes correspond to the *PR5* family (Reiss and Horstmann, 2001). *PR5* expression encodes a thaumatin-like protein (TLP2), with several putative properties e.g. antifungal activity and cell regulation during abiotic and biotic stress (Reiss and Horstmann, 2001; Hejgaard et al., 1991; Singh et al., 1989). Jasmonic acid is a further important resistance and cell signaling hormone (Creelman and Mullet, 1997). It is derived from the cell membrane associated linoleic acid and induce de novo synthesis of jasmonate-induced-proteins (JIP) (Simpson and Gardner, 1995; Schweizer et al., 1993; Farmer and Ryan, 1992). During fungal pathogenesis the plant metabolism is also influenced by plant sugars, which can regulate the gene expressions e.g. of ribulose-1,5-bisphosphate carboxylase small subunit (*RuBisCO*) (Proels and Hückelhoven, 2014; Eichmann et al., 2010; Swarbrick et al., 2006). Thereby, abscisic acid as an important plant hormone for plant development is also influenced (reviewed in Nambara and Marion-Poll (2005)). It is responsible for regulation of gene expression during stress responses and natural senescence procedures. In barley the dehydration-responsive factor 1 (*HvDRF1*) is involved in abscisic acid activation and mediated gene regulation as identified by Xu and Loveridge (2004). Until now, even this small setup of important regulators on the 'omic level during a pathogen infestation was not considered in plant phenotyping studies using hyperspectral imaging.

In the present chapter, gene expression profiles were linked to hyperspectral reflectance signatures. To elucidate functional correlations and benefits for plant resistance breeding, *Hordeum vulgare* L. – *Blumeria graminis* f.sp. *hordei* (*Bgh*) was used as model system. Besides a susceptible barley genotype (WT), two near-isogenic lines of *H. vulgare* cv. Ingrid M.C. 20 (mildew locus o 3 (*mlo3*) based resistance) and cv. Pallas 01 (Mildew locus a 1 and 12 (*Mla1*; *Mla12*) based resistance) were used to analyze different plant-pathogen interactions. The *mlo* dysfunction allows the induction of effective cell wall appositions (CWAs - papillae), which developed at the penetration site of *Bgh* during the first ~40 hours after inoculation (hai) and inhibit the penetration (Röpenack et al., 1998; Jørgensen, 1992a). The *Mla* based resistance is characteristic by fast local or single-cell hypersensitive responses (HR) against *Bgh* (Hückelhoven et al., 1999). Expression of seven genes was analyzed 0, 12, 24, 48 and 72 hai. A linear discriminant analysis (LDA) revealed significant synergistic effects between the hyperspectral signal and the corresponding gene activities during these early barley-*Bgh* interactions. The Relief algorithm was applied to determine relevant wavelengths to distinguish between *Bgh* inoculated and healthy barley and to characterize relevant spectral wavelengths for the gene expression profiles.

This method has been already used to select informative genes for cancer classification using microarray gene expression data (Wang and Makedon, 2004).

5.3 Materials and Methods

5.3.1 Plant material and cultivation

Plants were grown in commercial substrate (Klasmann-Deilmann GmbH, Germany) for 10 days in the greenhouse at 23/20 °C and a photoperiod of 16 hours. The primary leaves were then detached and transferred on phyto agar plates containing 0.34 mM benzimidazol. *H. vulgare* cv. Ingrid wild type (WT) was used as a genotype susceptible to powdery mildew. The corresponding near-isogenic line Ingrid M.C. 20, containing dysfunction in mildew locus o 3 (*mlo3*) (Hinze et al., 1991) was used to assess non race-specific papilla based resistance. *H. vulgare* cv. Pallas 01, with resistant mildew locus a 1 and a 12 (*Mla1*; *Mla12*) was used to analyze a hypersensitive response (Boyd et al., 1995; Kølster et al., 1986).

5.3.2 Pathogen and inoculation

The barley *mlo3* and *Mla1* avirulent *Bgh* isolate K1 was used to analyze resistance reactions over time (Shen et al., 2003; Zhou et al., 2001). *Bgh* K1 was maintained on cv. Tocada (KWS, Einbeck, Germnay) in a controlled environment. Twenty-four hours before inoculation the conidia of heavily infested plants were shaken off and discarded in order to assure homogenous and vital conidia for inoculation. Detached leaves on phyto agar were inoculated with a density of $\overline{X} = 329$ ($\pm$ 107) conidia/cm^2 from young powdery mildew pustules (7-10 dai). For each barley genotype, eight leaves were inoculated with *Bgh* isolate K1 and eight leaves were kept untreated as healthy control. The agar plates were sealed and incubated in a climate chamber at 19 °C, 1100 m^{-2}·*cd* illuminance and a photoperiod of 16 h per day. Development of *Bgh* and processes during resistance response of barley were histologically assessed, using Coomassie Brilliant Blue R-250 (CBB) and 3,3'-diaminobenzidine (DAB) staining (Thordal-Christensen et al., 1997; Wolf and Frič, 1981).

5.3.3 Total RNA extraction, reverse transcription-polymerase chain reaction and real time qPCR

RNA was isolated and purified from five pooled LN_2 homogenized barley leaves (~1 g powdered material) using NucleoSpin® RNA Plant kit and NucleoSpin® RNA Clean-up kit (Macherey-Nagel, Düren, Germany), according to the manufacturers recommendations. Total RNA was checked by qPCR using GoTag® G2 Hot Start Colorless Master Mix (Promega, Madison, USA). Therefore, the housekeeping gene *UBIQUITIN* was amplified, including genomic DNA as control sample. Subsequently, the qPCR product and RNA samples were stained with ethidium bromide in 2 % agarose gel to detect contaminations with genomic DNA. Samples with DNA contamination were secondly digested with DNase using TURBO DNA-free™ kit (Life Technologies, Carlsbad, USA) followed by the previous control step. The amount and quality of RNAs were photometrically analyzed using NanoDrop 2000 UV-VIS spectrophotometer (Thermo Scientific, Wilmington, USA).

For cDNA reverse synthesis 1 µg RNA was used. High-Capacity cDNA Reverse Transcription kit with RNase inhibitor (Applied Biosystems, Foster City, USA) was used for reverse transcription polymerase chain reaction following the manufacturers instructions. The cDNAs were

checked by ethidium bromide staining in 2 % agarose gel. Before performing real time qPCR, cDNA was diluted 1:50 with nuclease free water. PCR program was used for the Fast SYBR® Green Master Mix (Applied Biosystems, Foster City, USA) with adjusted annealing temperature to the primers used. The amplified genes of interest were quantified in a relative way to the appropriated mock samples and the fold change in gene expression was calculated via the $2^{-\Delta\Delta Ct}$ -method by Livak and Schmittgen (2001), using *UBIQUITIN* cDNA amplification for normalization. Used DNA oligonucleotide primers are shown in Table 5.1. Amplified real-time PCR products were proved on 2 % agarose gel after melting curve analysis at $55 - 95\,^{\circ}\mathrm{C}$ and compared to calculated fold changes in gene expression (as example Fig. 24).

Table 5.1: PCR primer sequences and product sizes in base pairs for cDNAs those analyzed by real time PCR. Acquisition temperatures were x_1=57 °C or x_2= 60 °C

Gene	**Accession number**	**Forward primer** (5' → 3') / **reverse primer** (5' → 3')	**Product size (bp)**
UBIQUITIN	M60175	[2]ACCCTCGCCGACTACAACAT / CAGTAGTGGCGGTCGAAGTG	263
HvDRF1	AY223807	[1]TCCTCTCGGTCAGATTTGCTGG / ACAGTCACCGGGTCAACTTCC	227
HvRuBisCO	U43493	[1]TCCTTTCCAGGGGCTCA / GAGGCAAGGCACCCACT	223
HvPR2	Barley1_01637	[2]TACTTCGCGTACCGTGACAA / GTGTAGGTCAGCCCGTTGTT	101
HvPR3	AJ276226	[1]CATCACGCAATCGGTGTTACG / TAGTCTCGTGGGAGGTCTGG	192
HvPR5	AY839295	[1]GCCGACCAACTACTCAATGT / AGGGCAGGTGAAGGTGCT	118
HvJIP23	X98124	[2]GGAGTGTTTGGTACCCCCAT / GGCACCAGTGGCATTGTAGA	250
HvGlb1	X56775	[2]CACATCAAGGTGACCACGTC / GGGTAGATGTTGGCCATGAG	200

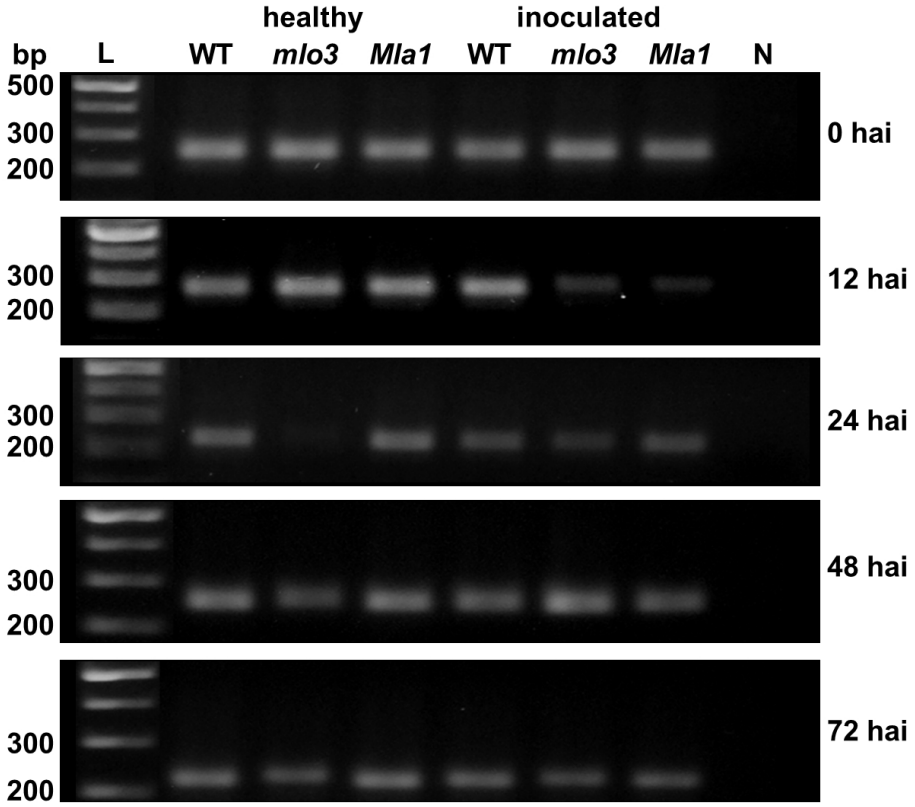

Figure 24: *HvRuBisCO* amplified gene product by real time PCR of healthy and *Bgh* inoculated cv. Ingrid WT, *mlo3* and cv. Pallas *Mla1* barley genotypes 0-72 hours after inoculation (hai) on a 2 % agarose gel stained by ethidium bromide (bp, base pairs; L, DNA ladder; N, negative control with RNA).

5.3.4 Hyperspectral image acquisition, reflectance extraction and histological observation

Hyperspectral images were acquired with a hyperspectral line scanner, (ImSpector PFD V10E, Spectral Imaging Ltd., Oulu, Finland) within a spectral range of 400 to 1000 nm and a spectral resolution of 2.73 nm which results in a spectral sampling of up to 0.78 nm/pixel, installed on a microscope (Kuska et al., 2015). Hyperspectral measurements were performed in the dark. Spectral binning and spatial binning were set to 1. Frame rate and exposure time were adjusted to the object. A magnification of 7.3x (~7.5 µm per pixel spatial resolution) was used. Hyperspectral data cubes were assessed every 3 hours from 0 hai until 48 hai, followed by daily measurements until 5 dai. To receive the relative reflectance a white reference bar (SphereOptics GmbH, Uhldingen-Mühlhofen, Germany) was recorded (W), followed by a dark current image (B_1). Subsequently, the leaf sample (I_0) and a corresponding dark current image (B_2) was recorded. Calculation of relative reflectance was according to the Formula 1 (chapter 3.3.3) using the software ENVI 5.1 + IDL 8.3 (ITT Visual Information Solutions, Boulder, USA). Following, spectral signals were smoothed by employing the Savitzky-Golay filter (Savitzky and Golay, 1964) and cutting reflectance values below 420 nm and above 830 nm because of high data noise. Parameters for the smoothing process were 12 supporting points to the left and right and 1 point in the middle, respectively and a third degree polynomial.

Spectral signatures of pixels from healthy and diseased regions were extracted manually. Therefore, a region of interest of about ~1000000 pixels was extracted. The arithmetic average was calculated for the regions of interest, as the basis for further analysis. Differences in hyperspectral reflectance among genotypes and over time were calculated according to (Carter and Knapp, 2001). Furthermore, data mining approaches following Kuska et al. (2015), and Kuska et al. (2017), were used to compute binary maps for *Bgh* disease detection on WT and *mlo3* barley as well as HRs on *Mla1*. Simplex Volume Maximization (SiVM) was applied to determine extreme signatures from hyperspectral images of all leaves and time points. Then all signatures were represented as a combination of the selected extremes. In this experiments, the number of extremes computed by SiVM were set to k=25. The probability based on the simplex distributions were then used for further analysis.

5.3.5 Linear Discriminant Analysis for the visualization of synergistic effects

The Linear Discriminant Analysis (LDA) can reduce the dimensionality of a dataset retaining the separability of the classes within the dataset. Visualizing the low-dimensional representation reveals the suitability of the features to separate the classes. LDA was applied to three different views on the plant status: (I) the spectral reflectance, (II) the gene activity and (III) the combination of both. For the calculation of the LDA transformations to two dimensions, each spectral observation is represented by five evenly distributed bands and each gene activity measurement is represented by three technical repetitions. The combined feature set includes all features using feature stacking.

5.3.6 RELIEF algorithm for feature selection

The selection of relevant features is an important preprocessing step for the reduction of processing time and improvement of result quality in hyperspectral data analysis. For the evaluation of feature relevance, multiple methods were developed (Guyon and Ellisseeff, 2003). Within this study the regressional RELIEF-F (Relief) algorithm for feature selection was used to gather additional information about the relation between single spectral bands and plant-physiological properties (Fig. 25). The Relief algorithm, as a filter algorithm, determines the relevance of features independently from a specific prediction algorithm. The algorithm is based on the idea that the values of relevant features are not arbitrary distributed in the feature space but that they are grouped by corresponding classes (Kira and Rendell, 1992). By analyzing the local neighborhood for all data points of a data set, the local characteristics can be transferred to the suitability of a single feature for a specific prediction tasks (Robnik-Šikonja and Kononenko, 1997) (Fig. 25). In the classification case (Fig. 25), the difference Δ in a feature value f_j of a data point X_i to the next data point from its class H_i (hit) and from a different class M_i (miss) is transferred to the relevance $R_i(f_j) = \Delta f_j((X_i, M)_i) - \Delta f_j((X_i, H)_i)$. Averaging the relevance across all n data points X_i, $i = 1...n$ gives a global estimation of feature relevance based on the local characteristics.

In this work, the Relief algorithm was used to determine the relevance as an indicator for interpretable relations within the data. It was applied to investigate the relevance of single wavebands of each genotype after inoculation. The significance of these differences were tested by applying the Welch's t-test. In addition, it was also possible to evaluate differences in the relevance of gene expression activities for the hyperspectral reflectance characteristics.

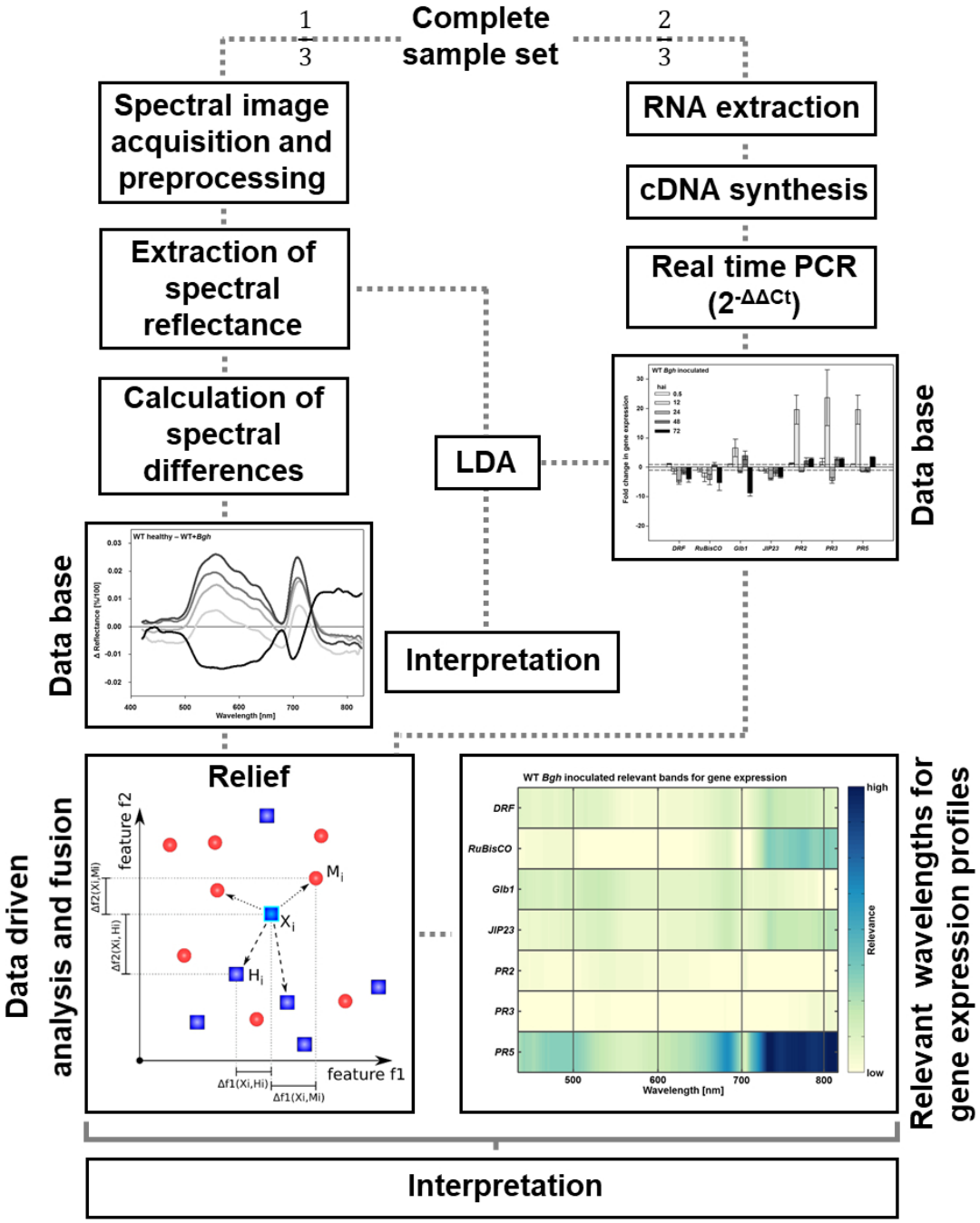

Figure 25: Link hyperspectral imaging data with gene expression profiles. Healthy and *B. graminis* f.sp. *hordei* inoculated primary leaves were used for hyperspectral imaging and RNA extraction, whereby destructive analysis requires 2/3 of the complete plant material. After hyperspectral image acquisition and normalization, the Savitzky-Golay-filter was applied to reduce data noise. Reflectance values were manually extracted from regions of interest. In parallel, RNA was used for reverse transcriptase to synthesize cDNA and to analyze gene expressions of selected genes using real time PCR. Linear Discriminant Analysis (LDA) was applied on the hyperspectral data, gene expression profiles and a combination of both data sets to visualize the suitability of the features for the separation of different barley-*Bgh* interactions. To determine relevance as indicator for interpretable relations between hyperspectral signatures and gene expression profiles the Relief algorithm was applied.

5.4 Results

5.4.1 Relevance of spectral wavelengths for discrimination of non-inoculated and inoculated barley

To discriminate between healthy and *Bgh* inoculated leaves, relevant wavebands were determined using the Relief algorithm (Fig. 26a, c, e). Hyperspectral reflectance from 0 to 120 hai were analyzed to identify key time points of changes in spectral reflectance for the different interactions. High relevance of the waveband is indicated by yellow color, low relevance by blue color. The compatible interaction (WT) reveals relevant wavelength from 520-660 nm and around 690 nm, at 6 hai and 48 hai (Fig. 26a). Waveband range of 400-520 nm shows high relevance 72 hai and 120 hai. The near infrared (NIR, 700-830 nm) range indicates higher relevance 36-48 hai and 96-120 hai, especially around 720 nm 120 hai. Secondary mycelia have been grown 72 hai on the WT, visualized by CBB staining (Fig. 26b) and no significant H_2O_2 generation could be observed 72 hai. Visible powdery mildew symptoms appeared 120 hai (not shown).

Bgh inoculated *mlo3* leaves showed high spectral relevance in wavelengths from 400-720 nm 0-48 hai (Fig. 26c). Wavebands with the highest relevance to discriminate between healthy and inoculated *mlo3* leaves were around 570 nm 36 hai and 48 hai. Later time points show similar relevance over the entire spectrum. The leaves did not show any symptoms. Microscopic observations at 72 hai by CBB and DAB staining indicated fully developed papilla, which stopped *Bgh* penetration and fungal development (Fig. 26d). Wavelengths with high relevance to determine inoculated *Mla1* leaves were indicated by the Relief algorithm at 400-600 nm and around 730 nm 72-120 hai (Fig. 26e). Wavelengths in the blue range provide relevance 12 and 24 hai. H_2O_2 generations were microscopically confirmed 72 hai using DAB staining, which indicates HRs against *Bgh* (Fig. 26f). After *Bgh* penetration, pathogen development was stopped by a HR at *Mla1* genotypes (Fig. 26f, CBB).

Overall, the Relief algorithm identified relevant changes in the spectral reflectance during early plant-pathogen interaction for all three barley-powdery mildew interactions specifically 12, 24, 48, 72 and 120 hai. The significance of spectral changes at these time points was analyzed using the Welch's t-test (Fig. 27). These specific time points were further used to calculate differences in the hyperspectral reflectance between healthy and *Bgh* inoculated leaves to assess subtle changes during barley-*Bgh* interactions.

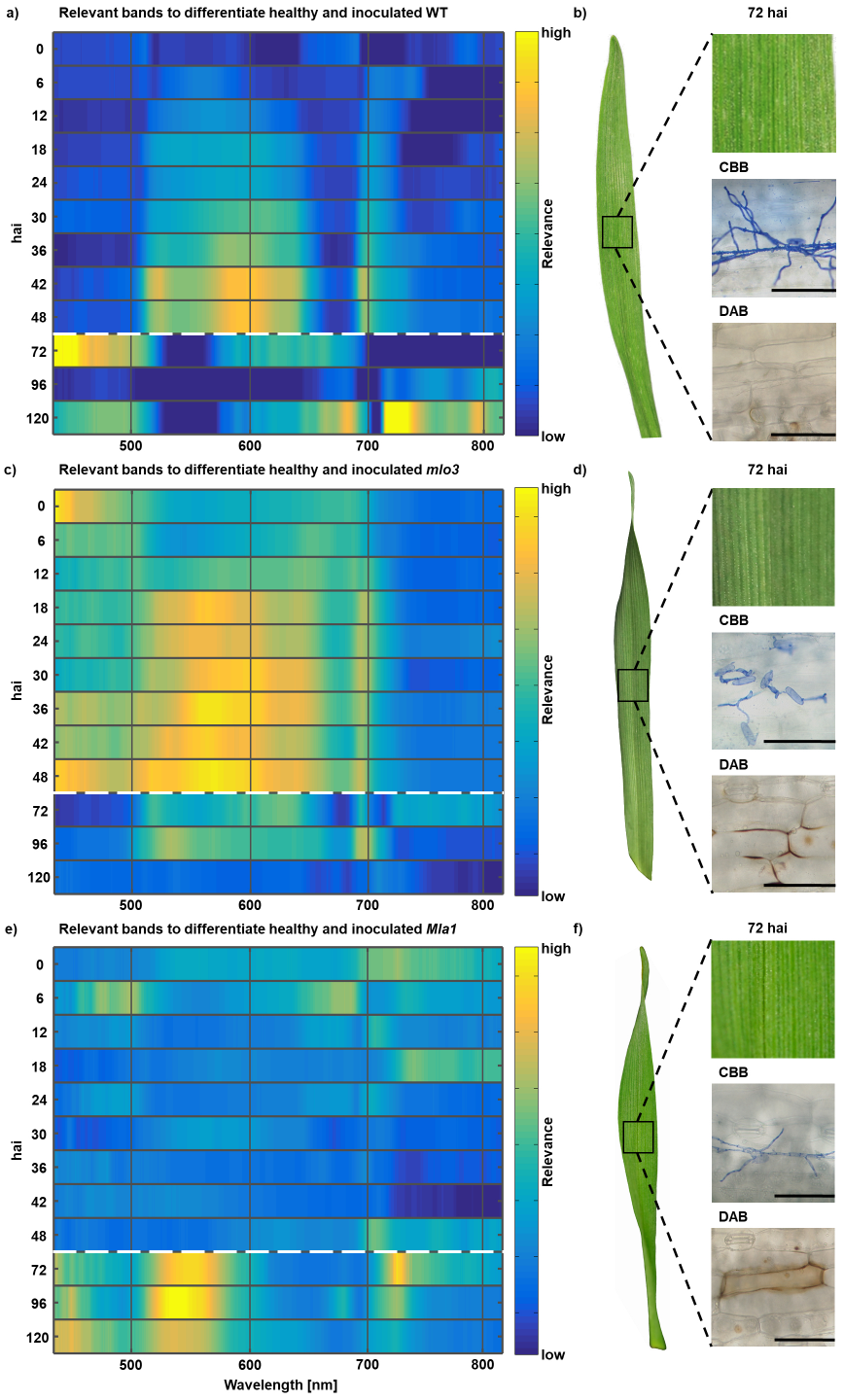

Figure 26: Relevant wavelength bands during susceptible WT as well as resistant *mlo3* and *Mla1* barley-*B. graminis* f.sp. *hordei* (*Bgh*) interactions 0-120 hours after inoculation (hai) (a, c, e). Corresponding RGB images were determined to analyze the phenotype 72 hai (b, d, f). Histological observations using coomassie brilliant blue R-250 (CBB) and 3,3'-diaminobenzidine (DAB) were used to assess the development of *Bgh* and resistance responses of barley (b, d, f). All three different interaction types showed different spectral relevance pattern. *Bgh* could only developed on susceptible WT leaves. Papillae were formed by *mlo3* leaves which prevented the penetration by *Bgh*. *Mla1* leaves undergoes a hypersensitive response at site of infection. (n = 8 replicates. Scale bars correspond to 100 µm).

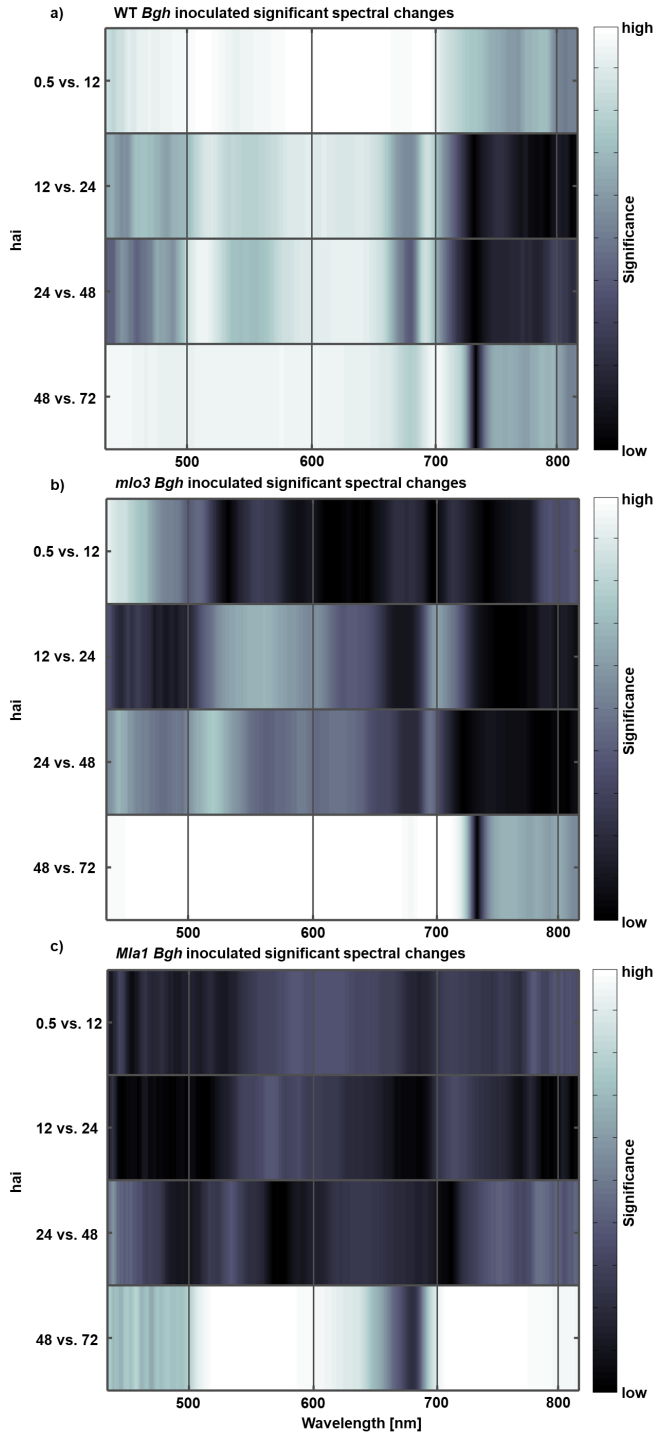

Figure 27: Welch's t-test to determine the significance of changes in hyperspectral reflectance 0.5 to 12, 12 to 24, 24 to 48 and 48 to 72 hai of *B. graminis* f.sp. *hordei* inoculated susceptible wild type (WT), *mlo3* and *Mla1* resistance barley. High significance is indicated in white and low significance of the wavelength band is indicated in black.

5.4.2 Early hyperspectral reflectance differences between powdery mildew susceptible, *mlo* and *Mla* resistant barley

Spectral differences were calculated for 0.5, 12, 24, 48 and 72 hai. At these time points symptoms were not macroscopically visible (Fig. 26b, d, f). First symptoms occurred 120 hai for the naked eye (not shown). For this reason, this time point was used as a macroscopically positive control but was no longer considered for further analysis. Instead, spectral signatures at 0.5 hai were used to assess influence of *Bgh* inoculation on the spectral reflectance. Calculations of difference spectra allowed an explicit analysis of significant wavelength ranges between healthy and inoculated genotypes (Fig. 28). All minus values correspond to a higher reflectance intensity of healthy leaves and all plus values to a higher reflectance intensity of *Bgh* inoculated leaves. Difference between healthy and inoculated WT leaves were marginal around ~0.0024 [$\Delta\%/100$] mainly in the NIR range 0.5 hai (Fig. 28a). The reflectance intensity of healthy WT leaves increased 400-670 nm and around 710 nm 12-48 hai. During these timepoints, reflectance in the NIR range was slightly higher in WT inoculated leaves. Conidia already penetrated epidermal cells and haustoria were developed. These spectral pattern changed 72 hai. The calculated difference signature exhibit higher reflectance intensities of inoculated leaves at 490-670 nm, around 700 nm and a decreased reflectance in the NIR (Fig. 28a). At this timepoint, *Bgh* is in the post penetration phase including first full developed haustoria and secondary mycelia.

Computed disease maps indicate powdery mildew infested spots 72 hai. Spectral differences between healthy and inoculated *mlo3* leaves exhibit a different pattern (Fig. 28b). Reflectance intensities were higher on healthy leaves over the entire spectrum 0 to 48 hai. During this time span, effective papillae were developed in *mlo3* inoculated leaves, but only subtle changes in the spectrum could be observed. Highly significant spectral changes were shown 400-720 nm 72 hai (Fig. 28c and 27b). The disease map of inoculated *mlo3* shows only black pixels, indicating healthy tissue.

Bgh inoculated *Mla1* show higher reflectance intensities at 500 to 850 nm from 0.5 until 48 hai (Fig. 28c). Early differences in reflectance were found in the NIR especially around 710 nm and 780 nm with a difference up to 0.027 [$\Delta\%/100$] 12 hai. During this time point of interaction, *Bgh* has developed an appressorium and starts to penetrate the epidermal cells and subsequently on the *Mla1* genotype a HR is induced. During the HR process, spectral difference pattern changed 72 hai (Fig. 28d). This spectral changes were highly significant from 500-650 nm and 690-830 nm (Fig. 27c). HR spots were not visible for the naked eye until 72 hai. Nevertheless, the applied HR map indicated pixels undergoing a HR in white.

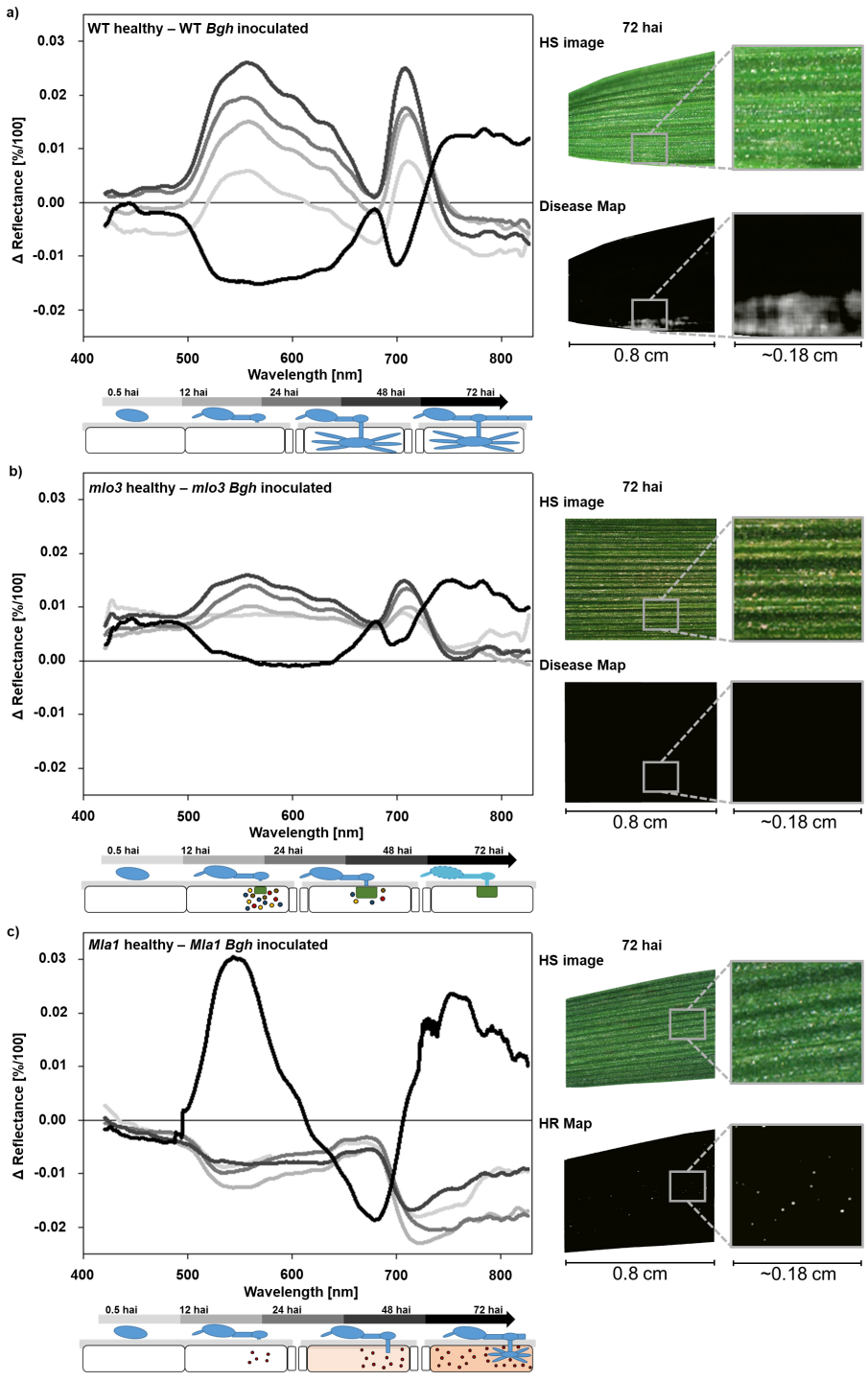

Figure 28: Spectral differences of healthy and inoculated with *B. graminis* f.sp. *hordei* (*Bgh*), susceptible WT (a), resistant *mlo3* (b) and *Mla1* (c), 0.5, 12, 24, 48 and 72 hai. Positive values in the difference plot demonstrate higher reflectance intensity of healthy leaves, negative values higher reflectance intensity of inoculated leaves. In addition, schemes of the interaction types development are illustrated. All interactions show a different spectral pattern with a change 72 hours after inoculation (hai). On pseudo RGB image from HSI, no symptoms are visible. Based on the reflectance spectrum, computed disease maps indicates *Bgh* infested pixels in white 72 hai. HR maps indicated pixels, which undergoes a hypersensitive response also in white 72 hai. (n = 8 biological replicates).

5.4.3 Gene expression profiles during barley-powdery mildew interactions

In order to elucidate transcriptional activity of near isogenic barley lines during *Bgh* interaction, seven genes, related to senescence and cell metabolism, cell signaling and resistance response were analyzed 0.5, 12, 24, 48 and 72 hai. *Bgh* inoculated WT showed down-regulated senescence corresponding genes, indicated by a negative change of *HvDRF* and *HvRuBisCO* (Fig. 29a). *HvDRF* was down-regulated from 24 until 72 hai. Instead, *HvRuBisCO* was down-regulated already 12 until 72 hai without significant differences compared to healthy leaves 48 hai. Resistance responses by WT leaves against *Bgh* were indicated by up-regulated *PR* genes 12 and 72 hai. Differences in transcriptional activity between *HvPR2*, *HvPR3* and *HvPR5* during 24 and 48 hai were present. Interestingly, *HvGlb1* showed higher transcriptional activity 12 and 48 hai in inoculated WT leaves, according to *Bgh* penetration time points. Down regulation of *HvJIP23* from 24 hai suggest that jasmonic acid is not an early key factor in this interaction system.

Gene expression-profile for *mlo3* inoculated leaves exhibit a different pattern compared to the other genotypes and treatments (Fig. 29c). *HvPR3* codes a chitinase 2 and was already up-regulated 0.5 hai. All tested genes were then down-regulated 12 hai, except *HvPR2* which had a higher transcriptional activity until 48 hai. *HvDRF*, *HvRuBisCO* and *PR* genes had a higher transcriptional activity in inoculated leaves compared to healthy *mlo3* leaves 48 hai.

Gene expression-profile of *Mla1* inoculated leaves refer to an initiate cellular degradation, approved by down regulated gene expression of mostly all genes 12 hai (Fig. 29e). *HvGlb1* and *HvJIP23* were the only genes in this system which were significantly up regulated 48 hai.

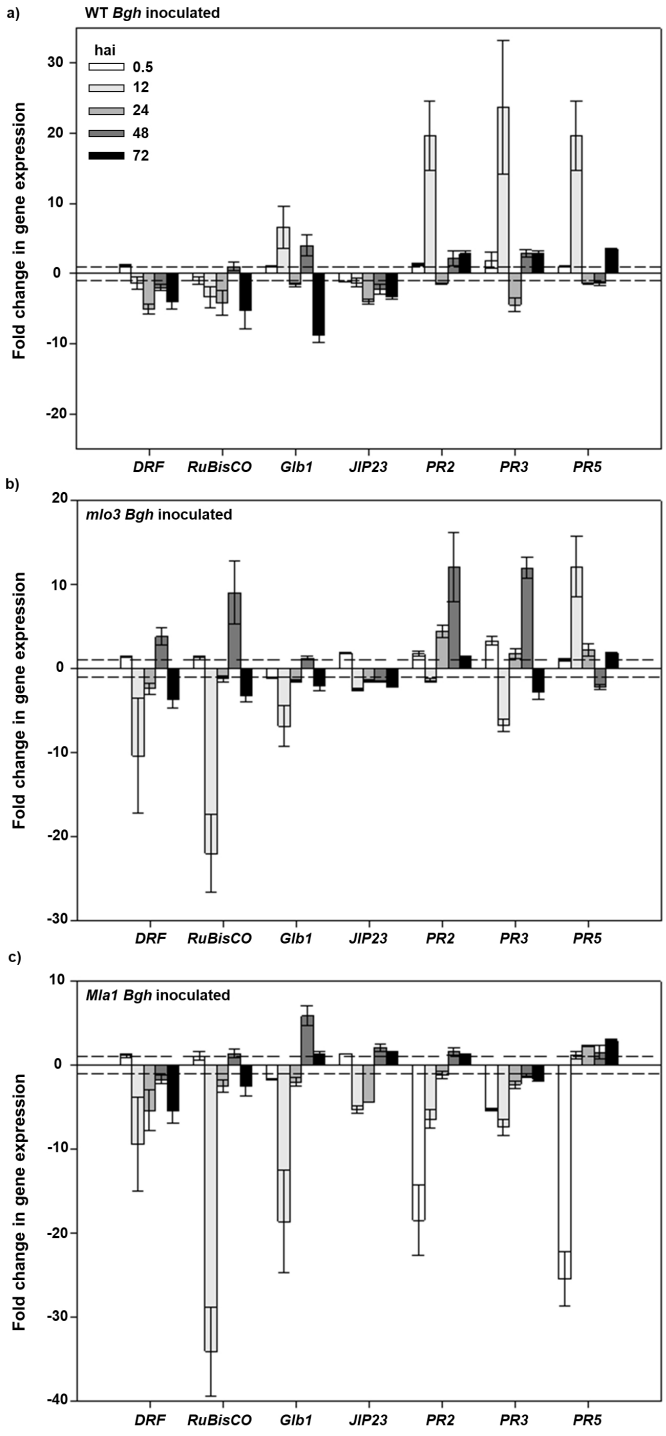

Figure 29: Gene expression profiles of inoculated with *B. graminis* f.sp. *hordei* (*Bgh*), susceptible WT (a), resistant *mlo3* (b) and *Mla1* (c), normalized to their appropriated mock samples 0.5, 12, 24, 48 and 72 hai. (n = 3 replicates; error bars indicate standard deviation).

5.4.4 Interrelations between hyperspectral signatures and gene expression profiles

To discriminate early *Bgh* pathogenesis on WT leaves and resistance responses on *mlo3* and *Mla1* leaves a LDA was applied on hyperspectral signatures, gene expression profiles and combined data sets (Fig. 30). The LDA classification by hyperspectral signatures revealed an improved discrimination of the barley-*Bgh* interaction types with ongoing pathogenesis (Fig. 30a). In contrast, LDA classification of the gene expression profiles of *Bgh* inoculated barley genotypes showed a discrimination during the early time points (Fig. 30b). Applying the LDA on the combined data sets of hyperspectral signatures and gene expression profiles revealed an efficient discrimination between the susceptible WT, *mlo3* and *Mla1* based resistant barley.

This shows significant synergistic effects between the hyperspectral signal and the corresponding gene activities carving out the subtle differences between the early plant adaptions.

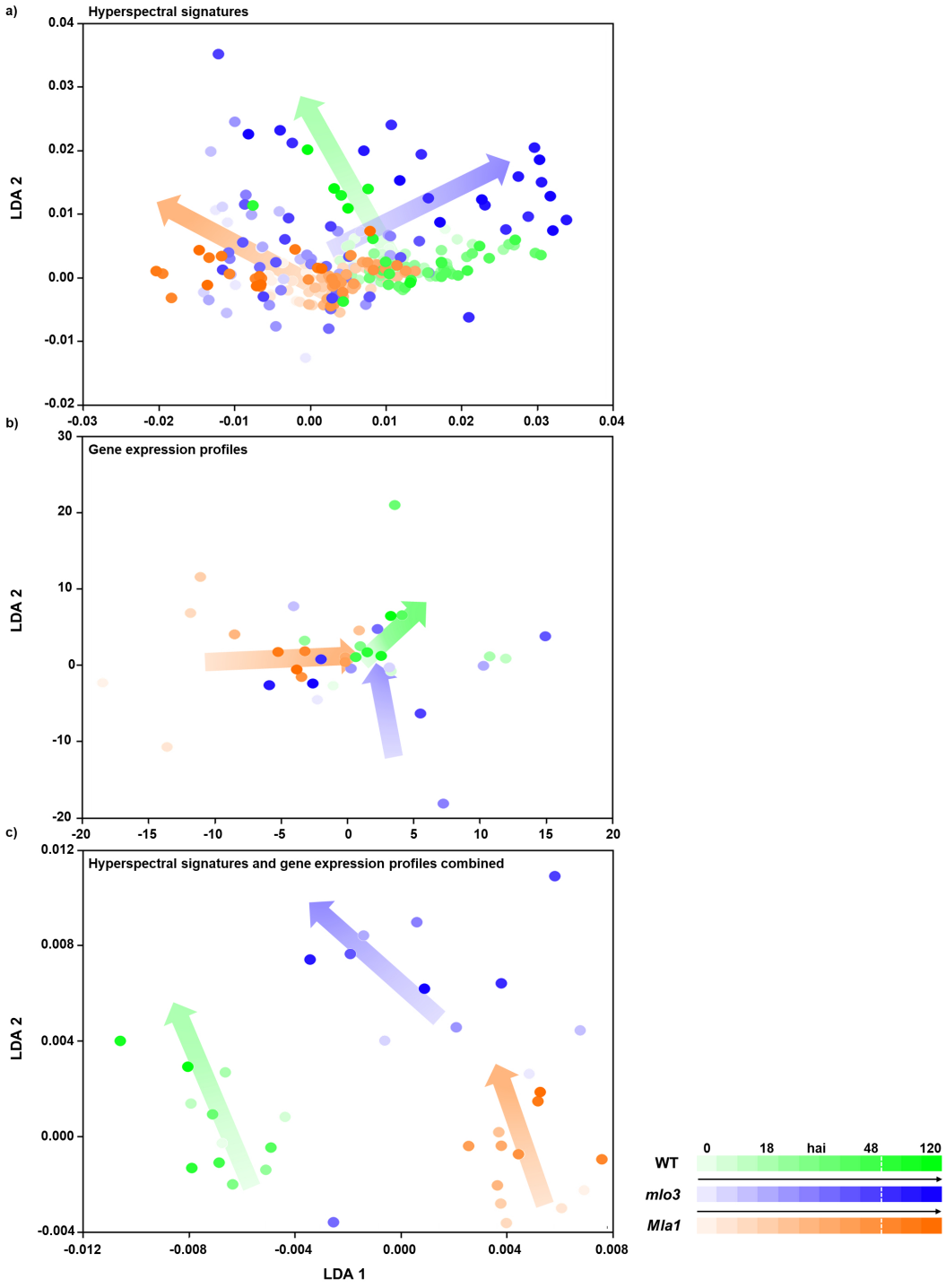

Figure 30: Separability of barley-*B. graminis* f.sp. *hordei* (*Bgh*) interactions based on hyperspectral signatures, gene expression profiles and combined data sets 0-72 hai. The suitability of features to differentiate *Bgh* inoculated susceptible wild type (WT) barley, papilla resistant (*mlo3*) and hypersensitive resistant (*Mla1*) barley were tested using a Linear Discriminant Analysis (LDA). Combining both data sets increased the separation between the different interaction types WT, *mlo3* and *Mla1*. (Arrows indicate the changed center of gravity per barley-*Bgh* interaction over the experimental period).

5.4.5 Relevant wavelength bands for the individual gene expression profiles

To analyze the coherence between spectral reflectance and gene expression profiles during barley-*Bgh* interactions, relevant wavelength bands and reflectance intensities for each gene were computed using the Relief algorithm. Wavebands with high relevance are indicated in blue, low relevance is indicated by beige color (Fig. 31).

Relevant wavebands for *HvDRF* expression profile of *Bgh* inoculated WT are around 730 nm (Fig. 31a). The NIR range is relevant for the expression profile of *HvRuBisCO*, *HvJIP23* and *HvPR5*. Wavebands at 400-530 nm and around 680 nm are relevant for *HvPR5* expression during WT-*Bgh* interaction, respectively.

Expression profile of *HvRuBisCO* of *Bgh* inoculated *mlo3* had varying relevant wavebands in the VIS-NIR range with the highest relevance around 730 nm (Fig. 31b). High relevance around 730 nm and 760-830 nm are shown as well for *HvJIP23*. *HvPR3* expression profile were related to reflectance at 400-530 nm, around 690 nm and 730 nm.

Relevant wavebands for gene expression profiles of *Bgh* inoculated *Mla1* leaves were mainly computed from 660-680 nm for almost all genes. Thereby, *HvDRF* profile shows no relevant wavebands in the VIS-NIR range. Wavebands from 520-650 nm, 660-680 nm and 700-750 nm show high relevance for the expression profile of *HvPR5*.

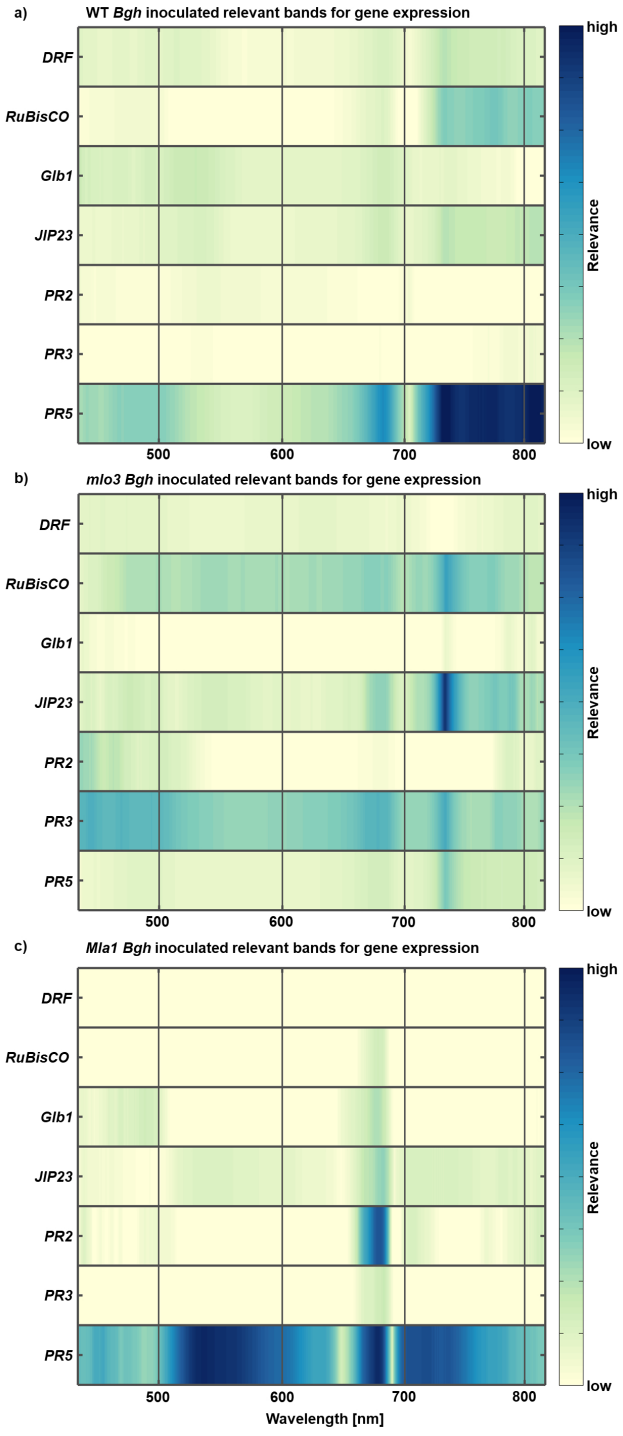

Figure 31: Relief algorithm to assess differences in the relevance of individual genes per wavelength band and barley genotype inoculated with *B. graminis* f.sp. *hordei* (*Bgh*), susceptible WT (a), resistant *mlo3* (b) and *Mla1* (c). High relevant wavelength bands for specific gene expression profile are indicated in blue and low relevant wavelength bands in beige.

5.5 Discussion

5.5.1 *Blumeria graminis* f.sp. *hordei* influence early spectral characteristics of barley

Previous studies on hyperspectral imaging of barley-*Bgh* interactions elucidated spectral characteristics of powdery mildew pathogenesis, as well as for *Mla1* and *mlo3* based resistance between 0 until 14 dai (Thomas et al., 2017; Kuska et al., 2015; Wahabzada et al., 2015a). Important time points varied depending on the interaction. Investigations by Kuska et al. (2017), indicated key moments in the plant-pathogen interaction to distinguish barley-*Bgh* interactions by hyperspectral imaging and histologic analysis 2-3 dai. In the present study the relevance of spectral changes during barley-*Bgh* interactions were revealed for the first time. Hyperspectral imaging of early time points (0-48 hai) revealed changes in the metabolism of inoculated WT and *mlo3* near-isogenic lines. During this interaction time, the senescence was decelerated in inoculated leaves, indicated by an stable reflectance intensity in the green range.

Barley leaves with a dysfunctional *mlo* gene had fully developed papillae 24-48 hai as described by Hückelhoven et al. (1999) and Thordal-Christensen et al. (1997). The former, complex cell wall aggregation (Chowdhury et al., 2014; Eggert et al., 2014) results in decreased reflectance from 420-660 nm and around 710 nm 1-2 dai. This may be explained by cytoplasmic streams in attacked epidermal cells (Bushnell and Bergquist, 1974). Similar spectral pattern for *Bgh* inoculated *mlo3* leaves were shown by Kuska et al. (2017), already 2 dai. *Mla1* based hypersensitive reaction which cause an early change 12 hai in the NIR range is correlated with plant physiological and structural changes (Carter and Knapp, 2001; Jacquemoud and Ustin, 2001). This indicates a rapid mode of action within the first 24 hours according to described process of *Mla* gene based HR (Hückelhoven et al., 1999). This process seems to decelerate 72 hai, displayed by a turnover of the difference reflectance. In previous studies, this turnover was spectrally determined in a *Bgh* inoculated *Mla1* already 48 hai (Kuska et al., 2017). This indicates a temporal dynamic of the *Mla* response against *Bgh* penetration. Nevertheless, the spectral difference pattern is similar, after the HR undergoing cells are necrotized.

5.5.2 Gene expression profiles and their link to spectral reflectance

The LDA analysis on hyperspectral signals or gene expression profiles indicated a high dispersion. This phenomenon derived from the temporal variability during the early individual interactions which are depended on the *Bgh* development and penetration time point (Wahabzada et al., 2015a, 2016). The opposed separability during the experimental period based on the chain process from gene to phenotype (Yin et al., 2004). In contrast, applying the LDA on the combined data sets differentiate all three barley-*Bgh* interactions independent from the time. This shows significant synergistic effects between the hyperspectral signal and the corresponding gene activities. These results open further analysis, investigating the temporal variability in the hyperspectral signal and gene expression profile as well as a functional link between both data sets.

Depending on the barley-*Bgh* interaction, different genes were expressed during plant-pathogen interaction. The *Bgh* infestation begins with the conidia developing an appressorium and starting to penetrate the epidermal cell wall using cell wall degrading enzymes and by an increased turgor pressure (Both et al., 2005). At this time point, *PR* genes are induced and a down regulation of *HvRuBisCO* has been already described in studies by Eichmann et al. (2010). During the compatible interaction, *PR5* showed broad functionality indicated in high frequency of relevant wavebands. *PR5* is reported as marker for systemic acquired resistance, but transcripted proteins are endo-ß-1,3-glucanases as well as endo-ß-1,4-xylanases with anti-fungal activity (Liu et al., 2010; Grenier et al., 1999; Morris et al., 1998; Hejgaard et al., 1991). A possible xylanase activity is indicated by high relevant wavelengths around 710 nm. Reflectance intensity around 700 nm is characterized by leaf and cell structure (Michéle et al., 2001; Gates et al., 1965). The cell structure is highly influenced by the cell wall in which xylan is a major component for the cell wall of monocotyl plants and can be degraded by endo-ß-1,4-xylanases (Faik, 2010). This coherency indicates that *PR5* activity is important during compatible barley-*Bgh* interaction.

Further important gene activity during compatible barley-*Bgh* interaction was revealed by upregulated *HvGlb1*, which is stimulated by gibberellic acid and transcripts a ß-1,3-glucanase mainly in aleurone cells to hydrolyze the cell walls (Wolf, 1992). Previous studies indicate an early up-regulation of ß-1,3-glucanases in *Bgh* inoculated barley leaves (Gregersen et al., 1997; Fric and Huttova, 1993). Similar upregulation profiles are caused by necrotrophic plant pathogens such as *Fusarium graminearum* infestation on barley roots which underlines a basal resistance response (Deshmukh and Kogel, 2007). Interestingly, a second overexpression of *HvGlb1* was during secondary mycelia growth which start a second penetration phase. Highest relevant wavelength bands for *HvGlb1* expression profile are in accordance with the mainly influenced wavelengths during early powdery mildew pathogenesis, which reveals *HvGlb1* as a possible *Bgh* penetration indicator (Thomas et al., 2017; Kuska et al., 2015; Wahabzada et al., 2015a; Mahlein et al., 2012).

The influence of *Bgh* on the gene expression of *JIP23* was as expected. After *Bgh* invaginates the epidermal cell and develops a functional haustorium, effector proteins are secreted by *Bgh* to successfully infest the plant and to overcome plant immunity (Ahmed et al., 2015; Robatzek and Somssich, 2002, 2001). Investigation by Scheler et al. (2016) provided evidence of early *HvJIP23* transcript suppression due to *Bgh* infestation which is strongly linked to jasmonate activity and its associated induced systemic resistance (Campos et al., 2014; Schweizer et al., 1993). In addition, jasmonates cause loss of chlorophyll, underlining their role in leaf senescence (Creelman and Mullet, 1997; Miyamoto et al., 1997). Relevant wavelength bands around 550 nm, 640-690 nm and 720-830 nm for *HvJIP23* expression profiles in *Bgh* inoculated WT leaves are known to correlate to the chlorophyll content, the photosynthetic activity and the leaf cell

structure (Zhao et al., 2016; Gates et al., 1965).

5.5.3 HSI reveals the metabolism during incompatible barley-powdery mildew interactions

Upregulated *HvDRF* and *HvRuBisCO* in *Bgh* inoculated *mlo3* are an evidence for a finished resistance response (reviewed in Rojas et al. (2014)). This result is in accordance with studies by Swarbrick et al. (2006) which analyzed a high transcript amount of *RuBisCO* related genes in a *Bgh* inoculated *mlo5* genotype from 3 dai. The *HvRuBisCO* expression profile in this study underlines relevant wavebands in the green and red range, elucidating the coherency of RuBisCO to the photosynthesis apparatus (Sicher and Bunce, 1997; Scholes et al., 1994). In addition, wavelength bands in the NIR are relevant due to the influence of RuBisCO on barley leaf cell development (Zielinski et al., 1989).

Further spectral coherency of gene expressions in *mlo3* were revealed for *HvPR3* expression, which is not known to be directly involved in barley *mlo* base resistance response. Relevant wavelength bands for *HvGlb1* expression profiles in *Bgh* inoculated *Mla1* reveals important spectral ranges for early *Bgh* infestation. If *HvGlb1* is a potential *Bgh* penetration indicator, these results are in accordance with studies by Kuska et al. (2017). They observed several successful penetrations of *Bgh* on resistant *Mla1* leaves which were later stopped by strong HRs. Interestingly, *HvPR2* expression profiles indicate high relevance to wavelengths around 680 nm. This spectral range is strongly influenced by the undergoing HR and associated cell death. Furthermore, *HvPR5* expression profiles and corresponding relevant wavelengths underline the important role of *HvPR* gene regulation during HR and cell collapsing.

The link between phenomic data and known parameters from 'omic and physiological studies is highly demanded to establish high-throughput phenotyping pipelines in crop breeding and crop improvement (Simko et al., 2017; Mahlein, 2016; Großkinsky et al., 2015). Results of the present study successfully prove a link between gene expression and hyperspectral reflectance. According to the hypotheses by Furbank and Tester (2011), it is also possible to study the function of genes using the phenomic information derived from the hyperspectral reflectance. The Relief algorithm determined the relevant wavelength bands for a specific gene expression profile and enabled the interpretation of the coherency based on the gene transcript responsibility. Until now, only few studies attempt to find these functional relations among spectral phenomics and genomic data. Recently, sugar beet inbred lines differing in two quantitative trait loci against *Cercospora* leaf spot could be differentiate according to disease severity using HSI (Leucker et al., 2017). This provides evidence that spectral technologies bear the potential to be implemented in exhaustive breeding processes. In a next step, the impact of proteins, secondary metabolites and hormones on spectral profiles during barley-*Bgh* interactions needs to be investigated. This would reveal a comprehensive phenotyping of a genotype and will support the development of hyperspectral-gene maps and will improve existing crop physiological modelling e.g. Yin et al. (2004). Then, assessed relevant wavebands of specific gene/protein/metabolite activities need to be validated by using knock-out mutants. This will establish novel approaches for plant-pathogen interaction studies and crop resistance breeding.

CHAPTER 6

Summary and outlook

Identification and characterization of resistance reactions of crop plants against fungal pathogens are essential to select resistant genotypes. Phenotyping of genotypes is realized by labor intensive visual plant ratings. To accelerate time and cost expensive visual rating in plant breeding, sensor based phenotyping-platforms are necessary. Hyperspectral imaging has been proved to be a promising tool to assess different plant parameters. However, the biological meaning of the reflected electromagnetic spectrum during a pathogenesis or subtle resistance reaction needs to be investigated and proven.

Therefore, the present study is focused on hyperspectral imaging to detect and characterize plant resistance responses. Two resistance reactions (*mlo* and *Mla* based resistance) of barley (*Hordeum vulgare* L.) against infections by *Blumeria graminis* f.sp. *hordei* (*Bgh*), the causal agent of powdery mildew on barley were used as a model system. The mildew locus o (*mlo*) gene based resistance of barley inhibit *Bgh* infestation by fast cell wall aggregations at sites of attempted fungal penetration, so called papilla. Mildew locus a (*Mla*) gene based resistance of barley leads to a hypersensitive response in a single cell or cell structures and finally necrotizes the penetrated cells.

Effects of the pathogenesis and resistance responses on the reflectance pattern of barley primary leaves were recorded during their temporal and spatial development on the microscopic scale. Histological and gene expression analysis were used to interpret the spectral information and the interaction processes on a small scale.

- Spatial, temporal and visual differences during barley-powdery mildew interactions were observed. First symptoms occurred 4 dai as small white spots on susceptible barley plants pathogenesis. Characteristic powdery mildew pustules appeared 5-6 dai, while new conidiophores were developed. Histological analysis using coomassie brilliant blue staining confirmed the specific ontogenesis of *Bgh* on susceptible plants.

  Resistant *mlo3* barley did not show any symptoms after inoculation with *Bgh*. The senescence of the detached and inoculated leaves were decelerated until 13 dai. Successful papillae were developed 1 dai and inhibit the penetration at the site of infections. Young papillae indicate H_2O_2 generations which were also observed in anticlinal cell walls using 3,3'-diaminobenzidine staining for histological observations.

Bgh penetrates epidermal cells of *Mla1* barley. Further development of *Bgh* was inhibited by a hypersensitive response (HR), indicated by high H_2O_2 generations from 1 dai. Cell structures undergoing a HR were macroscopically visible as small brown spots from 5 dai.

- Gene expression profiles for 0.5, 12, 24, 48 and 72 hai indicated different transcriptional processes during barley-powdery mildew interactions.

  Bgh inoculated susceptible barley showed down-regulation of senescence corresponding genes until 72 hai. Nevertheless, a resistance response by susceptible barley against *Bgh* was observed by up-regulated *PR* genes 12 and 72 hai. During *Bgh* penetration a ß-1-3,1-4-D-glucanase showed increased transcription activity.

  Inoculated *mlo3* leaves showed an increased activity of a *chitinase 2* and *PR2* transcript at early time points. With the exception of cell metabolism indicators, gene expression profiles of inoculated compared to healthy *mlo3* leaves were not significantly different from 72 hai.

  Proved genes of inoculated *Mla1* barley were mostly down regulated. Significant up regulated genes were a ß-1-3,1-4-D-glucanase and a jasmonate induced protein transcript at 48 hai. These gene expression profile indicated a *Bgh* penetration and induced HR.

- A hyperspectral imaging microscope measurement system was established in this study to determine spectral changes on the leaf and on the cellular level of barley during early resistance reactions against *Bgh*. In addition, a protocol with detached primary leaves of barley on an agar plate system was established and proved to ensure stable and reliable conditions during spectral measurements.

- Characteristic spectral signatures of susceptible barley were recorded with the new hyperspectral imaging microscope 0 to 14 days after inoculation.

  The reflectance spectrum of the inoculated susceptible leaves did not change until 2 dai, while the corresponding healthy leaves showed an increased reflectance intensity from 500-660 nm. An increase in reflectance in this specific wavelength range indicates natural senescence. Powdery mildew pathogenesis influence the reflectance 400-680 nm and around 690 nm and 710 nm from 3 dai. Reflectance in the blue range cause a convex bend pattern and the green peak increased at 550 nm 5 dai. The cellular structure of the leaves changed during the powdery mildew pathogenesis which is indicated in spectral changes of the near infrared (NIR) from 700-730 nm. Finally, the leaves necrotized and showed a plateau reflectance pattern from 550-650 nm.

  Calculating reflectance differences of *mlo3* healthy and inoculated leaves revealed changes from 480-670 nm, ~700 nm and 730-830 nm 2-3 dai. From then, the reflectance spectrum of inoculated *mlo3* barley did not change until 13 dai.

  Reflectance intensity decreased in the NIR from 720-830 nm during the hypersensitive response of *Bgh* inoculated *Mla1* barley 2 dai. In addition, reflectance spectra from 640-690 nm increased during HR. This spectral pattern became more prominent until 7 dai.

- By applying Simplex Volume Maximization (SiVM) as an advanced method from machine learning on hyperspectral imaging data, an automated extraction of characteristic spectral reflectance of barley-powdery mildew interactions was obtained. Differences between automated and manually assessed reflectance values were between 2-4 %.

  Spectral traces indicated reflectance differences between *Bgh* inoculated susceptible and *mlo3* resistant barley based on distances among traces and their directions. In addition,

spectral traces revealed the genotype specific hyperspectral dynamic for each interaction type.

SiVM reduces the data dimension because it decomposes a hyperspectral image into extreme data vectors and represent each spectral signature by a linear combination of them. This enabled a consecutive statistical analysis and interpretable image clustering. For *Bgh* inoculated susceptible leaves a binary map system was established which accurately indicated diseased spots from 3 dai and following. Retrospective analysis of the HR of *Mla1* barley against *Bgh* infection were improved by HR binary maps, which indicated subtle spots undergoing a HR from 2 dai. This allowed a precise selection of areas of interest for further hyperspectral image analysis.

- Relevant wavelengths and reflectance intensities during barley-powdery mildew interactions were determined by applying the Relief algorithm.

  Therefore, barley-powdery mildew interactions were hyperspectrally measured every 3 hours until 5 dai. During early pathogenesis, 500-660 nm was identified as the relevant functional spectral range. After *Bgh* established an haustoria, reflectance around 690-710 nm was also relevant. Before white pustules appeared, spectral ranges from 400 to 520 nm and 580-700 nm were important. Later pathogenesis stages showed 400-530 nm, 580-700 nm and 710-840 nm as relevant wavelength bands.

  During papilla formation, *mlo3* barley 400-690 nm and around 700 nm was revealed as relevant spectral range.

  The *Mla1* gene based hypersensitive response against *Bgh* showed ~500 nm, ~680 nm and 720-830 nm as relevant spectral ranges in early stages. After the HR was finished, spectral reflectance around 400 nm, ~550 nm and ~730 nm were relevant. Furthermore, the Relief algorithm assessed the highest relevant wavebands and spectral intensities 0.5, 12, 24, 48 and 72 hai for all three proved interaction types. Significance of the spectral changes was confirmed by Welch's t-test.

  The coherency between hyperspectral reflectance and gene expression profiles could be evaluated. Therefore, important wavelength bands and spectral intensities for seven genes were obtained by applying the Relief algorithm. The proved interaction types showed different gene expression profiles which was also indicated in the most relevant wavelengths for each gene. *HvRuBisCO* expression profiles exhibited relevant wavebands in the green and red range elucidating the coherency to the photosynthesis apparatus. Highest relevant wavelength bands for a ß-1-3,1-4-D-glucanase transcript activity in *Bgh* inoculated susceptible barley were around the blue, green and red range which are mainly influenced during early powdery mildew pathogenesis. *HvPR5* underlines an important role during HR and cell decomposition in *Mla1* barley and showed highly relevant bands in the green range and around 680 nm, as well as in the NIR.

Hyperspectral imaging can increase the objectivity of phenotyping processes and gives new insights into host-pathogen interactions. The analysis of individual interactions using hyperspectral imaging enables a specific characterization in space and time. In addition to its non-invasive nature in the detection of host-pathogen interactions, hyperspectral imaging opens new opportunities to investigate biological processes. According to this study, a coherency between gene transcriptional activity and the reflectance spectrum of plants is detectable. For the development of hyperspectral-gene maps further investigations are necessary. Therefore, a gene chip analysis of barley-powdery mildew interactions could provide a sufficient overview of gene activities

which must be linked to hyperspectral reflectance characteristics. Assessed relevant wavebands of specific gene activities can be then validated by knock-out mutants, such as using molecular cloning or clustered regularly interspaced short palindromic repeats (CRISPR) gene editing. This will also enable the identification of multiple resistant barley varieties using HSI.

For an exhaustive knowledge, the analysis of the spectral impact of proteins, secondary metabolites and hormones during barley-powdery mildew interactions and their relation to spectral properties is required. This will reveal a global phenotyping of individual genotypes.

Currently, a combination of hyperspectral imaging with histological and molecular methods is necessary for the characterization and interpretation of the spectral reflectance. But in a foreseeable future, hyperspectral imaging can reduce the lab effort of standardized analysis and could be used for basic biological studies. Parameters influencing the plant phenotype and current possible detections of different plant parameters by hyperspectral imaging are illustrated in Fig. 32.

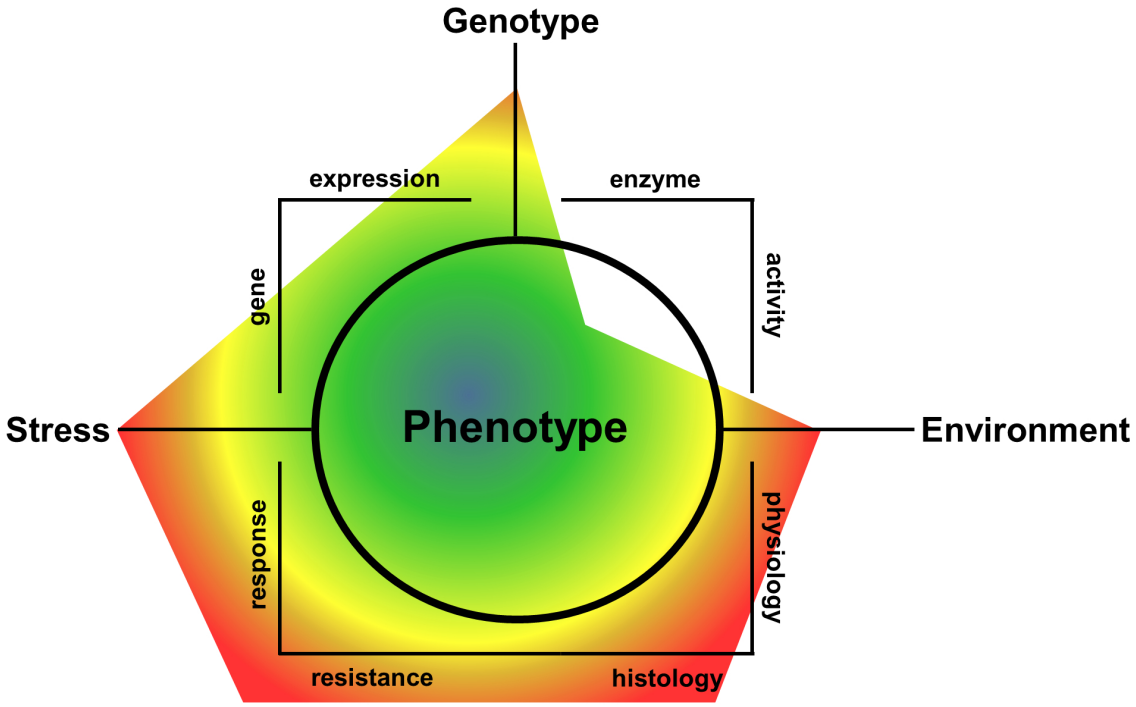

Figure 32: Parameters influencing the plant phenotype. Furthermore, plant parameters and phenotype relevant factors which can be detected and characterized using hyperspectral imaging are indicated by the coloured hexagon. Different stresses can be determined and assessed by hyperspectral imaging. Physiological and histological studies are mainly used for the biological interpretation of the reflectance spectrum like for plant pathogen resistance detection. In accordance to this study, the combination with gene expression profiles elucidates a functional link between hyperspectral reflectance and gene expressions. The influence of enzyme activities on the spectral reflectance pattern of plants is still unknown.

By applying data driven techniques such as SiVM or the Relief algorithm, an automatic extraction of significant spectral reflectance wavebands as well as relations to changes on the cellular and gene level was realized. The results of data drive approaches need to be validated by experts and have to be linked to biological processes. But data driven approaches also provide interpretable results and models of complex spectral data which are easy to understand even by non-experts e.g. spectral traces and binary maps of barley-powdery mildew interactions in this thesis. By machine learning, the assessment of different plant parameters was possible, like the differentiation of diseased and healthy plants or leaf areas. With this approach, all image pixels are considered by the computer in a fraction of time compared to human investigation. Nevertheless, the pixel allocation by the algorithm can be inaccurate. For a high accuracy and correct allocation a training data set with manually labeled parameters must be learned by the computer. Hereby, the biological interpretation is done before unknown data can be analyzed. These supervised approaches are easy to understand, but limit the results on the trained parameters. In a next step, a machine learning pipeline could be developed that collects representative spectral signatures of host-pathogen interactions for a hyperspectral library. Subsequently, this collection must be evaluated by experts. However, this will open a global and interactive collection of plant spectral reflectance properties.

As a basis, the new outcomes of this study support an accelerated and accurated analysis of hyperspectral images based on manual and automated approaches. The established hyperspectral imaging microscope provides the basis to determine subtle plant-pathogen interactions such as early pathogenesis and plant resistance responses. Furthermore, it was proven that spectral changes during powdery mildew pathogenesis, *mlo* and *Mla* based resistance reactions are biologically interpretable. Finally, a coherency between the plant phenotype and genotype was indentified by correlations between gene expression profiles of barley and spectral properties during barley-powdery mildew interactions. For plant resistance phenotyping the results from proximal sensing will be transferred on the plant and field scale. State-of-the-art phenotyping green house facilities will be the first step to establish high-throughput phenotyping pipelines. In such approaches the whole plant will be measured and new important parameters for hyperspectral imaging which expand the spectral plant pattern will be considered such as plant organs, plant architecture, leaf angle, leaf overlapping and focus plain.

References

Ahmed, A. A., Pedersen, C., Schultz-Larsen, T., Kwaaitaal, M., Jørgensen, H. J. L., and Thordal-Christensen, H. (2015). The barley powdery mildew candidate secreted effector protein CSEP0105 inhibits the chaperone activity of small heat shock protein. *Plant Physiology*, 168:321–333.

Aken, O. and Breusegem, F. (2015). Licensed to kill: Mitochondria, chloroplasts, and cell death. *Trends in Plant Science*, 20:754–766.

Arens, N., Backhaus, A., Döll, S., Fischer, S., Seiffert, U., and Mock, H. P. (2016). Non-invasive presymptomatic detection of *Cercospora beticola* infection and identification of early metabolic responses in sugar beet. *Frontiers in Plant Science*, 7:1377.

Assaad, F. F., Qiu, J. L., Youngs, H., Ehrhardt, D., Zimmerli, L., Kalde, M., Wanner, G., Peck, S. C., Edwards, H., Ramonell, K., Sommerville, C. R., and Thordal-Christensen, H. (2004). The PEN1 syntaxin defines a novel cellular compartment upon fungal attack and is required for the timely assembly of papillae. *Molecular Biology of the Cell*, 15:5118–5129.

Azevedo, C., Sadanandom, A., Kitagawa, K., Freialdenhoven, A., Shirasu, K., and Schulze-Lefert, P. (2002). The RAR1 Interactor SGT1, an essential component of *R* gene-triggered disease resistance. *Science*, 295:2073–2076.

Baxter, A., Mittler, R., and Suzuki, N. (2014). ROS as key players in plant stress signalling. *Journal of Experimental Botany*, 65:1229–1240.

Bayles, C. J., Ghemawat, M. S., and Aist, J. R. (1990). Inhibition by 2-deoxy-D-glucose of callose formation, papilla deposition, and resistance to powdery mildew in an ml-o barley mutant. *Physiological and Molecular Plant Pathology*, 36:63–72.

Behmann, J., Mahlein, A. K., Rumpf, T., Römer, C., and L., P. (2015). A review of advanced machine learning methods for the detection of biotic stress in precision crop protection. *Precision Agriculture*, 16:239–260.

Bell, A. A. (1981). Biochemical mechanisms of disease resistance. *Annual Review of Plant Physiology*, 32:21–81.

Benhamou, N., Joosten, M. H. A. J., and De Wit, P. J. G. M. (1990). Subcellular localization of chitinase and of potential substrate in tomato root tissue infected by *Fusarium oxysporum* f.sp. *radicis-lycopersici*. *Plant Physiology*, 92:1108–1120.

Bhat, R. A., Miklis, M., Schmelzer, E., Schulze-Lefert, P., and Panstruga, R. (2005). Recruitment and interaction dynamics of plant penetration resistance components in a plasma membrane microdomain. *Proceedings of the National Academy of Sciences USA*, 102:3135–3140.

Bieri, S., Mauch, S., Shen, Q. H., Peart, J., Devoto, A., Casais, C., Ceron, F., Schulze, S., Steinbiß, H. H., Shirasi, K., and Schulze-Lefert, P. (2004). *Rar1* positively controls steady state levels of barley *Mla* resistance proteins and enables sufficient *Mla6* accumulation for effective resistance. *The Plant Cell*, 16:3480–3495.

Blackburn, G. A. (2007). Hyperspectral remote sensing of plant pigments. *Journal of Experimental Botany*, 58:855–867.

Blanvillain, R., Young, B., Cai, Y. M., Hecht, V., Varoquaux, F., Delorme, V., Lancelin, J. M., Delseny, M., and Gallois, P. (2011). The *Arabidopsis* peptide kiss of death is an inducer of programmed cell death. *The EMBO Journal*, 30:1173–1183.

Blumer, S. (1967). Echte Mehltaupilze (*Erysiphaceae*). *VEB Gustav Fischer Verlag*.

Bock, C. H., Poole, G. H., Parker, P. E., and Gottwald, T. (2010). Plant disease severity estimated visually, by digital photography and image analysis, and by hyperspectral imaging. *Critical Reviews in Plant Sciences*, 29:59–107.

Bogaerts, J., Dierickx, B., De Moor, P., Tezcan, D. S., De Munck, K., and van Hoof, C. (2005). High-end CMOS active pixel sensor for hyperspectral imaging. *Proceedings of IEEE International Workshop on CCD and Advanced Image Sensors*, pages 39–43.

Borlaug, N. E. (2002). Feeding a world of 10 billion people: The miracle ahead. *In Vitro Cellular and Developmental Biology - Plant*, 38:221–228.

Both, M., Csukai, M., Stumpf, M. P. H., and Spanu, P. D. (2005). Gene expression profiles of *Blumeria graminis* indicate dynamic changes to primary metabolism during development of an obligate biotrophic pathogen. *The Plant Cell*, 17:2107–2122.

Boyd, L. A., Smith, P. H., Foster, E. M., and Brown, J. K. M. (1995). The effects of allelic variation at the Mla resistance locus in barley on the early development of *Erysiphe graminis* f.sp. *hordei* and host response. *Plant Journal*, 7:959–968.

Burns, D. A. (2008). Historical Development. In Burns, D. A. and Ciurczak, E. W., editors, *Handbook of near-infrared analysis 3rd edition*, chapter 1, pages 3–6. CRC Press Taylor and Francis Group USA.

Büschges, R., Hollricher, K., Panstruga, R., Simons, G., Wolter, M., Frijters, A., van Daelen, R., van der Lee, T., Diergaarde, P., Groenendijk, J., Töpsch, S., Vos, P., Salamini, F., and Schulze-Lefert, P. (1997). The barley *Mlo* gene: A novel control element of plant pathogen resistance. *Cell*, 88:695–705.

Bushnell, W. R. and Bergquist, S. E. (1974). Aggregation of host cytoplasm and the formation of papillae and haustoria in powdery mildew of barley. *Phytopathology*, 65:310–318.

Caldo, R. A., Nettleton, D., and P., W. R. (2004). Interaction-dependent gene expression in *Mla*-specified response to barley powdery mildew. *The Plant Cell*, 16:2514–2528.

Campos, M. L., Kang, J. H., and Howe, G. A. (2014). Jasmonate-triggered plant immunity. *Journal of Chemical Ecology*, 40:657–675.

Caplan, J., Padmanabhan, M., and Dinesh-Kumar, S. P. (2008). Plant NB-LRR immune receptors: From recognition to transcriptional reprogramming. *Cell Host and Microbe*, 3:126–135.

Carter, G. A. and Knapp, A. K. (2001). Leaf optical properties in higher plants: Linking spectral characteristics to stress and chlorophyll concentrations. *American Journal of Botany*, 88:677–684.

Chaerle, L., Hagenbeek, D., De Buyne, E., Valcke, R., and Van Der Straeten, D. (2004). Thermal and chlorophyll-fluorescence imaging distinguish plant-pathogen interactions at an early stage. *Plant and Cell Physiology*, 45:887–896.

Chaerle, L., Leinonen, I., Jones, H. G., and Van Der Straeten, D. (2007). Monitoring and screening plant populations with combined thermal and chlorophyll fluorescence imaging. *Journal of Experimental Botany*, 58:773–784.

Chang, C., Deshui, Y., Jiao, J., Jing, S., Schulze-Lefert, P., and Shen, Q. H. (2013). Barley Mla immune receptors directly interfere with antagonistically acting transcription factors to initiate disease resistance signalling. *Plant and Cell Physiology*, 25:1158–1173.

Chapman, A. V. E., Surana, P., Hunt, M. R., Fuerst, G., and Wise, R. (2016). Required for *Mla* Resistance 3, a new player in barley powdery mildew resistance? *Plant and Animal Genome Conference XXIV*, page P0911 (poster).

Cheng, J. H., Nicolai, B., and Sun, D. W. (2017). Hyperspectral imaging with multivariate analysis for technological parameters prediction and classification of muscle foods: A review. *Meat Science*, 123:182–191.

Chowdhury, J., Henderson, M., Schweizer, P., Burton, R. A., Fincher, G. B., and Little, A. (2014). Differential accumulation of callose, arabinoxylan and cellulose in nonpenetrated versus penetrated papillae on leaves of barley infected with *Blumeria graminis* f.sp. *hordei*. *New Phytologist*, 204:650–660.

Clay, K., Reinhart, K., Rudgers, J., Tintjer, T., Koslow, J., and L., F. S. (2008). Red Queen Communities. In Ostfeld, R. S., Keesing, F., and Eviner, V. T., editors, *Infectious Disease Ecology - The Effects of Ecosystems on Disease and of Disease on Ecosystems*, pages 145–178. A Princeton University Press USA.

Cobb, J. N., DeClerck, G., Greenberg, A., Clark, R., and McCouch, S. (2013). Next-generation phenotyping: Requirements and strategies for enhancing our understanding of genotype-phenotype relationships and its relevance to crop improvement. *Theoretical and Applied Genetics*, 126:867–887.

Collins, N. C., Thordal-Christensen, H., Lipka, V., Bau, S., Kombrink, E., Qiu, J. L., Hückelhoven, R., Stein, M., Freialdenhoven, A., Somerville, S. C., and Schulze-Lefert, S. (2003). SNARE-protein-mediated disease resistance at the plant cell wall. *Nature*, 425:973–977.

Consonni, C., Humphry, M. E., Hartmann, A. A., Livaja, M., Durner, J., Westphal, L., Vogel, J., Lipka, V., Kemmerling, B., Schulze-Lefert, P., Somerville, S. C., and Panstruga, R. (2006). Conserved requirement for a plant host cell protein in powdery mildew pathogenesis. *Nature*, 38:716–720.

Creelman, R. A. and Mullet, J. E. (1997). Biosynthesis and action of jasmonates in plants. *Annual Review of Plant Physiology*, 48:355–381.

Curran, P. J. (1989). Remote sensing of foliar chemistry. *Remote Sensing of Environment*, 30:271–278.

Dangl, J. L. and Jones, J. D. G. (2001). Plant pathogens and integrated defence response to infection. *Nature*, 411:826–833.

Delalieux, S., Aardt, J., Keulemans, W., Schrevens, E., and Coppin, P. (2007). Detection of biotic stress (*Venturia inaequalis*) in apple trees using hyperspectral data: Non-parametric statistical approaches and physiological implications. *European Journal of Agronomy*, 27:130–143.

Deshmukh, S. D. and Kogel, K. H. (2007). *Piriformospora indica* protects barley from root rot caused by *Fusarium graminearum*. *Journal of Plant Diseases and Protection*, 114:263–268.

Devoto, A., Piffanelli, P., Nilsson, I., Wallin, E., Panstruga, R., von Heijne, G., and Schulze-Lefert, P. (1999). Topology, subcellular localization, and sequence diversity of the Mlo family in plants. *Journal of Biological Chemistry*, 274:34993–35004.

Dore, I., Legrand, M., Cornelissen, B. J. C., and Bol, J. F. (1991). Subcellular localization of acidic and basic PR proteins in tobacco mosaic virus infected tobacco. *Archives of Virology*, 120:97–107.

Douchkov, D., Lueck, S., Hensel, G., Kumlehn, J., Rajaraman, J., Johrde, A., Doblin, M. S., Beahan, C. T., Kopischke, M., Fuchs, R., Lipka, V., Niks, R. E., Bulone, V., Chowdhury, J., Little, A., Burton, R. A., Bacic, A. N., Fincher, G. B., and Schweizer, P. (2016). The barley (*Hordeum vulgare*) cellulose synthase-like D2 gene (*HvCslD2*) mediates penetration resistance to host-adapted and nonhost isolates of the powdery mildew fungus. *New Phytologist*, 212:421–433.

Eggert, D., Naumann, M., Reimer, R., and Voigt, C. A. (2014). Nanoscale glucan polymer network causes pathogen resistance. *Scientific Reports*, 4:4159.

Eichmann, R., Bischof, M., Weis, C., Shaw, J., Lacomme, C., Schweizer, P., Duchkov, D., Hensel, G., Kumlehn, J., and Hückelhoven, R. (2010). Bax Inhibitor-1 is required for full susceptibility of barley to powdery mildew. *Molecular Plant-Microbe Interactions*, 23:1217–1227.

Ellingboe, A. H. (1980). Changing concepts in host-pathogen genetics. *Annual Review of Phytopathology*, 19:125–143.

Ellis, J. G., Lawrence, G. J., Luck, J. E., and N., D. P. (1999). Identification of regions in alleles of the flax rust resistance gene L that determine differences in gene-for-gene specificity. *The Plant Cell*, 11:495–506.

Faik, A. (2010). Xylan Biosynthesis: News from the grass. *Plant Physiology*, 153:396–402.

Farmer, E. E. and Ryan, C. (1992). Octadecanoid precursors of jasmonic acid activate the synthesis of wound-inducible proteinase inhibitors. *The Plant Cell*, 4:129–134.

Fiorani, F., Rascher, U., Jahnke, S., and Schurr, U. (2012). Imaging plants dynamics in heterogenic environments. *Current Opinion in Biotechnology*, 23:227–235.

Fiorani, F. and Schurr, U. (2013). Future scenarios for plant phenotyping. *Annual Review of Plant Biology*, 64:267–291.

Fischer, C. and Kakoulli, I. (2006). Multispectral and hyperspectral imaging technologies in conservation: Current research and potential applications. *Resources Conservation and Recycling*, 7:1–16.

Francis, S. A., Dewey, F. M., and Gurr, S. J. (1996). The role of cutinase in germling development and infection by *Erysiphe graminis* f. sp. *hordei*. *Physiological and Molecular Plant Pathology*, 49:201–211.

Freialdenhoven, A., Peterhänsel, C., Kurth, J., Kreuzaler, F., and Schulze-Lefert, P. (1996). Identification of genes required for the function of non-race-specific *mlo* resistance to powdery mildew in barley. *The Plant Cell*, 8:5–14.

Freytag, S., Arabatzis, N., Hahlbrock, K., and Schmelzer, E. (1994). Reversible cytoplasmic rearrangements precede wall apposition, hypersensitive cell death and defense-related gene activation in potato *Phytophthora infestans* interactions. *Planta*, 194:123–135.

Fric, F. and Huttova, J. (1993). Glucanase, glucan synthase and chitinase activity in barley genotypes susceptible or resistant to *Erysiphe graminis* f.sp. *hordei*. *Biologia Plantarum*, 35:95–101.

Friedli, M., Kirchgessner, N., Grieder, C., Liebisch, F., Mannale, M., and Walter, A. (2016). Terrestrial 3D laser scanning to track the increase in canopy height of both monocot and dicot crop species under field conditions. *Plant Methods*, 12:9.

Fu, Z. Q. and Dong, X. (2013). Systemic acquired resistance: Turning local infection into global defense. *Annual Review of Plant Biology*, 64:839–863.

Furbank, R. T. and Tester, M. (2011). Phenomics - technologies to relieve the phenotyping bottleneck. *Trends in Plant Science*, 16:635–644.

Gamon, J. A., Serrano, L., and Surfus, J. S. (1997). The photochemical reflectance index: An optical indicator of photosynthetic radiation use efficiency across species, functional types, and nutrient levels. *Oecologia*, 112:492–501.

Gamon, J. A. and Surfus, J. S. (1999). Assessing leaf pigment content and activity with a reflectometer. *New Phytologist*, 143:105–117.

Gates, D. M., Keegan, H. J., Schelter, J. C., and Weidner, V. R. (1965). Spectral properties of plants. *Applied Optics*, 4:11–20.

Gay, A., Thomas, H., Roca, M., James, C., Taylor, J., Rowland, J., and Ougham, H. (1987). Dynamic experimental evidence for the plasma membrane ATPase domain hypothesis of haustorial transport and for ionic coupling of the haustorium of *Erysiphe graminis* to the host cell (*Hordeum vulgare*). *New Phytologist*, 107:541–548.

Gay, A., Thomas, H., Roca, M., James, C., Taylor, J., Rowland, J., and Ougham, H. (2008). Nondestructive analysis of senescence in mesophyll cells by spectral resolution of protein synthesis-dependent pigment metabolism. *New Phytologist*, 179:663–674.

Giessen, J. E., W., H., and R., S. (1956). Die Gersten Athiopiens und Erythraas. *Zeitschrift für Pflanzenzüchtung*, 35:377–440.

Gitelson, A., Gritz, Y., and Merzlyak, M. N. (2003). Relationships between leaf chlorophyll content and spectral reflectance and algorithms for non-destructive chlorophyll assessment in higher plant leaves. *Journal of Plant Physiology*, 160:271–282.

Glawe, D. A. (2008). The powdery mildews: A review of the world's most familiar (yet poorly known) plant pathogens. *Annual Review of Phytopathology*, 46:27–51.

Green, J. R., Carver, T. L. W., and Gurr, S. J. (2002). The formation and function of infection and feeding structures. In Bélanger, R. R., Bushnell, W. R., Dik, A. J., and Carver, T. L. W., editors, *The Powdery Mildews - a Comprehensive Treatise*, pages 66–82. American Phytopathological Society (APS Press USA).

Greenberg, J. T. (1997). Programmed cell death in plant-pathogen interactions. *Annual Review of Plant Physiology and Plant Molecular Biology*, 48:525–545.

Greenberg, J. T. and Yao, N. (2004). The role and regulation of programmed cell death in plant-pathogen interactions. *Cellular Microbiology*, 6:201–211.

Gregersen, P. L., Thordal-Christensen, H., Forster, H., and Collinge, D. B. (1997). Differential gene transcript accumulation in barley leaf epidermis and mesophyll in response to attack by *Blumeria graminis* f.sp. *hordei* (syn. *Erysiphe graminis* f.sp. *hordei*). *Physiological and Molecular Plant Pathology*, 51:85–97.

Grenier, J., Potvin, C., Trudel, J., and Asselin, A. (1999). Some thaumatin-like proteins hydrolyse polymeric ß-1,3-glucans. *The Plant Journal*, 19:473–480.

Großkinsky, D., Svensgaard, J., Christensen, S., and Roitsch, T. (2015). Plant phenomics and the need for physiological phenotyping across scales to narrow the genotype-to-phenotype knowledge gap. *Journal of Experimental Botany*, 66:5429–5440.

Guyon, I. and Ellisseeff, A. (2003). An introduction to variable and feature selection. *Journal of Machine Learning Research*, 3:1157–1182.

Hacquard, S., Kracher, B., Maekawa, T., Vernaldi, S., Schulze-Lefert, P., and Themaat, E. V. L. (2013). Mosaic genome structure of the barley powdery mildew pathogen and conservation of transcriptional programs in divergent hosts. *Proceedings of the National Academy of Sciences USA*, 110:2219–2228.

Häffner, E., Konietzki, S., and Diederichsen, E. (2015). Keeping Control: The role of senescence and development in plant pathogenesis and defense. *Plants*, 4:449–488.

Haltermann, D. A. and Wise, R. P. (2004). A single-amino acid substitution in the sixth leucine-rich repeat of barley Mla6 and Mla13 alleviates dependence on Rar1 for disease resistance signaling. *The Plant Journal*, 38:215–226.

Hartmann, A., Czauderna, T., Hoffmann, R., Stein, N., and Schreiber, F. (2011). HTPheno: An image analysis pipeline for high-throughput plant phenotyping. *BMC Bioinformatics*, 12:148.

Heim, R. H. J., Jürgens, N., Große-Stoltenberg, A., and Oldeland, J. (2015). The effect of epidermal structures on leaf spectral signatures of ice plants (*Aizoaceae*). *Remote Sensing*, 7:16901–16914.

Hejgaard, J., Jacobsen, S., and Svendsen, I. (1991). Two antifungal thaumatin-like proteins from barley grain. *The FEBS Journal*, 291:127–131.

Hinze, K., Thompson, R. D., Ritter, E., Salamini, F., and Schulze-Lefert, P. (1991). Restriction fragment length polymorphism-mediated targeting of the ml-o resistance locus barley (*Hordeum vulgare*). *Proceedings of the National Academy of Sciences USA*, 88:3691–3695.

Hippe-Sanwald, S., Hermanns, M., and Somerville, S. C. (1992). Ultrastructural comparison of incompatible and compatible interactions in the barley powdery mildew disease. *Protoplasma*, 168:27–40.

Hubert, D. A., Tornero, P., Belkhadir, Y., Krishna, P., Takahashi, A., Shirasu, K., and Dangl, J. L. (2003). Cytosolic HSP90 associates with and modulates the Arabidopsis RPM1 disease resistance protein. *The EMBO Journal*, 22:5679–5689.

Hückelhoven, R., Fodor, J., Preis, C., and Kogel, K. H. (1999). Hypersensitive cell death and papilla formation in barley attacked by the powdery mildew fungus are associated with hydrogen peroxide but not with salicylic acid accumulation. *Plant Physiology*, 119:1251–1260.

Hückelhoven, R., Fodor, J., Trujillo, M., C., and Kogel, K. H. (2000). Barley *Mla* and *Rar* mutants compromised in the hypersensitive cell death response against *Blumeria graminis* f.sp. *hordei* are modified in their ability to accumulate reactive oxygen intermediates at sites of fungal invasion. *Planta*, 212:16–24.

Hückelhoven, R. and Kogel, K. H. (1998). Tissue-specific superoxide generation at interaction sites in resistant and susceptible near-isogenic barley lines attacked by the powdery mildew fungus (*Erysiphe graminis* f.sp. *hordei*). *Molecular Plant-Microbe Interactions*, 11:292–300.

Iori, A., Scala, V., Cesar, D., Pinzari, F., Dégidio, M. G., Fanelli, C., Fabbri, A. A., Reverberi, M., and Serranti, S. (2015). Hyperspectral and molecular analysis of *Stagonospora nodorum* blotch disease in durum wheat. *European Journal of Plant Pathology*, 141:689–702.

Jackson, R. D. (1983). Spectral indices in *n*-Space. *Remote Sensing of Environment*, 13:409–421.

Jacquemoud, S. and Baret, F. (1990). PROSPECT: A model of leaf optical properties spectra. *Remote Sensing of Environment*, 34:75–91.

Jacquemoud, S. and Ustin, S. L. (2001). Leaf optical properties: A state of the art. *Proceedings of the 8th international symposium physical measurements and signatures in remote sensing (CNES)*, pages 223–232.

Jones, J. D. G. and Dangl, J. L. (2006). The plant immune system. *Nature Reviews*, 444:323–329.

Jørgensen, J. H. (1992a). Discovery, characterization and exploitation of Mlo powdery mildew resistance in barley. *Euphytica*, 63:141–152.

Jørgensen, J. H. (1992b). Multigene families of powdery mildew resistance genes in locus *Mla* on barley chromosome 5. *Plant Breeding*, 108:53–59.

Jørgensen, J. H. (1994). Genetics of powdery mildew resistance in barley. *Critical Reviews in Plant Sciences*, 13:97–119.

Jørgensen, J. H. and Mortensen, K. (1977). Primary infection by *Erysiphe graminis* f.sp. *hordei* of barley mutants with resistance genes in the *mlo* locus. *Phytopathology*, 67:678–685.

Kailath, T. (1967). The divergence and Bhattacharyya distance measures in signal selection. *IEEE Transactions on Communications*, 15:52–60.

Kersting, K., Bauckhage, C., Wahabzada, M., Mahlein, A. K., Steiner, U., Oerke, E. C., Römer, C., and Plümer, L. (2016). Feeding the world with Big Data: Uncovering spectral characteristics and dynamics of stressed plants. In Lässig, J., Kersting, K., and Morik, K., editors, *Computational Sustainability*, pages 99–120. Springer International Publishing.

Kersting, K., Xu, Z., Wahabzada, M., Bauckhage, C., Thurau, C., Römer, C., Ballvora, A., Rascher, U., Leon, J., and Plümer, L. (2012a). Pre-symptomatic prediction of plant drought stress using Dirichlet-aggregation regression on hyperspectral images. *Proceedings of the twenty-sixth conference on artificial intelligence (AAAI). Special track on Computational Sustainability and AI*, pages 302–308.

Kersting, K., Xu, Z., Wahabzada, M., Thurau, C., Römer, C., Ballvora, A., Rascher, U., Leon, J., Bauckhage, C., and Plümer, L. (2012b). Simplex distributions for embedding data matrices over time. *Proceedings of the 12th SIAM international conference on data mining*, pages 295–306.

Kira, K. and Rendell, L. A. (1992). The feature selection problem: Traditional methods and a new algorithm. *Association for the Advancement of Artificial Intelligence*, 2:129–134.

Kirchgessner, N., Liebisch, F., Yu, K., Pfeifer, J., Friedli, M., Hund, A., and Walter, A. (2017). The ETH field phenotyping platform FIP: A cable-suspended multi-sensor system. *Functional Plant Biology*, 44:154–168.

Kirubakaran, S. I. and Sakthivel, N. (2007). Cloning and overexpression of antifungal barley chitinase gene in *Escherichia coli*. *Protein Expression and Purification*, 52:159–166.

Kleinhofs, A., Kilian, A., Maroof, M. A. S., Biyashev, R. M., Hayes, P., Chen, F. Q., Lapitan, N., Fenwick, A., Blake, T. K., Kanazin, V., Ananiev, E., Dahleen, L., Kudran, D., Bollinger, J., Knapp, S. J., Liu, B., Sorrells, M., Heun, M., Franckowiak, J. D., Hoffmann, D., Skadsen, R., and Steffenson, B. J. (1993). A molecular, isozyme and morphological map of barley (*Hordeum vulgare*) genome. *Theoretical and Applied Genetics*, 86:705–712.

Kobayashi, Y., Kobayashi, I., Funaki, Y., Fujimoto, S., Takemoto, T., and Kunoh, H. (1997). Dynamic reorganization of microfilaments and microtubules is necessary for the expression of non-host resistance in barley coleoptile cells. *The Plant Journal*, 11:525–537.

Kogel, K. H. and Hückelhoven, R. (1999). Superoxid generation in chemically activated resistance of barley in response to inoculation with powdery mildew fungus. *Journal of Phytopathology*, 147:1–14.

Kogel, K. H., Ortel, B., Jarosch, B., Atzorn, R., Schiffer, R., and Wasternack, C. (1995). Resistance in barley against the powdery mildew fungus (*Erysiphe graminis* f.sp. *hordei*) is not associated with enhanced levels of endogenous jasmonates . *European Journal of Plant Pathology*, 101:319–332.

Kolbe, W. (1982). Further studies on the fungicidal activity of Baytan cereal seed treatment and its effect on yield (1975-1981). *Pflanzenschutz-Nachrichten Bayer*, 35:72–103.

Kølster, P., Munk, L., Stølen, O., and Løhde, J. (1986). Near-isogenic barley lines with genes for resistance to powdery mildew. *Crop Science*, 26:903–907.

Krupinska, K. (2007). Date and activities of plastids during leaf senescence. In Wise, R. R. and Hoober, J. K., editors, *The structure and function of plastids*, pages 433–449. Springer Science and Business Media.

Kuska, M., Wahabzada, M., Leucker, M., Dehne, H. W., Kersting, K., Oerke, E. C., Steiner, U., and Mahlein, A. K. (2015). Hyperspectral phenotyping on the microscopic scale: Towards automated characterization of plant-pathogen interactions. *Plant Methods*, 11:28.

Kuska, M. T., Brugger, A., Thomas, S., Wahabzada, M., Kersting, K., Oerke, E. C., Steiner, U., and Mahlein, A. K. (2017). Spectral patterns reveal early resistance reactions of barley against *Blumeria graminis* f. sp. *hordei*. *Phytopathology*, [in press]:doi.org/10.1094/PHYTO–04–17–0128–R.

Lamb, C. and Dixon, R. A. (1997). The oxidative burst in plant disease resistance. *Annual Review of Plant Biology*, 48:251–275.

Le Maire, G., Francois, C., and Dufrene, E. (2004). Towards universal deciduous broad leaf chlorophyll indices using PROSPECT simulated database and hyperspectral reflectance measurements. *Remote Sensing of Environment*, 89:1–28.

Leavesley, S. J., Annamdevula, N., Boni, J., Stocker, S., Grant, K., Troyanovsky, B., Rich, T. C., and Alvarez, D. F. (2012). Hyperspectral imaging microscopy for identification and quantitative analysis of fluorescently-labeled cells in highly autofluorescent tissue. *Journal of Biophotonics*, 5:67–84.

Leucker, M., Mahlein, A. K., Steiner, U., and Oerke, E. C. (2016). Improvement of lesion phenotyping in *Cercospora beticola*-sugar beet interaction by hyperspectral imaging. *Phytopathology*, 106:177–184.

Leucker, M., Mahlein, A. K., Steiner, U., and Oerke, E. C. (2017). Hyperspectral imaging reveals the effect of sugar beet quantitative trait loci on *Cercospora* leaf spot resistance. *Functional Plant Biology*, 44:1–9.

Lillesaeter, O. (1982). Spectral reflectance of partly transmitting leaves: Laboratory measurements and mathematical modeling. *Remote Sensing of Environment*, 12:247–254.

Lipka, V. and Panstruga, R. (2005). Dynamic cellular response in plant-microbe interactions. *Current Opinion in Plant Biology*, 8:625–631.

Liu, J. J., Sturrock, R., and Ekramoddoullah, A. K. M. (2010). The superfamily of thaumatin-like proteins: Its origin, evolution, and expression towards biological function. *Plant Cell Reports*, 29:419–436.

Liu, Y. L., Burch-Smith, T., Schiff, M., Feng, S. H., and Dinesh-Kumar, S. P. (2004). Molecular chaperone Hsp90 associates with resistance protein N and its signaling proteins SGT1 and Rar1 to modulate an innate immune response in plants. *Journal of Biological Chemistry*, 279:2101–2108.

Livak, K. J. and Schmittgen, T. D. (2001). Analysis of relative gene expression data using real-time quantitative PCR and the $2^{-\Delta\Delta Ct}$ -method. *Methods*, 25:402–408.

Lu, X., Kracher, B., Saur, I. M. L., Bauer, S., Ellwood, S. R., Wise, R., Yaeno, T., Maekawa, T., and Schulze-Lefert, P. (2016). Allelic barley MLA immune receptors recognize sequence-unrelated avirulence effectors of the powdery mildew pathogen. *Proceedings of the National Academy of Sciences USA*, 133:6486–6495.

Lutze, G., Schott, H., Trommer, R., and Amelung, D. (1982). On the economic assessment of damage caused by major cereal diseases. *Nachrichtenblatt für den Pflanzenschutz in der DDR*, 36:198–201.

Lyngkjaer, M., Newton, A., Atzema, J., and Baker, S. (2000). The barley *mlo*-gene: An important powdery mildew resistance source. *Agronomie*, 20:745–756.

Ma, Z. and Michailides, T. J. (2005). Advances in understanding molecular mechanisms of fungicide resistance and molecular detection of resistant genotypes in phytopathogenic fungi. *Crop Protection*, 24:853–863.

Mahlein, A. K. (2016). Plant disease detection by imaging sensors - parallels and specific demands for precision agriculture and plant phenotyping. *Plant Disease*, 2:241–251.

Mahlein, A. K., Oerke, E. C., Steiner, U., and Dehne, H. W. (2012). Recent advances in sensing plant diseases for precision crop protection. *European Journal of Plant Pathology*, 133:197–209.

Mahlein, A. K., Rumpf, T., Dehne, H. W., Plümer, L., Steiner, and Oerke, E. C. (2013). Development of spectral indices for detecting and identifying plant diseases. *Remote Sensing of Environment*, 128:21–30.

Mahlein, A. K., Steiner, U., Dehne, H. W., and Oerke, E. C. (2010). Spectral signatures of sugar beet leaves for the detection and differentiation of diseases. *Precision Agriculture*, 11:413–431.

Maor, R. and Shirasu, K. (2005). The arms race continues: Battle strategies between plants and fungal pathogens. *Current Opinion in Microbiology*, 8:399–404.

Matile, P. and Hörtensteiner, S. (1999). Chlorophyll degradation. *Annual Review of Plant Physiology and Plant Molecular Biology*, 50:67–95.

Melis, A. and Harvey, G. W. (1981). Regulation of photosystem stoichiometry, chlorophyll a and chlorophyll b content and relation to chloroplast ultrastructure. *Biochimica et Biophysica Acta*, 637:138–145.

Merzlyak, M. N., Chivkunova, O. B., Solovchenko, A. E., and Naqvi, K. R. (2008). Light absorption by anthocyanins in juvenile, stressed, and senescing leaves. *Journal of Experimental Botany*, 59:3903–3911.

Michéle, R., Slaton, E., Raymond, H., and William, K. (2001). Estimating near-infrared leaf reflectance from leaf structural characteristics. *American Journal of Botany*, 88:278–284.

Miyamoto, K., Oka, M., and Ueda, J. (1997). Update on the possible mode of action of the jasmonates: Focus on the metabolism of cell wall polysaacharides in relation to growth and development. *Physiologia Plantarum*, 100:631–638.

Molitor, A., Zajic, D., Voll, L. M., Pons-Kühnemann, J., Samans, B., Kogel, K. H., and Waller, F. (2011). Barley leaf transcriptome and metabolite analysis reveals new aspects of compatibility and *Piriformospora indica*-mediated systemic induced resistance to powdery mildew. *Molecular Plant-Microbe Interactions*, 24:1427–1439.

Morris, S. W., Vernooij, B., Titatarn, S., Starret, M., Thomas, S., Wiltse, C. C., Frederiksen, R. A., Bhandhufalck, A., Hulbert, S., and Uknes, S. (1998). Induced resistance response in maiz. *Molecular Plant-Microbe Interactions*, 11:643–658.

Moscou, M. J., Lauter, N., Caldo, R. A., and Nettleton, D. Wise, R. P. (2011). Quantitative and temporal definition of the *Mla* transcriptional regulon during barley-powdery mildew interactions. *Molecular Plant-Microbe Interactions*, 24:694–705.

Mühle, E. (1971). Krankheiten und Schädlinge der Futtergräser. *Hirzel, Leipzig*, 1:422.

Muselimyan, N., Swift, L. M., Asfour, H., Chahbazian, T., Mazhari, R.and Mercader, M. A., and A., S. N. (2016). Seeing the invisible: Revealing atrial ablation lesions using hyperspectral imaging approach. *PLOS One*, 11:1–15.

Nair, R. and Rost, B. (2005). Mimicking cellular sorting improves prediction of subcellular localization. *Journal of Molecular Biology*, 348:85–100.

Nambara, E. and Marion-Poll, A. (2005). Abscisic acid biosynthesis and catabolism. *Annual Review of Plant Biology*, 56:165–185.

Nover, I. (1972). Untersuchungen mit einer für den Resistenzträger Lyallpur 3645 virulenten Rasse von *Erysiphe graminis* DC. f.sp. *hordei* Marchal. *Archiv Pflanzenschutz*, 8:439–445.

Nutter, F. W., Esker, P. D., and Netto, R. A. C. (2006). Disease assessment concepts and the advancements made in improving the accuracy and precision of plant disease data. *European Journal of Plant Pathology*, 115:95–103.

Nutter, F. W., Gleason, M. L., Jenco, J. H., and Christians, N. C. (1993). Assessing the accuracy, intra-rater repeatability, and inter-rater reliability of disease assessment systems. *Phytopathology*, 83:806–812.

Oerke, E. C. and Dehne, H. W. (2004). Safeguarding production–losses in major crops and the role of crop protection. *Crop Protection*, 23:275–285.

Oerke, E. C., Herzog, K., and Toepfer, R. (2016). Hyperspectral phenotyping of the reaction of grapevine genotypes to *Plasmopara viticola*. *Journal of Experimental Botany*, 67:5529–5543.

Oerke, E. C., Mahlein, A. K., and Steiner, U. (2014). Proximal sensing of plant diseases. In Gullino, M. L. and Bonants, P. J. M., editors, *Detection and Diagnostics of Plant Pathogens*, pages 55–68. Springer Netherlands.

Oerke, E. C., Steiner, U., Dehne, H. W., and Lindenthal, M. (2006). Thermal imaging of cucumber leaves affected by downy mildew and environmental conditions. *Journal of Experimental Botany*, 57:2121–2132.

Pan, W. J., Wang, X., Deng, Y. R., Li, J. H., Chen, W., Chiang, J. Y., Yang, J. B., and Zheng, L. (2015). Nondestructive and intuitive determination of circadian chlorophyll rhythms in soybean leaves using multispectral imaging. *Scientific Reports*, 5:11108.

Paulus, S., Behmann, J., Mahlein, A. K., Plümer, L., and Kuhlmann, H. (2014). Low-Cost 3D systems: Suitable tools for plant phenotyping. *Adam Hilger Series on Sensors*, 14:3001–3018.

Peterhänsel, C., Freialdenhoven, A., Kurth, J., Kolsch, R., and Schulze-Lefert, P. (1997). Interaction analyses of genes required for resistance responses to powdery mildew in barley reveal distinct pathways leading to leaf cell death. *The Plant Cell*, 9:1397–1409.

Pietrzykowski, E., Stone, C., Pinkard, E., and Mohammed, C. (2006). Effects of *Mycosphaerella* leaf disease on the spectral reflectance properties of juvenile *Eucalyptus globulus* foliage. *Forest Pathology*, 36:334–348.

Poland, J. A. and Rife, T. W. (2012). Genotyping-by-sequencing for plant breeding and genetics. *The Plant Genome*, 5:92–102.

Pretorius, Z. A., Singh, R. P., Wagoire, W. W., and Payne, T. S. (2000). Detection of virulence to wheat stem rust resistance gene *Sr31* in *Puccinia graminis* f.sp. *tritici* in Uganda. *Plant Disease*, 84:203.

Proels, R. K. and Hückelhoven, R. (2014). Cell-wall invertases, key enzymes in the modulation of plant metabolism during defence response. *Molecular Plant Pathology*, 15:858–864.

Pryce, J. E., Carver, T., and Gurr, S. J. (1999). The roles of cellulase enzymes and mechanical force in host penetration by *Erysiphe graminis* f.sp.*hordei*. *Physiological and Molecular Plant Pathology*, 55:175–182.

Rascher, U., Blossfeld, S., Fiorani, F., Jahnke, S., Jansen, M., Kuhn, A. J., Matsubara, S., Märtin, L. L. A., Merchant, A., Metzner, R., Müller-Linow, M., Nagel, K. A., Pieruschka, R., Pinto, F., Schreiber, C. M., Temperton, V. M., Thorpe, M. R., van Dusschoten, D., van Volkenburgh, E., Windt, C. W., and Schurr, U. (2011). Non-invasive approaches for phenotyping of enhanced performance traits in bean. *Functional Plant Biology*, 38:968–983.

Reiss, E. and Horstmann, C. (2001). *Drechslera teres*-infested barley *Hordeum vulgare* L. leaves accumulate eight isoforms of thaumatin-like proteins. *Physiological and Molecular Plant Pathology*, 58:183–188.

Robatzek, S. and Somssich, I. E. (2001). A new member of the *Arabidopsis WRKY* transcription factor family, *AtWRKY6*, is associated with both senesce- and defence-related processes. *The Plant Journal*, 28:123–133.

Robatzek, S. and Somssich, I. E. (2002). Targets of *AtWRKY6* regulation during plant senescence and pathogen defense. *Genes and Development*, 16:1139–1149.

Robnik-Šikonja, M. and Kononenko, I. (1997). An adaptation of Relief for attribute estimation in regression. *Machine Learning: Proceedings of the Fourteenth International Conference*, pages 296–304.

Rojas, C. M., Senthil-Kumar, M., Tzin, V., and Mysore, K. S. (2014). Regulation of primary plant metabolism during plant-pathogen interactions and its contribution to plant defense. *Frontiers in Plant Science*, 5:1–12.

Römer, C., Wahabzada, M., Ballvora, A., Pinto, F., Rossini, M., Panigada, C., Behmann, J., Léon, J., Thurau, C., Bauckhage, C., Kersting, K., Rascher, U., and Plümer, L. (2012). Early drought stress detection in cereals: Simplex volume maximisation for hyperspectral image analysis. *Functional Plant Biology*, 39:878–890.

Röpenack, E., Parr, A., and Schulze-Lefert, P. (1998). Structural analyses and dynamics of soluble and cell wall-bound phenolics in a broad spectrum resistance to the powdery mildew fungus in barley. *Journal of Biological Chemistry*, 273:9013–9022.

Roulin, S., Xu, P., Brown, A. H. D., and Fincher, G. (1997). Expression of specific (1-3)-[beta]-glucanase genes in leaves of near-isogenic resistant and susceptible barley lines infected with the leaf scald fungus (*Rhynchosporium secalis*). *Physiological and Molecular Plant Pathology*, 50:245–261.

Rouse, J. W., Haas, R. H., Schell, J. A., and Deering, D. W. (1974). Monitoring vegetation systems in the great plains with ERTS. *Proceeding of the third earth resources technology satellite-1 symposium*, pages 309–317.

Rumpf, T., Mahlein, A. K., Steiner, U., Oerke, E. C., Dehne, H. W., and Plümer, L. (2010). Early detection and classification of plant disease with Support Vector Machines based on hyperspectral reflectance. *Computers and Electronics in Agriculture*, 74:91–99.

Saisho, D. and Purugganan, M. D. (2007). Molecular phylogeography of domesticated barley traces expansion of agriculture in the old world. *Genetics*, 177:1765–1776.

Savitzky, A. and Golay, J. M. E. (1964). Smoothing and differentiation of data by simplified least squares procedures. *Analytical Chemistry*, 36:1627–1639.

Schaart, J. G., van de Weil, C. C. M., Lotz, L. A. P., and Smulders, M. J. M. (2016). Opportunities for products of new plant breeding techniques. *Trends in Plant Science*, 21:438–449.

Scheler, B., Schnepf, V., Galgenmüller, C., Ranf, S., and Hückelhoven, R. (2016). Barley disease susceptibility factor RACB acts in epidermal cell polarity and positioning of the nucleus. *Journal of Experimental Botany*, 67:3263–3275.

Scheumann, V., Schoch, S., and Rüdiger, W. (1999). Chlorophyll *b* reduction during senescence of barley seedlings. *Planta*, 209:364–370.

Schmelzer, E. (2002). Cell polarization, a crucial process in fungal defence. *Trends in Plant Science*, 7:411–415.

Scholes, J. D., Lee, P. J., Horton, P., and Lewis, D. H. (1994). Invertase: Understanding changes in the photosynthetic and carbohydrate metabolism of barley leaves infected with powdery mildew. *New Phytologist*, 126:213–222.

Schultz, R. A., Nielsen, T., Zavaleta, J. R., Runch, R., Wyatt, R., and Garner, H. R. (2001). Hyperspectral imaging: A novel approach for microscopic analysis. *Cytometry*, 43:239–247.

Schulze-Lefert, P. and Vogel, J. (2000). Closing the ranks to attack by powdery mildew. *Trends in Plant Science*, 5:343–348.

Schweizer, P., Gees, R., and Mosinger, E. (1993). Effect of jasmonic acid on the inter action of barley (*Hordeum vulgare* L.) with the powdery mildew *Erysiphe graminis* f.sp. *hordei*. *Plant Physiology*, 102:503–511.

Seeholzer, S., Tsuchimatsu, T., Jordan, T., Bieri, S., Pajonk, S., Yang, W., Jahoor, A., Shimizi, K. K., Keller, B., and Schulze-Lefert, P. (2010). Diversity at the Mla powdery mildew resistance locus from cultivated barley reveals sites of positive selection. *Molecular Plant-Microbe Interactions*, 23:497–509.

Seelig, H. D., Hoehn, A., Stodieck, L. S., Klaus, D. M., Adams, W. W., and Emery, W. J. (2008). The assessment of leaf water cotent using leaf reflectance ratios in the visible, near-, and short-wave-infrared. *International Journal of Remote Sensing*, 29:3701–3713.

Seiffert, U. and Schweizer, P. (2005). A pattern recognition tool for quantitative analysis of in planta hyphal growth of powdery mildew fungi. *Molecular Plant-Microbe Interactions*, 18:906–912.

Sendin, K., Williams, P. J., and Manley, M. (2016). Near infrared hyperspectral imaging in quality and safety evaluation of cereals. *Critical Reviews in Food Science and Nutrition*, doi: 10.1080/10408398.2016.1205548.

Shen, Q. H. and Schulze-Lefert, P. (2007). Rumble in the nuclear jungle: Compartmentalization, trafficking, and nuclear action of plant immune receptors. *The EMBO Journal*, 26:4293–4301.

Shen, Q. H., Zhou, F., Bieri, S., Haizel, T., Shirasu, K., and Schulze-Lefert, P. (2003). Recognition specificity and RAR1/SGT1 dependence in barley *Mla* disease resistance genes to the powdery mildew fungus. *The Plant Cell*, 15:732–744.

Shimelis, H. and Laing, M. (2012). Timelines in conventional crop improvement: Pre-breeding and breeding procedures. *Australian Journal of Crop Science*, 6:1542–1549.

Sicher, C. R. and Bunce, J. A. (1997). Relationship of photosynthetic acclimation to changes of Rubisco activity in field-grown winter wheat and barley during growth in elevated carbon dioxid. *Photosynthesis Research*, 52:27–38.

Simko, I., Jimenez-Berni, J. A., and Sirault, X. R. R. (2017). Phenomic approaches and tools for phytopathologists. *Phytopathology*, 107:6–17.

Simpson, T. D. and Gardner, H. W. (1995). Allene oxide synthase and allene oxide cyclase, enzymes of the jasmonic acid pathway, localized in glycine max tissues. *Plant Physiology*, 108:199–202.

Singh, N. K., Nelson, D. E., Kuhn, D., Hasegawa, P. M., and Bressan, R. A. (1989). Molecular cloning of osmotin and regulation of its expression by ABA and adaptation to low water potential. *Plant Physiology*, 90:1096–1101.

Skou, J. P. (1985). On the enhanced callose deposition in barley with *mlo* powdery mildew resistance genes. *Phytopathologische Zeitschrift*, 112:207–216.

Skou, J. P., Jørgensen, J., and Lilholt, U. (1984). Comparative studies on callose formation in powdery mildew compatible and incompatible barley. *Phytopathologische Zeitschrift*, 109:147–168.

Slaton, M. R., Hunt, R., and Smith, W. K. (2001). Estimating near-infrared leaf reflectance from leaf structural characteristics. *American Journal of Botany*, 88:278–284.

Steddom, K., Bredehoeft, M. W., Khan, M., and Rush, C. M. (2005). Comparison of visual and multispectral radiometric disease evaluations of *Cercospora* leaf spot of sugar beet. *Plant Disease*, 89:153–158.

Stein, M., Dittgen, J., Sanchez-Rodriguez, C., Hou, B. H., Molina, A., Schulze-Lefert, P., Lipka, V., and Somerville, S. (2006). *Arabidopsis PEN3/PDR8*, an ATP binding cassette transport, contributes to nonhost resistance to inappropriate pathogens that enter by direct penetration. *The Plant Cell*, 18:731–746.

Stergiopoulos, I. and Wit, J. G. M. (2009). Fungal effector proteins. *Annual Review of Phytopathology*, 47:233–263.

Strachan, I. B., Pattey, E., and Boisvert, J. B. (2002). Impact of nitrogen and environmental conditions on corn as detected by hyperspectral reflectance. *Remote Sensing of Environment*, 80:213–224.

Swarbrick, P., Schulze-Lefert, P., and Scholes, J. (2006). Metabolic consequences of susceptible and resistance (race-specific and broad-spectrum) in barley leaves challenged with powdery mildew. *Plant Cell and Environment*, 29:1061–1076.

Takahashi, A., Casais, C., Ichimura, K., and Shirasu, K. (2003). HSP90 interacts with RAR1 and SGT1 and is essential for RPS2-mediated disease resistance in *Arabidopsis*. *Proceedings of the National Academy of Sciences USA*, 100:11777–11782.

Tenenboim, H. and Brotman, Y. (2016). Omic relief for the biotically stressed: Metabolomics of plant biotic interactions. *Trends in Plant Science*, 21:781–791.

Thenkabail, P. S., Smith, R. B., and de Pauw, E. (2000). Hyperspectral vegetation indices and their relationships with agricultural crop characteristics. *Remote Sensing of Environment*, 71:158–182.

Thomas, S., Wahabzada, M., Kuska, M. T., Rascher, U., and Mahlein, A. K. (2017). Observation of plant-pathogen interaction by simultaneous hyperspectral imaging reflection and transmission measurements. *Functional Plant Biology*, 44:23–34.

Thordal-Christensen, H., Zhang, Z., Wei, Y., and Collinge, D. B. (1997). Subcellular localization of H_2O_2 in plants. H_2O_2 accumulation in papillae and hypersensitive response during the barley-powdery mildew interaction. *The Plant Journal*, 11:1187–1194.

Thurau, C., Kersting, K., and Bauckhage, C. (2010). Yes we can - Simplex Volume Maximization for descriptive web-scale matrix factorization. *International Conference on Information and Knowledge Management, Toronto, Canada*, 24:1785–1788.

Thurau, C., Kersting, K., Wahabzada, M., and Bauckhage, C. (2012). Descriptive matrix factorization for sustainability: Adopting the principle of opposites. *Data Mining and Knowledge Discovery*, 24:325–354.

Ustin, S. L. and Gamon, J. A. (2010). Remote sensing of plant functional types. *New Phytologist*, 186:795–816.

Virlet, N., Sabermanesh, K., Sadeghi-Tehran, P., and Hawkesford, M. J. (2017). Field scanalyzer: An automated robotic field phenotyping platform for detailed crop monitoring. *Functional Plant Biology*, 44:143–153.

Wahabzada, M., Mahlein, A. K., Bauckhage, C., Steiner, U., Oerke, E. C., and Kersting, K. (2015a). Metro maps of plant disease dynamics - automated mining of differences using hyperspectral images. *PLOS One*, 10:1–20.

Wahabzada, M., Mahlein, A. K., Bauckhage, C., Steiner, U., Oerke, E. C., and Kersting, K. (2016). Plant phenotyping using probabilistic topic models: Uncovering the hyperspectral language of plants. *Scientific Reports*, 6:22482.

Wahabzada, M., Paulus, S., Kersting, K., and Mahlein, A. K. (2015b). Automated interpretation of 3D laserscanned point clouds for plant organ segmentation. *BMC Bioinformatics*, 16:248.

Walters, D. R., Avrova, A., Bingham, I. J., Burnett, F. J., Fountaine, J., Havis, N. D., Hoad, S. P., Hughes, G., Looseley, M., Oxley, S. J. P., Renwick, A., Topp, C. F. E., and Newton, A. C. (2012). Control of foliar disease in barley: Towards an integrated approach. *European Journal of Plant Pathology*, 133:33–73.

Wang, Y. and Makedon, F. (2004). Application of Relief-F feature filtering algorithm to selecting informative genes for cancer classification using microarray data. *Proceedings of the IEEE computational systems bioinformatics conference*, pages 497–498.

Wei, F., Gobelman-Werner, K., Morrol, S. M., Kurth, J., Mao, L., Wing, R., Leister, D., Schulze-Lefert, P., and Wise, R. P. (1999). The *Mla* (powdery mildew) resistance cluster is associated with three NBS-LRR gene families and suppressed recombination within a 140-kb DNA interval on chromosome 5s (1HS) of barley. *Genetics*, 153:1929–1948.

Weißling, R. and Panstruga, R. (2012). Rapid quantification of plant-powdery mildew interactions by qPCR and conidiospore counts. *Plant Methods*, 8:35.

Wenzel, G. (1985). Strategies in unconventional breeding for disease resistance. *Annual Review of Phytopathology*, 23:149–172.

Wenzel, G. (2006). Molecular plant breeding: Achievements in green biotechnology and future perspectives. *Applied Microbiology and Biotechnology*, 70:642–650.

West, J. S., Bravo, C., Oberti, R., Lemaire, D., Moshou, D., and McCartney, H. A. (2003). The potential of optical canopy measurement for targeted control of field crop disease. *Annual Review of Phytopathology*, 41:593–614.

Wolf, G. and Frič, F. (1981). A rapid staining method for *Erysiphe graminis* f.sp. *hordei* in and whole barley leaves with a protein-specific dye. *Phytopathology*, 71:596–598.

Wolf, N. (1992). Structure of the genes encoding *Hordeum vulgare* (1-3, 1-4)-*ß*-glucanase isoenzymes I and II and functional analysis of their promoters in barley aleurone protoplasts. *Molecular Genetics and Genomics*, 234:33–42.

Wolfe, M. S. (1984). Trying to understand and control powdery mildew. *Plant Pathology*, 33:451–466.

Wright, D. P., Baldwin, B. C., Shephard, M. C., and Scholes, J. D. (1995a). Source-sink relationships in wheat leaves infected with powdery mildew. 1. Alterations in carbohydrate metabolism. *Physiological and Molecular Plant Pathology*, 47:237–253.

Wright, D. P., Baldwin, B. C., Shephard, M. C., and Scholes, J. D. (1995b). Source-sink relationships in wheat leaves infected with powdery mildew. 2. Changes in the regulation of the calvin cycle. *Physiological and Molecular Plant Pathology*, 47:255–267.

Xu, G. P. and Loveridge, C. W. (2004). *HvDRF1* is involved in abscisic acid-mediated gene regulation in barley and produces two forms of *AP2* transcriptional activators, interacting preferably with a CT-rich element. *The Plant Journal*, 37:326–339.

Xu, P., Wang, J., and Fincher, G. B. (1992). Evolution and differential expression of the (1-3)-[beta]-glucan endohydrolase encoding gene family in barley, *Hordeum vulgare*. *Plant Pathology*, 120:157–165.

Yendrek, C. R., Tomaz, T., Montes, C. M., Cao, Y., Morse, A. M., Brown, P. J., McIntyre, L. M., Leakey, A. D. B., and Ainsworth, E. A. (2016). High-throughput phenotyping of maize leaf physiological and biochemical traits using hyperspectral reflectance. *Plant Physiology*, [in press]:doi: 10.1104/pp.16.01447.

Yin, X., Struik, P. C., and Kropff, M. J. (2004). Role of crop physiology in predicting gene-to-phenotype relationships. *Trends in Plant Science*, 9:426–432.

Zhang, J. C., Pu, R. L., Wang, J. H., Huang, W. J., Yuan, L., and Luo, J. H. (2012). Detecting powdery mildew of winter wheat using leaf level hyperspectral measurements. *Computers and Electronics in Agriculture*, 85:13–23.

Zhao, Y. R., Li, X., Yu, K. Q., Cheng, F., and He, Y. (2016). Hyperspectral imaging for determining pigment contents in cucumber leaves in response to angular leaf spot disease. *Scientific Reports*, 6:27790.

Zhou, F., Kurth, J., Wei, F., Elliott, C., Valé, G., Yahiaoui, N., Keller, B., Somerville, S., Wise, R., and Schulze-Lefert, P. (2001). Cell-autonomous expression of barley *Mla1* confers race-specific resistance to the powdery mildew fungus via a *Rar1*-Independent signalling pathway. *The Plant Cell*, 13:337–350.

Zielinski, R. E., Werneke, J. M., and Jenkins, M. E. (1989). Coordinate expression of *Rubisco* activase and *Rubisco* during barley leaf cell development. *Plant Physiology*, 90:516–521.

Danksagung

Ich möchte mich an dieser Stelle bei allen Personen bedanken, die mich während meiner Promotionszeit und zur Erstellung meiner Dissertation in vielfältiger Weise unterstützt haben.

Mein größter und besonderer Dank gilt Frau PD Dr. A.-K. Mahlein vom Institut für Zuckerrübenforschung an der Universität Göttingen. Sie gab mir die Möglichkeit in Ihrer interdisziplinären Nachwuchsgruppe des CROP.SENSe.net Forschungsnetzwerkes an der Universität Bonn, an einer modernen Thematik zu arbeiten. Sie hat mich stets unterstützt und mir die spannende Thematik der 'hyperspektralen Sensoren' eröffnet und mir dabei auch Selbsttändigkeit gewährt. Ich bedanke mich besonders für die erstklassige Betreuung, die ermöglichten Fortbildungen und Auslandserfahrungen und für das entgegengebrachte Vertrauen. An dieser Stelle möchte ich auch Frau Prof. Dr. D. Bartels vom IMBIO-Molekulare Physiologie der Universität Bonn ganz herzlich für Ihr Interesse an meiner Arbeit und für die Übernahme des Koreferates danken.

Sehr herzlich möchte ich mich bei Frau PD Dr. U. Steiner bedanken, die mich auf die Möglichkeiten im Institut (INRES-Pflanzenkrankheiten und Pflanzenschutz) aufmerksam gemacht hat und auch folgend durch ihre vielfältigen Anregungen und mit konstruktiver Kritik meine Forschungssrbeit begleitet hat. An dieser Stelle möchte ich mich auch bei Herrn PD. Dr. E.-C. Oerke bedanken der ebenfalls durch vielfältigen Anregungen und mit konstruktiver Kritik das Entstehen dieser Arbeit maßgeblich beeinflusst hat. Mein herzlicher Dank geht auch an Herr Prof. Dr. H.-W. Dehne vom INRES-Pflanzenkrankheiten und Pflanzenschutz (ehem. Phytomedizin) der Universität Bonn für seine Unterstützung und warmherzige Aufnahme in seine Forschungsabteilung, schon während meiner Studienzeit. Ich danke allen Mitarbeitern und Doktoranden des Instituts für die kollegiale Zusammenarbeit und für die angenehme Arbeitsathmosphäre. Insbesondere danke ich Jennifer Stracke, Kerstin Lange, Carolin Sichtermann und Marlene Leucker für die vielfältige Unterstützung. Dr. M. Wahabzada und Dr. J. Behmann danke ich für die fachbereichübergreifende Arbeit zur Optimierung der Auswertung hyperspektraler Daten und für die Unterstützung bei der Fertigstellung meiner Dissertation. Vielen Dank, dass ich die Doktorarbeit mit euch zusammen erleben durfte.

Dieses Projekt wurde im Rahmen des Agroclusters CROP.SENSe.net Kompetenznetzwerk der Phänotypisierungsforschung durchgeführt. Dem BMBF danke ich für die finanzielle Unterstützung. Die Durchführung meines Forschungsaufenthalts in Dänemark ermöglichte das 'Jeff Schell' Stipendium der Bayer Science and Education Foundation, der ich in Dank verbunden bin. An dieser Stelle möchte ich mich bei Herrn Prof. Dr. T. Roitsch und Dr. D. K. Grosskinsky für die warmherzige Aufnahme in die Forschungsgruppe und Unterstützung meines Forschungsaufenthaltes bedanken.

Ich danke meiner Familie und meinen Freunden dafür, dass es sie gibt. Meiner Mutter Michalina Kuska und meiner Verlobten Nadine Pastuszka werde ich immer dankbar sein für die bedingungslose Unterstützung und dafür, dass sie an mich glauben. Ich danke meinem Bruder Benjamin, meiner Schwägerin Sandra, und Ihren Kindern Mia und Fabian Kuska. Ema Piecha, Mirela, Woitek, Elisa und Julia Szutka. Gabriele, Richard und René Pastuszka. Maria und Herbert Urbatzka. Beate und Francisco Carillo. Sandrina Kreuer, Tobias, und Marion Lewanczyk. Konrad Kosciow und Paula Marczyk. Theo Staschewski und Ursula Behr. Patrick Wolf und Diana Obliers. Nikolas Unger und Dunja Giebeler. Simon und Verena Selzer. Sebastian Mirgeler und Lisa Wagner. Manuel Mohr und Christine Prem. Nikolas Owtscharenko und Christina Braun. Fabian Vogel und Lara Deppe. Jannika Tangermann, Max Münchmeyer und Eduard Mann. Ganz besonders möchte ich mich auch bei Jan Obliers und Katrin Hänisch für Ihre Unterstützung während meines Studiums danken.

Die gemeinsame Zeit mit euch allen ist von unschätzbaren Wert.

Erklärung

Hiermit erkläre ich, dass ich die Arbeit ohne unzulässige Hilfe Dritter und ohne Benutzung anderer als der angegebenen Hilfsmittel angefertigt habe. Die aus fremden Quellen direkt oder indirekt übernommenen Informationen sind als solche kenntlich gemacht. Des Weiteren versichere ich, dass ich diese Dissertation nicht als Prüfungsarbeit für eine andere Prüfung oder die gleiche oder Teile der Abhandlung als Dissertation bei einer anderen Fakultät oder bei einem anderen Fachbereich eingereicht habe.

Bonn, den 25.08.2017

Matheus Thomas Kuska